ASYMMETRIC TURBULENT FLOW: ANALYSIS AND EXPERIMENT

by

Ertugrul ALP

A thesis submitted to the School of Graduate Studies in partial fulfillment of the requirements of the degree of

MASTER OF APPLIED SCIENCE

in the

Department of Mechanical Engineering
University of Ottawa
Ottawa, Canada

1974

ABSTRACT

An experimental and theoretical investigation of fully developed asymmetric turbulent flow in a channel is reported in the present study. All through the analysis the fluid properties were assumed to be constant.

The experimental programme consisted of providing detailed measurements of mean and turbulent characteristics of the flow in a large-aspect-ratio rectangular channel. One of the walls of the channel was smooth and the other roughened with transverse V-ribs. The dissimilar wall conditions imposed a strong asymmetry on both the mean and turbulent flow fields disclosing several features that are concealed in the symmetric flow situations.

The theoretical investigation was concerned with predicting the flow parameters of engineering interest. The integral method was used together with a turbulence model based on Prandtl's mixing length theory.

An attempt to close the equations with one empirical constant failed to successfully predict the parameters of interest. Thus, it was necessary to resort to the use of empirical functions for the parameters describing the maximum velocity and zero shear stress points. The results then were in excellent agreement with the experimentally determined values.

The results show the strong effect of asymmetry on engineering parameters. Furthermore, it is the roughness structure (including roughness geometry, relative roughness and roughness density) which influences the nature of asymmetry.

ACKNOWLEDGEMENTS

The author wishes to acknowledge with gratitude the advice and guidance of Dr. Y. Lee of University of Ottawa, who initiated the work and supervised its realization.

Sincere thanks are also due to the technical staff of the Mechanical Engineering Department, especially to Mr. E. Kelly, for their painstaking efforts for the construction of the apparatus, and also to Mrs. F. Perron for her efforts in typing this thesis.

TABLE OF CONTENTS

LIST OF TABLES

LIST OF FIGURES

NOMENCLATURE

A	cross sectional area of channel; constant
a	constant
$\vec{a}$	vector "a"
$\overleftrightarrow{a}$	tensor "a"
B, b	constants
C, C_1	constants
D	diameter; quantities defined by eqns. A.10.1 and A.12.1
F	body force
f	friction factor, $\frac{2\tau_w}{\rho u_{av}^2}$
g	gravitational acceleration
k	von Karman's constant, 0.4
k_s	sand roughness
l	mixing length
m	$\frac{z}{\varepsilon}$ or
n	constant
P	pressure; electrical power
p	pitch; distance between tips of roughness elements
Q	flow rate; heat transfer by convection from hot-wire probe
R	gas constant; electrical resistance; pipe radius

Re	Reynolds number, $\frac{u_{av} D_{hyd}}{\nu}$
s	distance between channel walls
T	temperature
Tu	turbulence intensity, $\frac{\sqrt{\overline{u'^2}}}{u}$
t	time
u	velocity in x-direction
u_{av}	average velocity in the channel, $\frac{Q}{A}$
V	anemometer output voltage
V_o	zero velocity voltage signal from anemometer
v	velocity in y-direction
w	velocity in z-direction
x	coordinate in the axial direction
y	coordinate perpendicular to the channel walls
z	coordinate parallel to the channel walls, perpendicular to the axial direction
z_{or}	parameter defined by equation 2.20, hydrodynamic roughness

Greek symbols

γ	specific weight, ρg
Δ	difference
δ	hydrodynamic boundary layer thickness

ϵ	physical roughness height
ϵ_M	eddy diffusivity
μ	absolute viscosity
ν	kinematic viscosity
ρ	density
σ	normal stress
τ	shear stress
τ_w	wall shear stress

Superscripts

$'$	fluctuating component
$-$	time averaged quantity
$+$	non-dimensionalized quantity, in case of velocities $u^+ = \frac{u}{u_\tau}$ in case of lengths $y^+ = \frac{y\, u_\tau}{\nu}$
$++$	quantity non-dimensionalized by using the friction velocity of the opposite wall

Subscripts

dP	double pitot tube
i	instantaneous
m	corresponding to the maximum velocity point
r	rough wall

rms	root mean square
s	smooth wall
t	turbulent
0 (zero)	corresponding to the zero shear stress point
δ	corresponding to conditions at δ, edge of boundary layer
∞	corresponding to conditions outside the boundary layer, potential flow

I. INTRODUCTION

1.1 Problem Background, Motivations and Objectives

Until recently detailed experimental studies of turbulent shear flows have been concerned with flows through relatively simple geometries such as flow in circular cross-sectional pipes or plane smooth channels. Investigations of channel flows with rough surface boundaries have also been largely confined to symmetric cases. The reasons of the earlier investigators for reserving themselves for these relatively simple cases are understandable: The nature of some of the turbulent flow properties, such as the mean velocity profiles and friction factors are most easily deductable when other effects such as compressibility, asymmetry and flow acceleration are not present. During recent years the data available on these more complex flows have increased and in the present study inclusion of asymmetry is carried out.

Until very recently theoretical approaches to the problem of predicting characteristics of turbulent shear flows have been confined to using integral analyses of the mean flow because of lack of availability of practical methods for the solution of a set of simultaneous partial differential equations closed with a set of empirical constants. Lately, especially in the last several years, this latter approach was successfully used for the solution of more complex turbulent shear problems through the use of high speed computers [1]. However, due to the complexity of this approach an approximate solution using the integral analyses together with a turbulence model based on Prandtl's mixing length theory is attempted in the present work as a preliminary study of the problem.

In the present study particular emphasis was placed on asymmetric flows where the characteristic flow properties exhibit stationary values, because it is these flow situations where some of the structural flow features, that are concealed in simple flows by virtue of symmetry or some other constraint, become prominent.

Asymmetric flows are encountered in many practical situations where technological requirements impose dissimilar boundary conditions. The nonuniform distribution of roughness or porosity or unequal curvatures of solid surface bounding the flow are some examples of such conditions. A practical example is the use of partially roughened or finned annulus in compact heat exchangers.

Bearing the above considerations in mind the main research objectives were set as follows:

1. To predict the fully developed mean flow parameters which are of direct engineering interest through theoretical considerations,

2. To measure these mean flow parameters experimentally in order to:
   i) Provide data to enable direct testing of theoretical predictions,
   ii) Provide data for a better understanding of fully developed yet strongly asymmetric flows,

3. To provide a basis for further study of the problem (e. g. Developing asymmetric flow).

1.2 Outline of the thesis

The thesis consists of five chapters, the first of which is the Introduction.

The second chapter introduces some fundamental notions and discusses possible approaches to the investigation of turbulent shear flows. It covers the basic equations and discusses, through a literature survey, some specific features of turbulent shear flows, that are relevant to the flow situations considered in the present work.

The main outcome of the present research is presented in chapters 3 and 4. Chapter 3 deals with the experimental studies covering the measurements of the main properties of the mean and fluctuating motion in a channel with one smooth and one roughened wall. A discussion of procedure and measurements is presented.

In Chapter 4 the relations used to predict the mean flow parameters are developed, followed by a description of the method of computation devised for the present work.

The main conclusions and recommendations for future work are presented in the closing chapter 5.

The relevant informations and/or details are given in 15 appendixes.

2. BASIC EQUATIONS AND LITERATURE SURVEY

2.1 Governing Physical Laws

2.1.1 Differential formulations

The general basic equations for conservation of mass and momentum of an incompressible fluid with constant viscosity can be written in vector form as follows [1]:

$\vec{V}$ = Velocity vector = $\vec{u} + \vec{v} + \vec{w}$

$$\nabla \cdot \vec{V} = 0 \tag{2.1}$$

$$\rho \left[\frac{\partial \vec{V}}{\partial t} + (\vec{V} \cdot \nabla) \vec{V} \right] = -\nabla P + \vec{F} + \mu \nabla^2 \vec{V} \tag{2.2}$$

Equations (2.2) are known as the incompressible Navier-Stokes equations. All terms in the above equations represent the instantaneous values of the quantities, which from now on will be designated by a subscript i. Introducing the time-averaged and fluctuating components of the quantities following O. Reynolds, [2], such as

$$u_i = u + u'$$

the following relations can be deduced for steady turbulent flow in the absence of body forces:

$$\nabla \cdot \vec{V} = 0$$
$$\nabla \cdot \vec{V}' = 0 \tag{2.4}$$

$$\rho \left[\left(\vec{V} \cdot \nabla \right) \vec{V} \right] = - \nabla P + \mu \nabla^2 \vec{V} + \nabla \cdot \overleftrightarrow{\tau}' \qquad (2.5)$$

where

$$\overleftrightarrow{\tau}' = \begin{pmatrix} \sigma'_x & \tau'_{xy} & \tau'_{xz} \\ \tau'_{xy} & \sigma'_y & \tau'_{yz} \\ \tau'_{xz} & \tau'_{yz} & \sigma'_z \end{pmatrix} = - \rho \begin{pmatrix} \overline{u'^2} & \overline{u'v'} & \overline{u'w'} \\ \overline{u'v'} & \overline{v'^2} & \overline{v'w'} \\ \overline{u'w'} & \overline{v'w'} & \overline{w'^2} \end{pmatrix} \qquad (2.6)$$

Care should be exercised in expanding the last term in eqn. (2.5) due to the tensorial nature of $\overleftrightarrow{\tau}'$.

The flow in the entrance region of a two dimensional duct belongs to a boundary-layer class of flows. The introduction of the so called "boundary-layer approximations" after L. Prandtl [3] into the above equations will yield

$$\frac{\partial u}{\partial x} + \frac{\partial v}{\partial y} = 0 \qquad (2.7)$$

$$\rho \left(u \frac{\partial u}{\partial x} + v \frac{\partial u}{\partial y} \right) = - \frac{dP}{dx} + \mu \frac{\partial^2 u}{\partial y^2} - \rho \left(\frac{\partial \overline{u'^2}}{\partial x} + \frac{\partial \overline{u'v'}}{\partial y} \right) \qquad (2.8)$$

For fully developed flow sufficiently far from the entrance, the flow is essentially one-dimensional with velocity field invariant in the streamwise (x) direction. When the conditions

$$\frac{\partial}{\partial x} = 0, \quad v = 0,$$

characterizing fully developed flow are imposed on eqn. (2.8) one obtains

$$\mu \frac{\partial^2 u}{\partial y^2} - \rho \frac{\partial \overline{u' v'}}{\partial y} - \frac{dP}{dx} = 0 \qquad (2.9)$$

with boundary conditions

$$\text{at } y = 0; \quad u = 0, \quad \overline{u' v'} = 0, \quad \mu \frac{\partial u}{\partial y} = \tau_w$$

$$\text{and} \quad \text{at } y = y_o ; \quad \tau = \mu \frac{\partial u}{\partial x} - \rho \overline{u' v'} = 0 \qquad (2.10)$$

It must be pointed out that in the last boundary condition, y_o represents the position of zero shear stress, not necessarily coincident with the zero positions of viscous or turbulent shear stresses, neither with the position of maximum velocity.

2.1.2 Integral formulations

The basic integral equations for conservation of mass and momentum of incompressible fluid flow in a duct can be written from the diagram describing the idealized model shown in figure 2.1.

Mass:

$$\frac{d}{dx} (u_{av} s) = \frac{d}{dx} \int_o^s u \, dy = 0 \qquad (2.11)$$

Momentum:

middle portion (potential flow);

$$\frac{dP}{dx} = -\rho u_\infty \frac{du_\infty}{dx} \qquad (2.12)$$

rough side;

$$\tau_{wr} = -\delta_r \frac{dP}{dx} - \frac{d}{dx}\int_{z_{or}}^{\delta_r} \rho u_r^2 \, dy_r + \rho u_\infty \frac{d}{dx}\int_{z_{or}}^{\delta_r} u_r \, dy_r \qquad (2.13)$$

smooth side;

$$\tau_{ws} = -\delta_s \frac{dP}{dx} - \frac{d}{dx}\int_{o}^{\delta_s} \rho u_s^2 \, dy_s + \rho u_\infty \frac{d}{dx}\int_{o}^{\delta_s} u_s \, dy_s \qquad (2.14)$$

The details of the derivation are presented in Appendix 1.

The momentum integral method for the boundary layer due to T. von Karman [4] has been a powerful tool for the prediction of boundary layers so far. Together with an assumed velocity field it forms the basis of many existing solutions of the boundary layer. It can in fact be derived through a partial integration of equation (2.8) [5].

The parameter z_{or} encountered in equation (2.13) which is the lower limit of the momentum integrals will be given due consideration in section 2.2.

For the fully developed region the momentum equations simplify to (see Appendix 2 for a derivation from equation (2.9)) :

rough side:

$$\tau_{wr} = - y_{or} \frac{dP}{dx} \qquad (2.15)$$

smooth side:

$$\tau_{ws} = - y_{os} \frac{dP}{dx}$$

where $y_{os} + y_{or} = s$

These last two equations enable the wall shear stresses to be calculated from the measured pressure gradient and zero shear point y_o. This method has been employed in the present experimental work.

2.1.3 Summary: Physical Model

The considerations in section 2.1.1 are relevant to channels with both smooth and rough walls. In the latter case, however, depending upon the type of roughness, the local flow mechanism in the vicinity of the rough wall may not fully satisfy the boundary layer approximations. Large scale roughness may cause flow recirculation in the wake zone of the roughness elements, where some of the neglected terms in the momentum equations become important. In the present analysis, the momentum integral equation was broken into smooth and rough side equations and, to take care of the above mentioned complication, the parameter z_{or} was introduced in the rough side equation. This will be further mentioned in section 2.2 where the velocity fields to be used in the present analysis are discussed.

The assumptions introduced in the derivation of equations (2.11 - 2.14) are as follows:

1. Flow is steady turbulent everywhere,
2. Working fluid is a constant-property Newtonian fluid,
3. Flow is uniform at the entrance,
4. Flow outside the boundary layer is potential flow,
5. Body forces are absent,
6. Boundary layer approximations are valid,

$$\text{namely} \quad \frac{\partial u}{\partial y} >> \frac{\partial u}{\partial x} \quad , \quad \frac{\partial v}{\partial x} \quad , \quad \frac{\partial v}{\partial y}$$

$$\frac{\partial P}{\partial x} \simeq \frac{dP}{dx} \quad , \quad \frac{\partial P}{\partial y} = 0$$

2.2 Mean Velocity Field

The simplified equations of motion presented in the previous section are not enough to predict the mean flow parameters which the present study is seeking for. A turbulence model is necessary to give the velocity profiles encountered in the flow situations involved. In the present work a model based on L. Prandtl's mixing length theory [6] is adopted. A physical interpretation of the mixing length can be given in the following way: The mixing length is that distance in the transverse direction which must be covered by an agglomeration of fluid particles travelling with its original mean velocity in order to make the difference between its velocity and the velocity in the new lamina equal to the mean transverse fluctuation in turbulent flow [5]. Using this concept of mixing length an expression for turbulent shear stress can be reached:

$$\tau_t = \rho l^2 \left|\frac{du}{dy}\right| \frac{du}{dy} \qquad (2.17)$$

Together with the assumptions that mixing length is proportional to the wall distance through a constant k and that shear stress does not change with wall distance, we get the following expression for the velocity profile in turbulent flow near a wall:

$$u = \frac{u_\tau}{k} \ln y + C_1 \qquad (2.18)$$

Through dimensional analysis considerations equation (2.18) can better be written for hydrodynamically smooth walls as [5]

$$\frac{u_s}{u_{\tau_s}} = \frac{1}{k} \ln \frac{y_s u_{\tau_s}}{\nu} + C \qquad (2.19)$$

and for rough walls as

$$\frac{u_r}{u_{\tau_r}} = \frac{1}{k} \ln \frac{y_r}{z_{or}} \qquad (2.20)$$

where $z_{or} = m\epsilon$, the hydrodynamic or characteristic roughness. Here m is a function used to incorporate the roughness shape and density into the theory.

A number of expressions for the velocity profile near a smooth wall are available in literature [7-14]. Among these the expression due to Reichardt [7] was chosen to be used in the present study because of its simple, continuous form valid for $y > 0$, including the so called "laminar sub-layer" as well:

$$u_s^+ = \frac{1}{k} \ln(1 + k y^+) + 7.8 \left[1 - \exp\left(-\frac{y^+}{11}\right) - \frac{y^+}{11} \exp\left(-\frac{y^+}{3}\right)\right] \qquad (2.21)$$

where k = 0.4, von Karman's constant.

The above profile simplifies to the expression due to Prandtl and Taylor [10] for large y^+ ($>\sim 100$, see Appendix 14, also see Table 4 for the experimental $y^+_{ms} = s^+ - y^{++}_{mr}$ values).

$$u^+ = \frac{1}{k} \ln y^+ + C \qquad (2.22)$$

with k = 0.4 again and the value of C = 5.52, adjusted to have numerical agreement with equation (2.21).

For the rough wall profile (2.20) a number of and varying values of m are reported in the literature for different shape and density of roughness elements.

For sand roughness J. Nikuradse [15] reports a value of $m = \frac{1}{30}$. For camouflage paints on aeroplanes $m = \frac{1}{18.75}$ [16], for different types of vegetation on earth $m = \frac{1}{7.5}$ [17]. Gef froy, Jude, Paumard [18] report values varying from $= \frac{1}{7.65}$ to $\frac{1}{3400}$ with $\frac{p}{\epsilon}$ varying between 9 and 20, respectively, for sinusoidal undulations in a pipe. Through a survey to determine the effect of roughness density λ, Simpson [19] found $m = \frac{1}{9400}$ for $\lambda = 1$ varying to $m = \frac{1}{3.45}$ for $\lambda = 5$, for different roughness shapes. In this case λ was defined as the ratio of the total surface area to the total roughness frontal area normal to the flow. In a detailed experimental survey of flow in an asymmetric rectangular channel with rectangular ribs ($\frac{p}{\epsilon} = 10$) Hanjalic [20] suggests a value of $m = \frac{1}{3.83}$. All the above values of m were calculated through reported data so as to fit the nomenclature of the present study.

In view of the widely varying values of m with no apparent correlation reported in the literature, it was obvious that further work was necessary to establish relations between roughness structures on walls and velocity profiles.

In the above equation (2.20) the parameter z_{or} may be interpreted as a hypothetical distance from the wall where the velocity is assumed to be zero. This shift of the reference point for the rough wall velocity profile has been shown to depend on the roughness Reynolds number $\frac{\varepsilon u_\tau}{\nu}$ (which is a measure of the roughness structure through the wall shear stress) by Clauser [21] on the basis of experiments conducted with two-dimensional roughness elements. Hama [22] has subsequently verified Clauser's generalization for three-dimensional roughness and Perry and Joubert [23] have extended experimentally their results to the boundary layer with adverse pressure gradient. Wu [24] has reported a similar shift for a rough surface with uniform spherical particles arranged in a random and compact form.

The reported data suggest that this point is somewhere between the root and the tip of the physical roughness height. Exactly where for a particular roughness structure remains to be found through experiments.

2.3 Eddy Diffusivity Models

The concept of eddy diffusivity, first initiated by Bussinesq [25], can be introduced into the analysis if we rewrite equation (2.9) as

$$\frac{\partial}{\partial y}\left(\mu \frac{\partial u}{\partial y} - \rho \overline{u'v'}\right) - \frac{dP}{dx} = 0 , \qquad (2.23)$$

the quantity in the parantheses corresponding to the shear stress τ in the channel:

$$\tau = \mu \frac{\partial u}{\partial y} - \rho \overline{u' v'} \qquad (2.24)$$

If we put

$$\tau_t = - \rho \overline{u' v'} = \rho \varepsilon_M \frac{\partial u}{\partial y} \qquad (2.25)$$

we get

$$\frac{\tau}{\rho} = (\nu + \varepsilon_M) \frac{du}{dy} \qquad (2.26)$$

This last equation, together with an eddy diffusivity model, has been extensively used to predict turbulent transport for a wide variety of flow geometries [7, 26-29]. However, especially in asymmetric flows, where the stationary values of the mean and fluctuating velocities do not coincide, the concept of eddy diffusivity as used above presents some difficulties. As discussed by Lee and Barrow [30], at points where the velocity gradient is zero, shear stress is not necessarily zero, whereas equation (2.26) predicts it to be zero.

The mean and fluctuating motion are closely interconnected as indicated by the appearance of the turbulent stresses in the mean momentum equation, and mean velocity gradients in the stress equations. It would seem that the statistically averaged fluctuating velocities would follow the behaviour of the mean motion and that both mean and fluctuating fields can be treated uniquely. However, the reported non-coincidence of the stationary values of the mean and fluctuating velocities [20, 31, 32] infers that universal treatment of

the two fields together is not possible. A partial explanation of this non-universality may be taken from Townsend's [33] suggestion that the fluctuating motion consists of an "active" component which interacts locally with the mean motion and, also of an "inactive" component, governed by far-away conditions and, therefore not directly correlated with the mean motion. A discussion of why the zero shear and zero velocity gradient points are not necessarily coincident in turbulent flows is given in Reference [32] through an analysis of Navier-Stokes and von Karman's momentum equations.

2.4 Engineering Flow Parameters

Although a wealth of information is available in literature on pressure drop measurements and friction factors for flow of fluids in channels with rough boundaries, a great majority of them are purely experimental and confined to symmetric flows in pipes.

Streeter [34] has experimentally shown that in artificially roughened pipes, f is mainly a function of Re and $\frac{s}{\varepsilon}$ and also deduced that shape of roughness has as much effect as the size of the roughness. In an attempt to find the optimum heat transfer surfaces over a wire wrapped tube, Sheriff and Gumley [35] also reported empirical correlations for friction factors. Kidd [36] explored heat transfer and pressure drop characteristics of gas flow inside spirally corrugated tubes. A friction correlation based on the law of the wall similarity, together with experimental pressure drop measurements in tubes with repeated-rib roughness, is reported in Reference [37]. Finally, friction measurements in rectangular channels [38] and in annuli [39] with walls of non-identical roughness were given in the literature. In these last two works a method due to Hall [40] was

employed to separate the friction factor due to each surface. This so called "Hall's transformation theory" is based on the assumption that the stationary values of mean and fluctuating velocity fields coincide. Discussions of the breakdown of this theory are given in References [32] and [38].

The above listed references contain little or no theoretical analysis. One notable exception is the study reported by Launder and Hanjalic [41] on turbulence structure in an asymmetric rectangular channel together with theoretical predictions of mean flow parameters.

3. EXPERIMENTAL STUDIES

3.1 Experimental Apparatus and Instrumentation - General

The experimental programme undertaken was designed to meet the overall research objectives described before. The working fluid was chosen as air in atmospheric conditions due to purposes of economical construction of test facilities and also availability of information on physical properties. Asymmetry was decided to be induced into the flow by artificially roughening the channel walls only partially. The channel shape had also to be of some practical importance. Thus a clear choice was a rectangular duct of large aspect ratios with one of the wider sides roughened, approximating flow conditions between two parallel plates or in an annulus with a radius ratio close to 1.

The main experimental programme consisted of providing detailed measurements of static pressure drop along the channel length, mean velocity profiles, mean velocity gradient profiles and profiles of longitudinal velocity fluctuations at different ports along the channel length with different spacings between plates.

The static pressure measurements were made with an MKS pressure transducer the calibration of which was checked against a micromanometer at frequent intervals. Velocities and velocity fluctuations were measured with DISA hot-wire probes. Velocity profiles were also checked with single pitot tube readings. Velocity gradients were measured with a double pitot tube. The traverses were made either manually or with a motor driven DISA traversing mechanism.

3.2 Apparatus

The experimental test section and the auxiliary apparatus is shown schematically in figure 3.1 and photographs of the channel assembly are given in figures 3.2. The channel walls were made of 1/2 inch - thick aluminium, 11 feet long, 16-3/8" wide. Three interchangeable plates were used, two of which were roughened by machining 60° V-grooves in the transverse direction. Machined rather than added roughness was chosen to facilitate heat transfer studies at a later stage. The machining was done on a milling machine, with a feed of 460 mm/min at 2860 rpm of cutter speed. The height of the grooves was 0.0804 inches (figure 3.3). The pitch to height ratio of the roughness elements was 1:1 for the present study. One of the roughened plates was provided with 14 velocity measuring ports of 1-3/4" dia. with center pieces to fit these ports (figure 3.4). A round 3-3/8" dia. 1/2" thick aluminium piece was welded on the main plate to provide support to the base of the traversing mechanism which was fixed to the plate by 1/4" dia. allan screws. 1/8" dia. holes were provided in the middle of the center pieces for smooth movement of total and hot-wire probes. The machining was done with these center pieces fixed to place, to provide a flush fit with the grooves. The other two plates were provided with static pressure holes of 0.025" dia., at four inch intervals along the center line (figure 3, 5). Thus provision was made to examine both asymmetric and rough-symmetric flows.

The main plates were mounted vertically on their sides to avoid the problem of sagging on a steel frame specifically designed for the purpose of changing the spacing between the plates. The top and bottom of the channel were closed with 1/2" thick transparent

plexiglass pieces through which the position of the probes could be examined. Using different widths of these plexiglass spacings the ratio $\frac{s}{\epsilon}$ of the channel could be controlled with discrete intervals. Four different sized spacers were used to provide $\frac{s}{\epsilon}$ ratios of 10.5, 16.7, 29.2 and 35.45.

An entrance section was designed with uniform flow considerations in mind, using an approximate solution of the potential flow equations with a practicable area drop ratio [42].

A diffuser section was designed to connect the channel to the diffuser box, which in turn was connected to the fan (specification: 6000 cfm at 14" H_2O, 1785 rpm, 19.8 BHP; driven by constant rpm electric motor). The diffuser box (wooden, 44" x 42" x 30") was equipped with two movable gates inside on the fan side, to facilitate the control of flow rate of air.

An entrance box (wooden, the same size as the diffuser box) was placed in front of the entrance section to provide a connection between the channel and the flow rate meter and also act as a settling chamber. The flow rate meter was placed upstream rather than downstream bearing in mind possible heat transfer experiments on the apparatus.

3.3 Instrumentation

3.3.1 Pitot-tube and pressure measurement system

Some of the velocity distributions were measured with a flattened-tip pitot tube as a check of the preliminary hot-wire probe traverses. The pitot tube was made from hypodermic stainless steel tubing, 0.035" O.D. and 0.020" I.D. Internal tip height was about

0.006" (figure 3.6). The pitot tube measurements were checked against the velocities attained in the DISA hot-wire calibration equipment and no appreciable difference was found between mean readings.

Static pressure holes 0.025 in. dia., were drilled on the plates, every 4 in. along the center line (figure 3.5). These were connected to the pressure measuring network of tubes through 1/8" I.D. pressure connectors, which were fixed onto the plates by screws. The tubing used was 3/8" O.D., 1/4" I.D. Jayflex-180 plastic tubing. The ends of each of these tubes were connected to a common manifold with one output going to the pressure measuring instrument. The signals through the pressure taps could be turned on and off by clamps which were placed before the manifold (figure 3.7).

Pressure measurements were made by MKS differential pressure transducers (types 77H-1 and 77H-1000). The output from the transducers were measured with the MKS Baratron type 77 electronic pressure meter [43], and these measurements were checked frequently against a micro-manometer. All pressure measurements were made relative to the atmosphere, i.e. one of the transducer inputs was open to the ambient.

3.3.2 Double pitot tube

The position of maximum velocity was found by means of a double pitot tube consisting of two flattened-tip pitot tubes 2 mm apart (figure 3.8) [20, 44]. No appreciable difference was found between the two pitot tubes when placed in a uniform stream during the calibration stage.

3.3.3 Hot wire probes and signal processing system

In measuring the mean velocity profiles and the longitudinal velocity fluctuation, the standard DISA miniature hot wire probes in conjunction with a DISA 55D00 series constant temperature anometer system were used. The probes were of type 55P11 (55F31 in the older specifications), made of platinum plated tungsten wires, 5 μm in dia. and 1.25 mm in length [45].

The signals from the probes were fed to type 55D01 anemometer unit, the output of which was in turn connected to a 55D10 linearizer. This output was connected to an auxiliary unit, 55D25. The linearized and filtered signals were measured with an RMS voltmeter, 55D35, and a digital voltmeter, 55D30. The RMS values of the fluctuations and the mean value of the output were then fed into the data recording system (see sec. 3.3.5) together with the output from the traversing mechanism (see sec. 3.3.4). Flowcharts of these measurements are given in figures 3.9 a,b.

3.3.4 Traversing mechanism

The mechanism used to traverse the probes (both pitot-tube and hot wire) was the DISA 55H01 Traversing mechanism supported by a traversing mechanism base which could be secured (figure 3.10) onto the plate carrying the velocity-measuring ports by three capscrews. The traversing mechanism was operated either with a manual drive unit or by electrical pulses via the DISA 52 C01 stepper motor, the latter of which was remotely controlled from the DISA 52B01 Sweep Drive Unit. The output level corresponding to a given probe position could be read on the 3-digit mechanical counter or could be automatically recorded.

3.3.5 Data recording system

The static pressure drops were recorded manually; however, all the rest of the measurements were suitable for automatic recording. For this purpose a Hewlett-Packard HP-5050B digital recorder was used in conjunction with an HP2901 A Input scanner and an HP2401C Integrating digital voltmeter (figure 3.11). Together with the HP automatic data acquisition system consisting of the above three units, an HP 7004B X-Y recorder was used for graphical representation of the recorded variables (figure 3.12). When the magnitude of the fluctuations relative to the mean input was too large to get a traceable curve, an RC-circuit was used at the y-input terminals of the X-Y recorder to decrease sensitivity.

3.3.6 Flowrate meter

The flow rate meter to measure the flow rate in the channel, and in turn to calculate the average velocity, was an orifice plate put between two pieces of aluminium pipe of 6.065" I.D. The orifice plate itself was designed according to ISO recommendation R541 with vena contracta taps [46,47]. Due to difficulties in following the geometrical requirements given in this recommendation a calibration of the whole unit was decided to be made (see section 3.4.1.). The front piece, 30" long, was open to the atmosphere, whereas the downstream end was connected to the entrance box, used as a settling chamber (figures 3.13 a,b).

3.4 Calibration of Instruments

3.4.1 Flowrate meter

The calibration of the orifice plate was made by connecting the downstream end of the entrance box to a settling chamber-

copper pipe assembly. The pipe itself had an I. D. of 3. 814 in. and it was 18 feet long. A detailed description of this apparatus is given in ref. [48]. A traversing mechanism located at about 30 equivalent diameters from the bell-mouthed entrance to the pipe facilitated the measurement of velocity profiles throughout the cross section of the pipe. These velocity profiles, measured by using a single pitot tube, were integrated numerically using the trapezoid rule to give the flow rate for a given pressure drop across the orifice plate. It can be shown through the use of Bernoulli's equation that flow rate is proportional to the square root of the orifice pressure drop [49]. The calibration curve Q versus $\sqrt{\Delta P_{orif}}$ drawn in this way is shown in figure 3.14. The accuracy of the calibration was estimated to be $\pm$ 1.5% in the range considered.

3.4.2 Hot wire probes

Fundamentally, velocity measurements with a constant temperature anemometer are performed by measuring the electric power, which must be supplied to the probe from the anemometer in order to keep the probe sensor at a certain temperature, higher than the temperature of the medium under measurement. The requisite amount of power, P, will then be equal to the amount of power, Q, removed by the flow. Q will, assuming everything else to be constant, be a measure of the velocity. However, this power P, which is proportional to the output voltage of the anemometer is a nonlinear function of the flow velocity U under measurement. This nonlinearity is not very important in measurements of small degrees of turbulence, in which case a small section of the calibration curve may be considered sufficiently

linear. At higher degrees of turbulence, the distortion caused by the curvature of the calibration curve becomes noticeable; also, measurements at varying degrees of mean flow velocity are rendered difficult by the consequent sensitivity variations. Mathematical treatment of results obtained in both the last mentioned cases is not a very satisfactory solution, and an electronic circuit to take care of the linearization problem is to be preferred [45].

The fundamental relationship between the flow velocity u and the amount of heat, Q, removed per unit of time can be formulated as

$$Q = P = A + B (u)^n \qquad (3.1)$$

A and B are constants, assuming constant temperature and constant density. The exponent n has an almost constant value over a wide range of Reynolds numbers. Equation 3.1 above can be put into the following form (Appendix 3):

$$\log \left(\frac{V^2}{V_o^2} - 1 \right) = n \log u + C \qquad (3.2)$$

where V_o is constant and thus a linear calibration curve can be drawn in this manner. However then the relationship between the fluctuating and the mean components of hot-wire signals and the velocity is relatively complicated (Appendix 4):

$$\frac{u'}{u} = \frac{V'}{V} \frac{1}{n} \left(\frac{V^2}{V^2 - V_o^2} \right) \qquad (3.3)$$

Through an electronic linearizer which will take care of the non-linear dependence of V on u the following simple form can be reached:

$$V = B\ u \tag{3.4}$$

where B is another constant and

$$\frac{u'}{u} = \frac{V'}{V} \tag{3.5}$$

During calibration, the hot-wire probe was placed in an air stream of known velocity and the linearized voltage output from the anemometer was recorded. DISA type 55D41/42 calibration unit was used for the purpose of supplying a known velocity to the probe [45]. A DISA type 55A67 adapter was used to match the geometry of the flow in the experimental apparatus (figure 3.15). A typical calibration curve is shown in figure 3.16. No account of drift between calibrations was taken into consideration.

3.5 Experimental procedure, data reduction and discussion of measurements

3.5.1 General

Before any experimental measurement, the electronic instruments were turned on for at least two hours to attain steady state conditions and avoid drift due to warm up. Then the necessary adjustments on the anemometer system and the pressure measuring meter were made. The apparatus was run for at least 20 minutes which was found to be sufficient to attain

steady state conditions in the flow. For a given channel width s the following measurements were made:

i) Static pressure drop versus channel length x.

ii) Static pressure drop at fully developed conditions versus Reynolds number.

iii) Velocity profiles U vs. y along x at 5 locations, using pitot tube or hot-wire probe.

iv) Velocity profiles U vs. y at fully developed conditions.

v) $\sqrt{\overline{u'^2}}$ vs. y along x at 5 locations.

vi) $\sqrt{\overline{u'^2}}$ vs. y at fully developed conditions.

vii) Double pitot tube readings ΔP_{dP} vs. y at fully developed conditions.

The Reynolds number range covered was approximately from 20,000 to 130,000.

All measurements were repeated for 2 different channel widths. Steps (iv), (vi) and (vii) were repeated for 4 different channel widths.

The hot-wire calibrations were done before and after each run. The temperature and pressure of the ambient were recorded before each run.

3.5.2 Static pressure measurements

Due to rapid random fluctuations in the pressure readouts both from the electronic meter and the inclined-arm micronamometer, an estimate of the average readout had to be made. The error introduced in this manner is estimated to be less than $\pm$ 0.5% considering the maximum and minimum values of the instantaneous

readouts. Since the accuracy of the meter checked against the manometer was better than this, no account of the latter accuracy was taken into consideration.

$\frac{dP}{dx}$ values were calculated as a function of x by fitting a straight line into the data points taken six at a time by polynomial regression and taking the slope of this line as the $\frac{dP}{dx}$ in the middle of the range of the 6 points (figures 3.17, 3.18). A FORTRAN program was written for this purpose and the subroutine REGR was used from the IBM Scientific Subroutine Package (SSP) for the straight line fit [50].

Fully developed $\frac{dP}{dx}$ values were computed using the same subroutine, however this time using the data for 5 points covering an x range of 4 ft at the extreme downstream end of the test section (figure 3.19). Fully developed friction factor values were computed in the same program using the relation obtained from a fully developed momentum balance (Appendix 5):

$$f = \frac{2\tau_w}{\rho u_{av}^2} = \frac{s}{\rho u_{av}^2} \left(\frac{dP}{dx}\right) \qquad (3.6)$$

(see section 3.5.8 for the evaluation of ρ, u_{av} and errors involved).

3.5.3 Free stream turbulence intensities

V_{rms} values of the signals from a hot-wire probe located at x = 0 were recorded for different Reynolds numbers and turbulence intensities were calculated for the uniform flow at the entrance through the relations,

$$Tu = \frac{\sqrt{u'^2}}{u} = \frac{V_{rms}}{V} \qquad (3.7)$$

Results can be seen in figure 3.20.

3.5.4 Determination of the probe position relative to the walls

The probe position relative to the walls was determined by advancing the probe towards the smooth wall until the probe just touched the wall and this point was taken as the reference point for the y-coordinate. The touching of the probe was checked visually through the transparent top wall of the channel. For hot wire probes, the touching could not be done, so a dummy probe of the same dimensions was used and the reference point noted. Then the working probe was mounted onto the probe support and the traverse carried out. The repeatability of the position of the probe was given as $\pm$ 0.2 mm for the stepper motor [45], and a resolution of 0.01 mm and 0.02 mm for the manual drive and the stepper motor respectively. Thus the uncertainty in the y_s measurement was estimated to be less than $\pm$ 1.5% of channel width for the smallest channel.

3.5.5 Mean velocity profiles

The mean velocity profiles were recorded either manually or through the data acquisition system and the X-Y recorder. Some graphs displayed on the X-Y recorder is shown in figures 3.21 a and 3.22 a for both developing and developed regions. The asymmetry of the flow should be noted. The fluctuations shown are a qualitative measure of the fluctuations of instantaneous velocity, however, are not representative of the actual magnitudes and frequency due to damping of the signal through

the various electronic apparatus.

The numerical data corresponding to these graphical displays were fed into the computer (IBM 360, Model 65) through a FORTRAN program and plotted in the form (see section 2.2).

$$u = a \log y + b \tag{3.8}$$

This was repeated for both $y = y_s$ and $y = y_r$. A straight line was fit by least squares method to the portions close to the walls and the corresponding slopes and u-axis intersections were computed (see figure 3.23).

If the velocity profiles

$$\frac{u_s}{u_{\tau_s}} = \frac{1}{k} \ln \frac{y_s u_{\tau_s}}{\nu} + C \tag{2.19}$$

and

$$\frac{u_r}{u_{\tau_r}} = \frac{1}{k} \ln \frac{y_r}{z_{or}} \tag{2.20}$$

are considered, u_{τ_s} and u_{τ_r} can be computed from the above mentioned slopes, and C and z_{or} from the intersections. For this, a value of k, von Karman's constant, should be assumed and here $k = 0.4$ was chosen. The results for one value of s is shown in Table 1. Values of friction factor was calculated using the quantities computed in this manner and plotted together with the otherwise computed friction factors in figure 3.24 a. The discrepancy is obvious and is probably due to a combination of errors in y, the estimation of u_τ from the slope of the straight line, and choice of k. The effect of a small change in y reference point is shown in Table 2.

3.5.6 Maximum mean velocity points

The maximum mean velocity points were found by making a double pitot tube traverse in y direction and recording the pressure difference between the pitot tubes (figure 3.25). This reading is a measure of the velocity gradient and the place where the curve cuts the $\Delta P_{dpitot} = 0$ line corresponds to the maximum velocity point. The uncertainty involved was estimated to be $\pm$ 1 mm and is much better than an estimate from the velocity profile itself where the uncertainty could be as much as $\pm$ 3 mm for a flatter profile.

3.5.7 Eddy diffusivity

The calculation of eddy diffusivity distribution was done by using the experimental outputs corresponding to double pitot tube traverses of the channel width. Rearranging equation 2.26 and using the linear shear stress distribution (see Appendix 6) we get

$$\frac{\epsilon_m}{\nu} = \frac{\tau_w}{\mu} \cdot \frac{\left(1 - \frac{y}{y_o}\right)}{\frac{du}{dy}} - 1 \qquad (3.9)$$

In the computation for the smooth and rough wall portions of the flow, the corresponding wall shear stress (see section 3.5.9) was used. The conversion of the double pitot tube results into $\frac{du}{dy}$ was made through the use of the relation (see Appendix 7)

$$\frac{du}{dy} \simeq \frac{1}{\rho_{air}} \cdot \frac{1}{u} \cdot \frac{\Delta P_{dpitot}}{\Delta y} \qquad (3.10)$$

Considering the fluctuations in the output from the double pitot tube, the uncertainty in ΔP_{dpitot} is estimated to be less

than $\pm$ 2.5% of maximum reading drawn on the X-Y recorder.

The result for one set of calculations is shown in figure 3.26. Eddy diffusivity becomes indeterminable at the maximum velocity point and it becomes negative (see sec. 5.1.2) near this point.

3.5.8 $\sqrt{\overline{u'^2}}$ measurements

The longitudinal fluctuating velocity components were measured with hot wire probes and recorded either manully or through the data acquisition system simultaneously with the mean velocity. The minimum V_{ms} point was estimated from graphs drawn on the X-Y recorder (Figure 3.22). The uncertainty involved in this case was estimated to be $\pm$ 1.5 mm.

3.5.9 Engineering flow parameters

A list of mean flow parameters considered, together with a summary of the expressions relating them, is given in Appendix 8. These expressions constitute a system of 17 equations, containing 32 parameters. Therefore 15 of these parameters should be supplied, experimentally or otherwise, to close the equations. These 15 parameters can be considered in four groups:

i) Geometrical parameters : A, D_{hyd}, s, ϵ, p

ii) Physical properties of working fluid: ρ, μ

iii) Experimental flow variables: $\frac{dP}{dx}$, y_{or}, y_{mr}, $\frac{du_s}{dy_s}$, $\frac{du_r}{dy_r}$, Q

iv) Independent variables: y_s, y_r

The only independent quantities among the geometric parameters are s, p and ϵ. s could be measured to an accuracy of $\pm$ 0.002 in. with a knowledge of ϵ to $\pm$ 0.001 in.

Values of dynamic viscosity μ was taken from Reference [51] corresponding to the ambient temperature.

The density of the air was calculated from the ideal gas equation of state $P = \rho RT$, again corresponding to the ambient conditions. Accuracy of P and T measurements were $\pm$ 0.1 mm Hg and $\pm$ 0.5°C respectively.

The accuracy of the Q measurement was estimated to be $\pm$ 1.5 % in section 3.4.1. In view of the higher accuracies in measurements of geometrical parameters, it can be concluded that the uncertainty involved in the u_{av} and Re largely depends on the flow rate measurement.

A closer examination of the 15 inputs mentioned above and a consideration of dimensional analysis techniques will reveal that the effects of all of those parameters can be incorporated in the effects of the following four main dimensionless groups:

$$\frac{s}{\epsilon}, \quad \frac{p}{\epsilon}, \quad Re, \quad f$$

The first two are geometric parameters. Re and f are used to relate the geometric properties, fluid properties and flow variables.

The major engineering interest from the type of experiments undertaken in the present study is to find the correlations between the above dimensionless variables. The rest of the parameters

considered are mainly for further understanding of the physical flow. The results of the experimental investigations in terms of the relevant dimensionless groups are presented in figure 3.24 a. Results regarding the other variables of interest are given in figures 3.27 - 3.29 and Table 3.

An attempt to theoretically predict the relationship between the above mentioned dimensionless groups is made in the next section.

4. THEORETICAL STUDIES - PREDICTION OF FULLY DEVELOPED ASYMMETRIC FLOWS

4.1 Relations between flow parameters

Using the definitions for the Reynolds number Re and average velocity U_{av} (see nomenclature), and the chosen velocity fields (equations 2.20, 2.21), the expression for Re can be derived in terms of the mean flow parameters (Appendix 9).

$$Re = \frac{2\,(1 + k\,y^{+}_{ms})}{k^2}\left[\ln\,(1 + y^{+}_{ms}) - 1\right] + 15.6\left[y^{+}_{ms} - 11\,(1 - \exp\left(\frac{y^{+}_{ms}}{11}\right)) + \frac{9}{11}\left(1 + \frac{y^{+}_{ms}}{3}\right)\exp\left(-\frac{y^{+}_{ms}}{3}\right) - \frac{9}{11}\right] + 2\,\frac{y^{++}_{mr}}{k}\left[\ln y^{+}_{ms} + Ck - \frac{u_{\tau_r}}{u_{\tau_s}}\right] + 2\,\frac{z^{++}_{or}}{k}\,\frac{u_{\tau_r}}{u_{\tau_s}} \qquad (4.1)$$

The main aim of the analysis is to predict the friction factor f as a function of Re for the particular flow geometry in consideration. The expression for f can also be derived through its definition in terms of the parameters encountered in equation 4.1 (Appendix 10)

A relation for the ratio $\frac{u_{\tau_r}}{u_{\tau_s}}$ can be reached using equations 2.15 and 2.16 (Appendix 10). The unknown parameter z^{++}_{or} can be eliminated by matching the rough and smooth wall profiles at the

maximum velocity point (see Appendix 11). In the above derivations the velocity profiles were assumed to be valid from the wall until the maximum velocity point.

An examination of the expressions for f and Re reveals that an input of the maximum velocity and zero shear stress points is necessary. The zero shear point approximately corresponds to the point where the fluctuations of the axial velocity component is a minimum [20, 52]. Thus these points were experimentally measured and input into the equations. All the other parameters of interest such as $\tau_{\omega r}$, $\tau_{\omega s}$ and m are byproducts of the computations.

4.2 Method of Calculation

4.2.1 Calculations with m as a constant

As a first step in the theoretical analysis an attempt was made to predict the friction factors without any new empirical inputs into the equations. The widely used assumption of the coincidence of the stationary values of the mean and fluctuating velocity fields was introducted into the equations by putting

$$y_o = y_m$$

Together with this assumption a constant value of $m = \frac{1}{30}$ was used to close the equations. This value for m is based on Nikuradse's experiments on rough pipes in the completely rough flow regime [5].

The relevant equations incorporating the above considerations are given in Appendix 12. The system of equations 4.1, A.10.1,

A.10.2, A.12.1 and A.12.2 can be solved for f and y_m by independently specifying Re. However, from a computational point of view it was found more economical to specify u_{τ_s} and compute y_m and Re, instead of specifying Re and computing y_m and u_{τ_s}. The computation was carried out numerically on the computer. A simplified flowchart of the program is given in Appendix 13. The results of the calculations are presented in figure 3.24 b.

In view of the results obtained with $m = \frac{1}{30}$, all the computations were repeated with another value of $m = \frac{1}{10}$. These results are presented together with the above results.

4.2.2 Calculations with m left as a variable

The results of calculations described in section 4.21 do not agree well with the results of experiments conducted in the test facilities constructed for the present study. Thus it was decided to disregard the assumptions used in the previous section and use the equations derived in section 4.1 in their full form. m was left as a variable function of Reynolds number and $\frac{s}{\epsilon}$ to be computed through the above mentioned equations. The data for y_o and y_m were supplied empirically. The computation was carried out in a similar manner to the one described in the previous section, however this time using equation A.11.3 instead of A.12.1 and A.12.2. A flowchart of the computer program used is given in Appendix 15. The results of calculations are presented in figure 3.24 a.

5. DISCUSSION OF RESULTS AND CONCLUSIONS

5.1 Zero shear stress and maximum mean velocity points

The most important parameters in the analysis are the locations of zero shear stress and maximum mean velocity points, since they are the only experimental inputs used in the prediction of mean flow parameters. The variation of the position of these points, as shown in figures 3.27-32, indicates strong dependence on Re, $\frac{s}{\epsilon}$, and $\frac{p}{\epsilon}$. The first observation is that they do not coincide. They get proportionately closer to the smooth wall with increase of Reynolds number and decrease of $\frac{s}{\epsilon}$. This latter results simply reflects the greater effect of a physical roughness element as it occupies a larger portion of the space between the walls. The variation with Reynolds number indicates stronger diffusion of turbulent eddies from the rough towards the smooth side as the velocity is increased and as the momentum exchange near the rough wall becomes more vigorous.

The effect of $\frac{p}{\epsilon}$ could not be found directly using the results of present experiments only but indirectly by comparing with Hanjalic's [20] results (figures 3.29 - 30). The Reynolds number used in these figures is based on the maximum velocity in the channel rather than the average velocity. Hanjalic's results were not available in terms of u_{av}. Hence, the present data were translated into Hanjalic's terms using the actual measured u_m in a channel corresponding to a particular u_{av}. The positions of the zero shear and maximum velocity points deviate more from the centerline of the channel towards the smooth wall for a larger $\frac{p}{\epsilon}$, i.e. for a lower roughness density at the same $\frac{s}{\epsilon}$ ratio. At first, this

may seem unexpected since a higher roughness density would seem to imply a more vigorous momentum exchange than a lower roughness density, and hence a smaller $\frac{y_{os}}{s}$ ratio. However, a closer examination of vortex patterns between roughness elements of different pitches [53, 54] reveals the possibility that at a higher roughness density the flow will tend to skip over the tips of the elements, but at a lower density the flow will find some time to re-attach and when it faces a new element it will be thrown into the stream, shedding vigorous eddies. Thus the points under consideration are even further displaced from the rough wall. The non-coincidence of the two points and the larger displacement of the zero-shear point than the maximum velocity point simply indicate the stronger effect of dissimilar boundary conditions on the turbulent flow field rather than the mean motion. To be able to say anything more about the functional relationship between roughness density and positions of zero shear and maximum velocity in a channel, further studies of separation, re-attachment and vortex structures on roughened walls should be done.

5.2 Mean velocity fields

The logarithmic velocity profiles chosen for the present study represent well the actual velocity fields encountered, except very near the rough wall, in a region of about 1.5 ϵ from the roughness root (figure 3.23). This deviation may be attributed to the vortex structures mentioned in the previous section, which possibly prevail between the roughness elements. It is an indication of the failure of the mixing length hypothesis and the assumptions used in the derivation of the logarithmic law (section 2.2) very near a rough wall.

The experimental velocity profile seems flatter near the maximum velocity point than those that the logarithmic profiles indicate. This is the region where the velocity field is influenced by the two walls and where the flow is retarded by the effect of the opposite wall. This flattening might introduce some error in the calculation of z_{or} and m since they are computed by matching the two wall profiles at the maximum velocity point. However, this error is probably much less than the errors involved in the calculations through the profile method (see the scatter of results presented in Table 1).

Between the sublayers very near the walls and the above mentioned region, the velocity profiles accord well with the law-of-the-wall profiles. Thus as far as the mean flow properties are concerned, the fluid particles within these regions are unaware of the nature of the opposite surface.

In section 2.2 a large variation of the parameter m was cited referring to the relevant literature. Variation of m with Reynolds number is not mentioned in any of these references, although in some, variation with roughness density $\frac{p}{\epsilon}$ is reported. The observed Re dependence of m(Table 3) during the present experimental programme(Table 3) led to a further survey of more recent literature and a similar reported behaviour was found in the work of Wang and Tullis [55]. A variation of m from $\frac{1}{29}$ to $\frac{1}{33.6}$ in a Reynolds number range of 7.2×10^5 to 2.53×10^6 was calculated through the data reported in [55] to match the present nomenclature. This is the same type of variation found in the present study, namely a decrease of m with increase of Re, and a similar order of magnitude for m. The interpretation of $z_{or} = m \cdot \epsilon$ as the point where the velocity

is assumed to be zero leads to the conclusions that, first, the virtual origin of velocity is under the roughness top, near the root, and second, as the velocity in the channel is increased, this origin is further suppressed towards the roughness roots, at least in the range of Reynolds numbers considered. Importance of z_{or} is further discussed in the next section.

5.3 Friction factors

Experimentally measured friction factors from the present study are in the same order of magnitude as the ones taken from the classical Moody diagram corresponding to the same relative roughness in a circular pipe (see figure 3.24 a). The differences, which might be significant in certain critical applications, are in the shape of the function f versus Re. Moody diagram predicts a constant friction factor in the Reynolds number range considered, since the flow in a pipe is completely rough in this range [5,56]. Present study indicates a seemingly transition range type of flow, between completely smooth and completely rough regimes. This is due to the asymmetry in the roughness distribution on the channel walls. The combination of completely rough flow on one side and smooth flow on the other produces the type of observed behaviour, namely the variation of total friction factor with both Re and $\frac{s}{\varepsilon}$, $\left(\text{or } \frac{\varepsilon}{D}\right)$.

There is another problem in using the Moody diagram when types of unfamiliar roughness structures are encountered. From a strictly design point of view, if the test channel had rough walls on both sides, one would still tend to use the same relative roughness value used above in order to calculate the friction factor from the Moody

chart. This in turn would predict exactly the same friction factor for both rough-rough and rough-smooth channels. And obviously, this cannot be the case. The problem arises due to the use of the concept of equivalent sand roughness in the classical diagram. An equivalent sand roughness should be defined for each particular roughness structure on a wall to be able to use the Moody chart. This sand roughness should also be a function of Reynolds number in case of asymmetric roughness distribution. The use of the parameter z_{or}, which is connected to the equivalent sand roughness through the logarithmic rough wall profile, is introduced in the present study to provide a step in the theoretical analysis of the behaviour of flow near a rough wall. It is conceptually easier to visualize z_{or} (as a point where the gross velocity profile reaches zero near the roughness root) than an equivalent sand roughness which has no sound physical basis. An equivalent sand roughness is simply defined as that value which gives the actual coefficient of resistance when inserted into the equation [5].

$$f = \left(2 \log \frac{R}{k_s} + 1.74\right)^{-2} / 4$$

Thus $z_{or} = m \varepsilon$ is more amenable to theoretical analysis than k_s. It might be possible to predict m through the type of studies mentioned at the end of section 5.1 and then proceed for the evaluation of the positions of zero shear and maximum velocity in a channel.

In the present study, since no theoretical prediction of the above mentioned parameters were available for the particular geometry used, empirical inputs of m, and then y_o and y_m were employed. Friction factors calculated with m as a constant did not agree at all with the experimentally measured values (figure 3.24 b). Those

calculated with experimental y_o and y_m, on the other hand, gave excellent results in predicting the friction factors (figure 3.24 a), again proving the strong dependence of m on Re and $\frac{s}{\epsilon}$.

5.4 Concluding remarks and future research

The research objectives stated earlier were on the whole achieved both experimentally and theoretically. A summary of the findings may be given as follows:

1. Friction factors for a fully developed asymmetric turbulent flow were predicted through integral analysis techniques.
2. For the above prediction empirical inputs of y_o and y_m are necessary.
3. The parameter m is a function of Re and $\frac{s}{\epsilon}$.

The following are suggestions for future research:

1. A more rigorous method of analysis is necessary for a better prediction of mean flow parameters; an improvement may be achieved through the exact method.
2. Further investigations on effect of $\frac{p}{\epsilon}$ are necessary for a better understanding of flow structures.
3. The prediction of flow parameters is then to be extended to Heat and Mass Transfer mechanisms.

REFERENCES

[1] Spalding, D. B., Patankar, S. V., "Heat and Mass Transfer in Boundary Layers", Morgan-Grampian, London (1967).

[2] Reynolds, O., "On the dynamic theory of incompressible viscous fluids and the determination of criterion", Phil. Trans. Roy. Soc., T186-A123 (1895).

[3] Prandtl, L., "Über Flüssigkeitsbewegung bei sehr kleiner Reibung", Proc. of the Third Intern. Math. Congr. Heidelberg (1904); also "Collected Works", v. 3, pp. 575-584 (1961).

[4] von Karmàn, T., "Über laminare und turbulente Reibung", ZAMM 1, pp. 233-255 (1912); also "Collected Works", v. 2, pp. 70-97, London (1956).

[5] Schlichting, H., "Boundary-Layer Theory", McGraw-Hill, 6th edition (1968).

[6] Prandtl, L., "Über die ausgebildete Turbulenz", ZAMM 5, pp. 136-139 (1925); also "Collected Works", v. 2, pp. 736-751 (1961).

[7] Reichardt, H., "Vollstandige Darstellung der turbulenten Geschwindigkeitsverteilung in glatten Leitungen", ZAMM 31, pp. 208-219 (1951).

[8] von Karman, T., "The analogy between fluid friction and heat transfer", Trans. ASME 61, p. 705 (1939).

[9] Deissler, R. G., "Analytical and experimental investigation of adiabatic turbulent flow in smooth tubes", NACA TN 2138 (1950).

[10] Kay, J.M. "Fluid Mechanics and Heat Transfer", Camb. Univ. Press, London (1957).

[11] van Driest, E.R., "On turbulent flow near a wall", Jour. of Aero. Sci., v. 23, p. 1007 (1956).

[12] Rannie, W.D., "Heat transfer in turbulent shear flow", Jour. of Aero. Sci., v. 23, p. 485 (1956).

[13] Spalding, D.V., "Single formula for the law of the wall", Jour. of Appl. Mech., ASME, v. 28, pp. 455-458 (1961).

[14] Wasan, D.T., Tien, C.L., Wilkie, C.R., "Theoretical correlation of velocity and eddy viscosity for flow close to a pipe wall", Jour. of A.I.Ch.E. v. 9, p. 567 (1963).

[15] Nikuradse, J., "Strömungsgesetze in rauhen Rohren", Forsh. Arb. Ing. - Wes., No. 361 (1933).

[16] Young, A.D., "The drag effects of roughness at high subcritical speeds", Jour. of Roy. Aero. Soc., v. 18, p. 534 (1950).

[17] Paeshke, W., "Experimentelle Untersuchungen zum Raughigekeits - und Stabilitätsproblem in der bodennahen Luftschicht", Z. Geophysik, v. 13, p. 14 (1937).

[18] Geffroy, J., Jude, P., Paumard, G., "Contribution à l'étude de la convection forcée par surfaces corruguées", Fourth Int. Heat Transfer Conf., FC 5.1, Paris (1970).

[19] Simpson, R.L., "A generalized correlation of roughness density effects on the turbulent boundary layer", AIAA Jour., v. 2, pp. 242-244 (1973).

[20] Hanjalic, K., "Two-dimensional asymmetric turbulent flow in ducts", Ph.D. Thesis, Univ. of London (1970).

[21] Clauser, F.H., "Turbulent boundary layers in adverse pressure gradients", Jour. of Aero. Sci., v. 21, pp. 91-108 (1954).

[22] Hama, F.R., "Boundary layer characteristics for smooth and rough surfaces", Trans. of Soc. of Naval Arch. and Marine Eng., v. 62, pp. 333-358 (1954).

[23] Perry, A.F., Joubert, P.N., "Rough wall boundary layer in adverse pressure gradients", J. of Fluid Mech., v. 17, pp. 193-211 (1963).

[24] Wu, J., "Flow in turbulent wall layer over uniform roughness", J. of Appl. Mech. v. 40, pp. 863-867 (1973).

[25] Bussinesq, J., "Théorie de l'écoulement tourbillant", Mém. prés. Acad. Sci. XXIII, 46, Paris (1877); quoted from [5], chapter 19.

[26] Deissler, R.G., "Turbulent heat transfer and friction in the entrance regions of smooth passages", Trans. ASME, pp. 1221-1233 (1955).

[27] Park, S.D., Lee, Y., "Diabatic turbulent flow in the entrance region of concentric annuli," EIC, v. 14, n. B-3 (1971).

[28] Sparrow, E.M., Eckert, E.R.G., Minkowycz, W.J., "Heat transfer and skin friction for turbulent boundary layer flow longitudinal to a circular cylinder", J. of Appl. Mech., pp. 37-43 (1963).

[29] Levy, S., "Turbulent flow in annulus", J. Heat Transfer, v. 89, pp. 25-31 (1967).

[30] Lee, Y., Barrow, H., "Turbulent flow and heat transfer in concentric annuli", Proceedings, I. Mech. Eng., v. 178, pp. 1-16, (1963-64).

[31] Eskinazi, S., Yeh, H., "An investigation on fully developed flows in curved channels", Jour. of Aero Sci., v. 23, pp. 23-24 (1956).

[32] Kjellstrom, B., Hedberg, S., "On shear stress distributions for flow in smooth and partially rough annuli", Aktiebolaget Atomenergi AE-243, Sweden (1966).

[33] Townsend, A.A., "Equilibrium layers and wall turbulence", J. Fluid Mech., v. 11, pp. 97-120 (1961).

[34] Streeter, V.L., "Frictional resistance in artificially roughened pipes", Proc. Amer. Soc. Civil Eng., v. 61, p. 163 (1935).

[35] Sheriff, N., Gumley, P., "Heat transfer and friction properties of surfaces with discrete roughness", Int. J. Heat Mass Transfer, v. 9, pp. 1297-1320 (1966).

[36] Kidd, G.J. Jr., "Heat transfer and pressure drop characteristics of gas flow inside spirally corrugated tubes", ASME - paper 69-WA/HT-3 (1969).

[37] Webb, R.L., Eckert, E.R.G., Goldstein, R.J., "Heat Transfer and friction in tubes with repeated - rib roughness", Int. J. Heat Mass Transfer, v. 14, pp. 601-617 (1971).

[38] Wilkie, D., Cowin, M., Burnett, P., Burgoyne, T., "Friction factor measurements in a rectangular channel with walls of identical and non-identical roughness", Int. J. Heat Mass Transfer, v. 10, pp. 611-621 (1967).

[39] Furber, B.N., Cox, D.N., "Heat Transfer and pressure drop measurements in channels with Whitworth thread form roughness", J. Mech. Eng. Sci., v. 9, pp. 339-350 (1967).

[40] Hall, W.B., "Heat transfer in channels having rough and smooth surface", J. Mech. Eng. Sci., v. 4, p. 287 (1962).

[41] Hanjalic, K., Launder, B.E., "Fully developed asymmetric flow in a plane channel", J. Fluid Mech., v. 51, pp. 301-335 (1972).

[42] Cheers, F., "Note on wind tunnel contractions", ARC R and M 2137 (1945).

[43] Instruction Manual, MKS Baratron Type 77, MKS Instruments Inc., Burlington, Massachusetts (1967).

[44] Durst, F., Launder, B.E., Akesson, H., "The determination of the position of maximum velocity in turbulent shear flow", Aero. J. Roy. Aero. Soc., v. 75, pp. 196-199 (1971).

[45] DISA Hot-wire anemometer system instruction and service manuals, DISA Elektronik A/S, Denmark (1968, 1973).

[46] ISO Recommendation R540, "Measurement of fluid flow by means of orifice plates and nozzles", 1st edition (1967).

[47] Spiller, R.L., "The art and practice of orifice flow metering", Instrumentation Technology, v. 18, pp. 52-56 (1971).

[48] Park, S.D., "Developing turbulent flow and heat transfer in concentric annuli, an analytical and experimental study", Ph. D. Thesis, Univ. of Ottawa (1971).

[49] Massey, B.S., "Mechanics of Fluids", van Nostrand Reinhold Co., London (1971).

[50] IBM SSP/360 manual.

[51] Eckert, E.R.G., Drake, R.M. Jr., "Heat and Mass Transfer", McGraw-Hill, Appendix of property values (1959).

[52] Brighton, J.A., Jones, J.B., "Fully developed turbulent flow in annuli", J. Basic Eng., ser. D., v. 86, pp. 835-844 (1964).

[53] Rampf, H., Feurstein, G., "Wärmeübergang und Druckverlust an dreiecksformigen Raughigkeiten in turbulenter Ringspaltströmung", Fourth Int. Heat Transfer Conf., FC5.3 Paris (1970).

[54] Williams, F., Watts, J., "The development of rough surfaces with improved heat transfer performance and a study of the mechanisms involved", Fourth Int. Heat Transfer Conf., FC5.5, Paris (1970).

[55] Wang, J., Tullis, J.P., "Turbulent flow in the entry region of a rough pipe", ASME paper 73-WA/FE-3 (1973).

[56] Tennekes, H., Lumley, J.L., "A First Course in Turbulence", The MIT Press, Cambridge, Massachusetts, and London, England (1972).

APPENDIX 1

Derivation of Integral Equations

A.1.1 Middle portion

Continuity equation (from figure 2.1):

$$(s - \delta_r - \delta_s) \frac{d u_\infty}{dx} = v_{\delta_r} + v_{\delta_s} \qquad (A.1.1)$$

Momentum equation:

$$(s - \delta_r - \delta_s)\, dP + d(\rho u_\infty^2)(s - \delta_r - \delta_s)$$

$$= \rho (u_\infty v_{\delta_r} dx + u_\infty v_{\delta_s} dx)$$

$$(s - \delta_r - \delta_s) \frac{d}{dx} (p + \rho u_\infty^2) = \rho u_\infty (v_{\delta_r} + v_{\delta_s})$$

using continuity eqn. A.1.1

$$(s - \delta_r - \delta_s) \left[\frac{dP}{dx} + 2 \rho u_\infty \frac{d u_\infty}{dx} \right]$$

$$= (s - \delta_r - \delta_s)\, \rho\, u_\infty \frac{d u_\infty}{dx}$$

$$dP = - \rho u_\infty d u_\infty \qquad (A.1.2)$$

A.1.2 Rough side

Continuity equation

$$\frac{d}{dx} \int_{z_{or}}^{\delta_r} \rho u_r \, dy_r = - \rho v_{\delta_r} \qquad (A.1.3)$$

Momentum equation:

$$\tau_{\omega} dx + (\delta_r - z_{or}) dP = - d \int_{z_{or}}^{\delta_r} \rho u_r^2 dy_r - u_{\delta_r} \rho v_{\delta_r} dx$$

Using continuity equation A.1.3 and

$$u_{\delta_r} = u_{\infty}$$

and also assuming $z_{or} \ll \delta_r$

$$\tau_{\omega r} = - \delta_r \frac{dP}{dx} - \frac{d}{dx} \int_{z_{or}}^{\delta_r} \rho u_r^2 dy_r + \rho u_{\infty} \frac{d}{dx} \int_{z_{or}}^{\delta_r} u_r dy_r \qquad (A.1.4)$$

A.1.3 Smooth side:

Continuity equation:

$$\frac{d}{dx} \int_{o}^{\delta_s} \rho u_s dy_s = - \rho v_{\delta_s} \qquad (A.1.5)$$

Momentum equation:

$$\tau_{\omega s} dx + \delta_s dP = - d \int_{o}^{\delta_s} \rho u_s^2 dy_s - u_{\delta_s} \rho v_{\delta_s} dx$$

Using continuity equation A1.5 and

$$u_{\delta_s} = u_{\infty}$$

$$\tau_{w\,s} = -\delta_s \frac{dP}{dx} - \frac{d}{dx}\int_0^{\delta_s} \rho u_s^2 \, dy_s + \rho u_\infty \frac{d}{dx}\int_0^{\delta_s} u_s \, dy_s \qquad \text{(A.1.6)}$$

A.1.4 Adding equations A.1.1, A.1.3 and A.1.5, the continuity equation for the whole channel becomes

$$\frac{d}{dx}\int_0^{s} u \, dy = 0$$

with the understanding that u is in three portions with corresponding upper and lower limits of validity in the channel.

APPENDIX 2

Derivation of fully developed region momentum equations from equation 2.9

$$\mu \frac{\partial^2 u}{\partial y^2} - \rho \frac{\partial \overline{u' v'}}{\partial y} - \frac{dP}{dx} = 0$$

$$\frac{\partial}{\partial y} \left(\mu \frac{\partial u}{\partial y} - \rho \overline{u' v'} \right) = \frac{dP}{dx}$$

integrating once

$$\mu \frac{\partial u}{\partial y} - \rho \overline{u' v'} = y \frac{dP}{dx} + C$$

Using the boundary condition,

$$\text{at } y = 0; \ \overline{u' v'} = 0, \ \mu \frac{\partial u}{\partial y} = \tau_w$$

$$\mu \frac{\partial u}{\partial y} - \rho \overline{u' v'} = y \frac{dP}{dx} + \tau_w \qquad \text{(A.2.1)}$$

and using the other boundary condition,

$$\text{at } y = y_o ; \ \tau = \mu \frac{\partial u}{\partial x} - \rho \overline{u' v'} = 0$$

$$0 = y_o \frac{dP}{dx} + \tau_w$$

$$\text{or} \qquad \tau_w = - y_o \frac{dP}{dx} \qquad \text{(A.2.2)}$$

APPENDIX 3

Relation between air velocity and hot-wire anemometer output signals

King's law for the removal of heat from a heated wire can be written as [45]:

$$Q = P = (A + B\,u^n)\,\Delta T \qquad (A.3.1)$$

where Q = rate of heat transferred from the hot wire

P = electrical power input

ΔT = temperature difference between the hot-wire and the surrounding medium

u = air velocity

n, A, B = constants

Now, electrical power input $P = \dfrac{V^2}{R}$

where V = voltage input to the wire

R = resistance of the wire

Therefore equation A.3.1 becomes

$$V^2 = R(A + B\,u^n)\,\Delta T$$

At $u = 0$, $V = V_o$ (to keep the wire at a constant temperature)

$$V^2 = V_o^2 + BR\,\Delta T\,u^n \qquad (A.3.2)$$

dividing by V_o^2

$$\frac{V^2}{V_o^2} = 1 + \frac{BR\,\Delta T}{V_o^2}\, u^n$$

$$\frac{V^2}{V_o^2} - 1 = C\,u^n \quad \text{where } C = \frac{BR\,\Delta T}{V_o^2}$$

$$\log\left(\frac{V^2}{V_o^2} - 1\right) = n \log u + C \qquad (A.3.3)$$

APPENDIX 4

Relation between the fluctuating and the mean components of hot-wire signals and velocities

1. In the case of non-linearized signals (see equation A.3.2) we have

$$V^2 = V_o^2 + C_1 u^n \qquad \text{(A.4.1)}$$

differentiating

$$2 V dV = C_1 n u^{n-1} du$$

dividing by $2 V^2$ and multiplying the R.H.S. with $\frac{u}{u}$

$$\frac{dV}{V} = \frac{C_1 n u^n}{2 V^2} \frac{du}{u}$$

rearranging

$$\frac{du}{u} = \frac{2 V^2}{n C_1 u^n} \frac{dV}{V}$$

$$\frac{du}{u} = \frac{dV}{V} \cdot \frac{2}{n} \left(\frac{V^2}{V^2 - V_o^2} \right) \qquad \text{(A.4.2)}$$

du and dV yet remain to be related to u' and V'.

Going back to equation A.4.1 and introducing

$$V = \bar{V} + V' \text{ and } u = \bar{u} + u'$$

where the bar over the symbols denotes time averaged values and ' denotes the fluctuating components,

$$(\bar{V} + V')^2 = V_o^2 + C_1 (\bar{u} + u')^n$$

expanding the terms

$$\bar{V}^2 + 2\bar{V}V' + V'^2 = V_o^2 + C_1 \left(\bar{u}^n + n\bar{u}^{n-1}u' + \frac{n(n-1)}{2!}\bar{u}^{n-2}u'^2 + \ldots \right) \quad (A.4.3)$$

retaining only the first two terms of the expansions

$$\bar{V}^2 + 2\bar{V}V' \simeq V_o^2 + C_1\bar{u}^n + C_1 n\bar{u}^{n-1}u'$$

since $\bar{V}^2 = V_o^2 + C_1\bar{u}^n$

$$2\bar{V}V' \simeq C_1 n\bar{u}^{n-1}u'$$

$$V' \simeq \frac{n}{2}\frac{C_1\bar{u}^{n-1}}{\bar{V}}\bar{u}'$$

multiplying the R.H.S. by $\frac{\bar{u}}{\bar{u}}$ and recognizing that $C_1\bar{u}^n = \bar{V}^2 - V_o^2$

$$V' \simeq \frac{n}{2}\frac{\bar{V}^2 - V_o^2}{\bar{V}}\frac{u'}{\bar{u}}$$

dividing by $\bar{V}$ and rearranging

$$\frac{u'}{u} \simeq \frac{V'}{\bar{V}}\frac{n}{2}\left(\frac{\bar{V}^2}{\bar{V}^2 - V_o^2}\right) \quad (A.4.4)$$

Comparisons of equations A.4.2 and A.4.4 will reveal that replacing du and dV by u' and V', and u and V by $\bar{u}$ and $\bar{V}$, respectively, is equivalent to omitting the higher order terms in equation A.4.3, which was done in the above derivation.

2. In the case of linearized signals voltage-velocity relationship is of the form:

$$V = B\,u$$

$$dV = B\,du$$

$$\frac{du}{u} = \frac{dV}{V}$$

or,

$$V = B\,u$$

$$\bar{V} + V' = B\,(\bar{u} + u')$$

$$\bar{V} = B\,\bar{u}\ ,\quad V' = B\,u'$$

therefore

$$\frac{u'}{\bar{u}} = \frac{V'}{\bar{V}}$$

APPENDIX 5

Calculation of experimental friction factors

Rough side:

$$f_r = \frac{2\,\tau_{wr}}{\rho\,u_{av}^2} \quad \text{(Definition)} \qquad \text{(A. 5. 1)}$$

and using equation 2.15

$$f_r = \frac{2\,y_{or}}{\rho\,u_{av}^2}\left(-\frac{dP}{dx}\right) \qquad \text{(A. 5. 2)}$$

Smooth side:

$$f_s = \frac{\tau_{ws}}{\rho\,u_{av}^2} \quad \text{(Definition)} \qquad \text{(A. 5. 3)}$$

and using equation 2.16

$$f_s = \frac{2\,y_{os}}{\rho\,u_{av}^2}\left(-\frac{dP}{dx}\right) \qquad \text{(A. 5. 4)}$$

Friction factor for the whole channel:

Making a fully developed momentum balance on a fluid element of thickness dx and height s, one obtains

$$\tau_{wr} + \tau_{ws} = s\left(-\frac{dP}{dx}\right)$$

Now, total f can be defined by

$$f = \frac{\tau_{wr} + \tau_{ws}}{\rho\,u_{av}^2} \quad \text{(Definition)} \qquad \text{(A. 5. 5)}$$

and using the above equation

$$f = \frac{s}{\rho u_{av}^2} \left(- \frac{dP}{dx} \right) \qquad (A.5.6)$$

From equations A.5.1 and A.5.3

$$f = \frac{f_r + f_s}{2}$$

APPENDIX 6

Fully developed shear stress distribution

Substituting equation 2.24 into equation A.2.1

$$\tau = y \frac{dP}{dx} + \tau_w \qquad (A.6.1)$$

dividing by τ_w

$$\frac{\tau}{\tau_w} = \frac{y}{\tau_w} \frac{dP}{dx} + 1$$

substituting the result from equation A.2.2 into the right hand side and simplifying

$$\frac{\tau}{\tau_w} = 1 - \frac{y}{y_o}$$

The relations A.6.1 and A.2.2 can be directly written down by a force balance on an infinitesimal fluid element of thickness dx and height y and y_o, respectively.

APPENDIX 7

Relation between $\frac{du}{dy}$ and double pitot tube measurements

$dy \simeq \Delta y = 2$ mm (distance between 2 pitot tubes, see sec. 3.3.2)

Writing the Bernouilli equation

$$\frac{P_1 - P_{st}}{\gamma_{air}} = \frac{u_1^2}{2g} \quad \text{for pitot tube number (1)}$$

and

$$\frac{P_2 - P_{st}}{\gamma_{air}} = \frac{u_2^2}{2g} \quad \text{for pitot tube number (2)}$$

substracting the above relations from each other

$$\frac{P_1 - P_2}{\gamma_{air}} = \frac{u_1^2 - u_2^2}{2g}$$

$$\frac{P_1 - P_2}{\gamma_{air}} = \frac{(u_1 - u_2)(u_1 + u_2)}{2g}$$

Assuming the velocity profile between the tips of the pitot tubes is linear, and the velocity at the center is u and $u_1 - u_2 = \Delta u$, we get

$$\frac{P_1 - P_2}{\gamma_{air}} = \frac{\Delta u \, (2 \cdot u)}{2g}$$

Putting $P_1 - P_2 = \Delta P_{dpitot}$, dividing by Δy and rearranging

$$\frac{\Delta u}{\Delta y} = \frac{1}{\rho_{air}} \cdot \frac{1}{u} \cdot \frac{\Delta P_{dpitot}}{\Delta y}$$

$$\frac{du}{dy} \simeq \frac{1}{\rho_{air}} \cdot \frac{1}{u} \cdot \frac{\Delta P_{dpitot}}{\Delta y}$$

APPENDIX 8

Summary of relations between mean flow parameters

$$u_{\tau r} = \frac{\tau_{w r}}{\rho} \qquad \text{(Definition)}$$

$$u_{\tau s} = \frac{\tau_{w s}}{\rho} \qquad \text{(Definition)}$$

$$f_s = \frac{2\,\tau_{w s}}{\rho\, u_{av}^2} \qquad \text{(Definition)}$$

$$f_r = \frac{2\,\tau_{w r}}{\rho\, u_{av}^2} \qquad \text{(Definition)}$$

$$f = \frac{f_s + f_r}{2} \qquad \text{(Appendix 5)}$$

$$\tau_{w r} = - y_{or} \frac{dP}{dx} \qquad \text{(Appendix 2)}$$

$$\tau_{w s} = - y_{os} \frac{dP}{dx} \qquad \text{(Appendix 2)}$$

$$\tau_{w r} + \tau_{w s} = - s \frac{dP}{dx} \qquad \text{(Appendix 5)}$$

$$\frac{\tau_r}{\tau_{w r}} = \left(1 - \frac{y_r}{y_{or}}\right) \qquad \text{(Appendix 6)}$$

$$\frac{\tau_s}{\tau_{w s}} = \left(1 - \frac{y_s}{y_{os}}\right) \qquad \text{(Appendix 6)}$$

$$Re = \frac{u_{av} D_{hyd}}{\nu} \qquad \text{(Definition)}$$

$$z_{or} = y_{mr} \exp\left[-\frac{u_{\tau s}}{u_{\tau r}} \left\{ \ln\left(\frac{u_{\tau s} s}{\nu} - \frac{u_{\tau s} y_{mr}}{\nu} \right) + Ck \right\} \right] \qquad \text{(Appendix 11)}$$

$$u_{av} = \frac{Q}{A} \qquad \text{(Definition)}$$

$$s = y_{or} + y_{os} \qquad \text{(Definition)}$$

$$m = \frac{z_{or}}{\varepsilon} \qquad \text{(Definition)}$$

$$\frac{\varepsilon_{Ms}}{\gamma} = \frac{\tau_{ws}}{\mu} \frac{\left(1 - \frac{y_s}{y_{os}} \right)}{\frac{d u_s}{d y_s}} - 1 \qquad \text{(equation 3.9)}$$

$$\frac{\varepsilon_{Mr}}{\gamma} = \frac{\tau_{wr}}{\mu} \frac{\left(1 - \frac{y_r}{y_{or}} \right)}{\frac{d u_r}{d y_r}} - 1 \qquad \text{(equation 3.9)}$$

APPENDIX 9

Reynolds number Re in terms of mean flow parameters

$$u_{av} = \frac{\int u \, dA}{A} = \frac{\int_o^{y_{ms}} u_s \, dA + \int_{z_{or}}^{y_{mr}} u_r \, dA}{A} \qquad (A.9.1)$$

$$u_s = u_{\tau s} \left\{ \frac{1}{k} \ln \left(1 + k \frac{y u_{\tau s}}{\nu}\right) + 7.8 \left[1 - \exp\left(- \frac{y u_{\tau s}}{11 \nu} \right) - \frac{y u_{\tau s}}{11 \nu} \exp\left(- \frac{y u_{\tau s}}{3 \nu} \right) \right] \right\}$$

$$u_r = u_{\tau r} \left(\frac{1}{k} \ln \frac{y}{z_{or}} \right)$$

$$dA = l \, dy$$

$$A = l \, s$$

Substitution of the above quantities into equation A.9.1 and integration gives:

$$u_{ay} = \frac{\nu}{s} \left\{ \frac{1 + k y^+_{ms}}{k^2} \left[\ln (1 + k y^+_{ms}) - 1 \right] + 7.8 \left[y^+_{ms} - 11 \left(1 - \exp\left(- \frac{y^+_{ms}}{11} \right)\right)\right] \right.$$

$$+ \frac{9}{11}\left(1 + \frac{y_{ms}^{+}}{3}\right)\exp\left(-\frac{y_{ms}^{+}}{3}\right) - \frac{9}{11}\Bigg]$$

$$+ \frac{y_{mr}^{++}}{k}\left[\ln y_{ms}^{+} + C\,k - \frac{u_{\tau r}}{u_{\tau s}}\right] + \frac{z_{or}^{++}}{k}\,\frac{u_{\tau r}}{u_{\tau s}}\Bigg\} \qquad (A.9.2)$$

Equation 4.1 follows using the definition of Re.

APPENDIX 10

Friction factor f in terms of mean flow parameters

$$\frac{\tau_{w r}}{\tau_{w s}} = \frac{y_{or}}{y_{os}} = \frac{y_{or}}{s - y_{or}} = \frac{1}{\frac{s}{y_{or}} - 1}$$

$$\frac{u_{\tau r}}{u_{\tau s}} = \frac{1}{\sqrt{\frac{s}{y_{or}} - 1}} \equiv \frac{1}{D} \qquad \text{(A.10.1)}$$

$$f_r = \frac{2\,\tau_{w r}}{\rho\, u_{av}^2}$$

$$= 2\left(\frac{u_{\tau r}}{u_{av}}\right)^2$$

$$= \frac{2}{D^2}\left(\frac{u_{\tau s}}{u_{av}}\right)^2$$

$$f_s = \frac{2\,\tau_{w s}}{\rho\, u_{av}^2}$$

$$= 2\left(\frac{u_{\tau s}}{u_{av}}\right)^2$$

Let $\Omega = \frac{u_{\tau s}}{u_{av}}$, then using equation A.9.2), Ω becomes

$$\Omega = \frac{s^+}{E}, \text{ where}$$

$$E = \frac{1 + k\, y_{ms}^{+}}{k^2} \left[\ln (1 + k\, y_{ms}^{+}) - 1 \right] + 7.8$$

$$\left[y_{ms}^{+} - 11 \left(1 - \exp\left(-\frac{y_{ms}^{+}}{11}\right)\right) \right] + \frac{9}{11} \left(1 + \frac{y_{ms}^{+}}{3}\right)$$

$$\exp\left(-\frac{y_{ms}^{+}}{3}\right) - \frac{9}{11} \Bigg]$$

$$+ \frac{1}{k} \left[y_{mr}^{++} \left(\ln y_{ms}^{+} + C\, k - \frac{1}{D}\right) + \frac{z_{or}^{++}}{D} \right]$$

$$y_{ms}^{+} = s^{+} - y_{mr}^{++}$$

and $$f = \Omega^2 \left(1 + \frac{1}{D^2}\right) \qquad \text{(A.10.2)}$$

APPENDIX II

Matching of smooth and rough wall velocity profiles at the maximum velocity point

$$u_m = \frac{u_{\tau r}}{k} \ln\left(\frac{y_{mr}}{z_{or}}\right) = \frac{u_{\tau s}}{k} \ln\left(\frac{y_{ms}\, u_{\tau s}}{\nu}\right) + C\, u_{\tau s}$$

$$y_{ms} = s - y_{mr}$$

rearranging

$$\ln y_{mr} - \ln z_{or} = \frac{u_{\tau s}}{u_{\tau r}} \left\{ \ln\left[\frac{(s - y_{mr})\, u_{\tau s}}{\nu}\right] + C\, k \right\}$$

$$z_{or} = y_{mr} \exp\left[- \frac{u_{\tau s}}{u_{\tau r}} \left\{ \ln \frac{(s - y_{mr})\, u_{\tau s}}{\nu} + C\, k \right\} \right]$$

(A. II. 1)

multiplying both sides by $\frac{u_{\tau s}}{\nu}$

$$z_{or}^{++} = y_{mr}^{++} \exp\left\{ - \frac{u_{\tau s}}{u_{\tau r}} \left[\ln (s^{+} - y_{mr}^{++}) + C\, k \right] \right\}$$

(A. II. 2)

using relation (A. 10. 1)

$$z_{or}^{++} = y_{mr}^{++} \exp\left\{ -D\left[\ln\left(s^{+} - y_{mr}^{++}\right) + C\,k \right] \right\} \qquad \text{(A. 11. 3)}$$

APPENDIX 12

Relations for f and Re with m as a constant

Putting $m = \text{const} = \frac{1}{30}$, equation A. 11. 1 becomes

$$z_{or} = m\,\epsilon = y_{mr} \exp\left\{-D\left[\ln\left(s^{+} - y_{mr}^{++}\right) + C\,k\right]\right\}$$

Putting $y_o \doteq y_m$, D becomes

$$D = \sqrt{\frac{s}{y_{mr}} - 1} \qquad \text{(A. 12. 1)}$$

$$m\,\epsilon = y_{mr} \exp\left\{-\sqrt{\frac{s}{y_{mr}} - 1}\left[\ln \frac{(s - y_{mr})\,u_{\tau s}}{\nu} + C\,k\right]\right\}$$

(A. 12. 2)

Equations 4. 1 and A. 20. 2 stay the same, however the above expression for D should be used.

APPENDIX 13

Flowchart of theoretical calculations with m = const

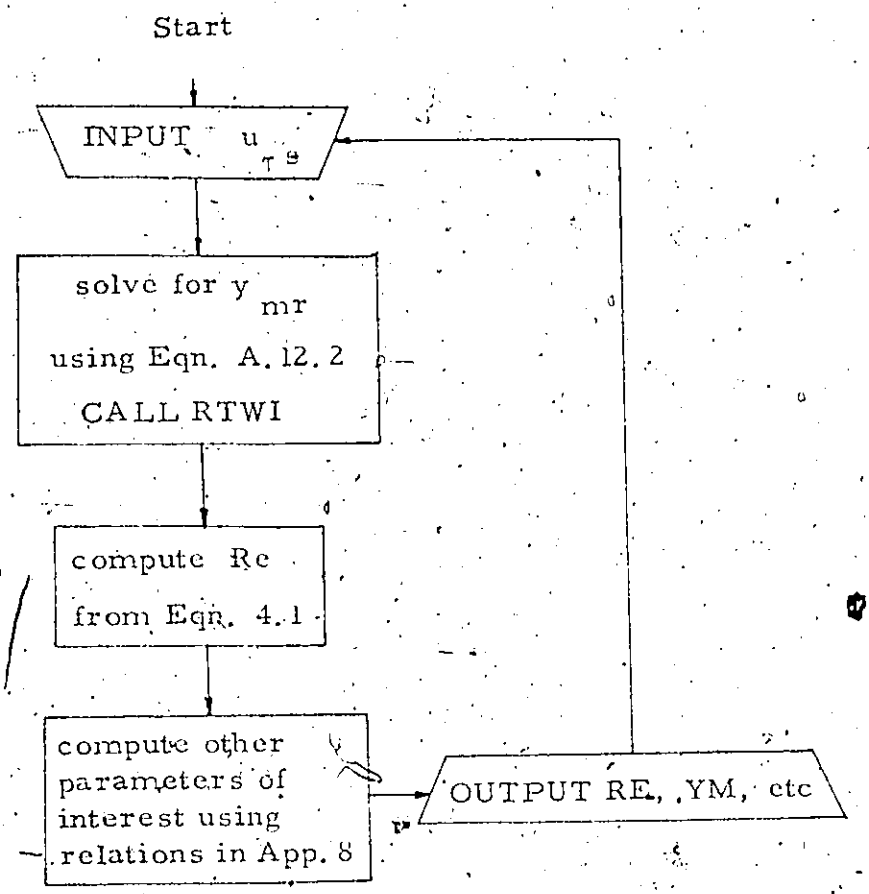

The program is open ended. The non-linear equation A.12.2 was solved by the subroutine RTWI, which utilizes the Wegstein's iteration method [38].

APPENDIX 14

Variation of C with y^+

y_s^+	C
1	1.01
4	0.55
9	2.36
16	4.0
25	4.94
36	5.38
64	5.58
81	5.58
100	5.57
121	5.56
144	5.55
196	5.54
256	5.53
324	5.53
361	5.52
400	5.52
484	5.52
576	5.52
676	5.52
900	5.52

APPENDIX 15

Flowchart of theoretical calculations with m as a variable

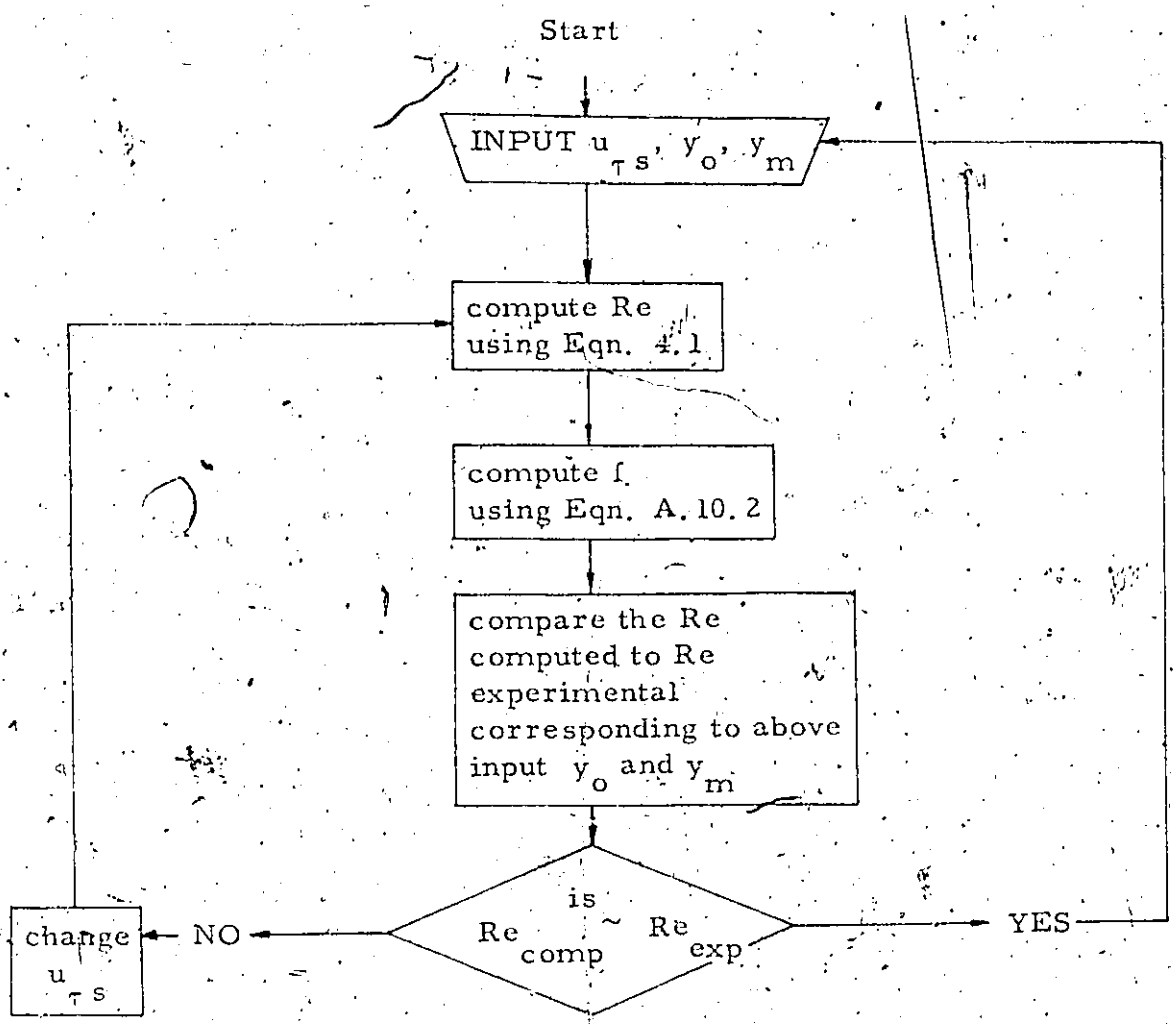

TABLE 1

Results from profile method

$\frac{s}{\epsilon} = 10.5$

x = 0.25 ft

Re	z_{or} (ft)	m	f_r	C	f_s	f
36800	0.0039	1.7	0.134	7.8	0.0077	0.071
47500	0.0011	5.94	0.047	10.5	0.0056	0.026
56700	0.0045	1.49	0.17	17.3	0.0034	0.087
75200	0.0031	2.14	0.125	12.9	0.0044	0.065

x = 1 ft

Re	z_{or} (ft)	m	f_r	C	f_s	f
23500	0.0019	3.45	0.05	6.76	0.0085	0.029
47000	0.0029	2.26	0.066	8.3	0.0058	0.036
75100	0.0035	1.92	0.083	10.2	0.0046	0.044

x = 5 ft

Re	z_{or} (ft)	m	f_r	C	f_s	f
23800	0.0038	1.74	0.07	15.2	0.0033	0.0370
47000	0.0039	1.69	0.085	14.3	0.0039	0.044
75500	0.0034	1.94	0.072	13.3	0.0037	0.038

x = 10 ft

Re	z_{or} (ft)	m	f_r	C	f_s	f
24800	0.004	1.65	0.085	10.7	0.006	0.0455
48600	0.0052	1.28	0.098	10.2	0.009	0.052
78000	0.0046	1.39	0.09	13.4	0.0036	0.047

TABLE 2

Effect of a small error in y measurement on results from profile method

$\frac{s}{\epsilon} = 10.5$

$x = 10$ ft

$Re = 48600$

	Results with experimental y_s	Results with $y_s + 0.1$ mm	% change	Results with $y_s - 0.09$ mm	% change
$u_{\tau r}$	= 13.02 ft/sec	12.82	-1.5	13.19	+1.3
z_{or}	= 0.0052 ft	0.005	-4	0.0054	+ 4
τ_{or}	= 0.4 lb_f/ft^2	0.392	-2	0.415	+ 3.8
f_r	= 0.098	0.0954	-2.7	0.1	+ 2
$u_{\tau s}$	= 2.91 ft/sec	3.38	+16	2.32	- 20
C	= 10.2	6.6	+35	16.5	+ 64
τ_{os}	= 0.02 lb_f/ft^2	0.027	+35	0.013	- 35
f_s	= 0.0049	0.0066	+35	0.0031	- 39
f	= 0.0516	0.051	-1.16	0.052	0.78
m	= 1.28	1.33	+3.9	1.24	-3.1

TABLE 3

Experimental results

$\frac{s}{c} = 29.2$

$x = 120$ in

Re_c	u_m (ft/sec)	Re_m	$\frac{y_{mr}}{s}$	$\frac{y_{or}}{s}$	$\frac{dP}{dx}$ $\left(\frac{mm\ Hg}{in}\right)$
23100	13.1	25500	0.595	0.71	0.0006
28000	16.4	32000	0.599	0.703	0.00085
33800	20.6	40400	0.606	0.718	0.0012
55000	34.4	67000	0.636	0.72	0.0031
66500	41.0	80000	0.64	0.719	0.0045
76000	45.9	89900	0.645	0.731	0.0059
87000	51.2	100000	0.64	0.742	0.0077
107000	62.3	121700	0.653	0.738	0.0116
132000	76.5	149500	0.674	0.748	0.0175

Table 3 (continued) Experimental results, $\frac{s}{\varepsilon} = 29.2$, $x = 120$ in

Re	$\tau_{w\,r}\left(\frac{lb_f}{ft^2}\right)$	$\tau_{w\,s}\left(\frac{lb_f}{ft^2}\right)$	$u_{\tau\,r}\left(\frac{ft}{sec}\right)$	$u_{\tau\,s}\left(\frac{ft}{sec}\right)$	f_r	f_s	f	$\frac{l}{m}$
21900	0.0025	0.0011	1.05	0.69	0.01725	0.00739	0.0123	10.3
27900	0.0037	0.0016	1.28	0.84	0.01591	0.00682	0.0114	11.7
34900	0.0058	0.0025	1.60	1.05	0.01583	0.00678	0.0113	13.6
41600	0.0078	0.0034	1.85	1.21	0.0150	0.00648	0.0107	14.9
51700	0.013	0.0055	2.37	1.55	0.0160	0.00685	0.0114	17.6
63000	0.018	0.0076	2.78	1.82	0.0147	0.00629	0.0105	19.5
74300	0.025	0.0108	3.32	2.17	0.0151	0.0065	0.0108	21.9
84100	0.033	0.014	3.80	2.49	0.0155	0.0066	0.0111	23.9
96200	0.046	0.020	4.48	2.93	0.0165	0.0071	0.0118	26.7
114000	0.062	0.026	5.19	3.40	0.0197	0.0067	0.0112	29.3

TABLE 4

Results of Theoretical Computations

$\frac{s}{\epsilon} = 10.5$

Re	$\frac{y_{mr}^{++}}{s^+}$ (exp)	s^+	z_{or}^{++}	f_r	f_s	f
17600	0.72	628	4.8	0.024	0.0092	0.0167
35300	0.73	1158	8.57	0.0234	0.0078	0.0155
48500	0.74	1540	11.36	0.0231	0.0073	0.0152
73000	0.755	2240	18.4	0.0240	0.0068	0.0154

$\frac{s}{\epsilon} = 29.2$

Re	$\frac{y_{mr}^{++}}{s^+}$ (exp)	s^+	z_{or}^{++}	f_r	f_s	f
23400	0.59	805	2.85	0.0177	0.0072	0.0125
34000	0.606	1123	3.75	0.017	0.0067	0.0118
57400	0.636	1798	5.06	0.0154	0.0060	0.0107
80200	0.645	2432	6.80	0.0153	0.0056	0.0104
115200	0.653	3365	8.77	0.0147	0.0052	0.0100

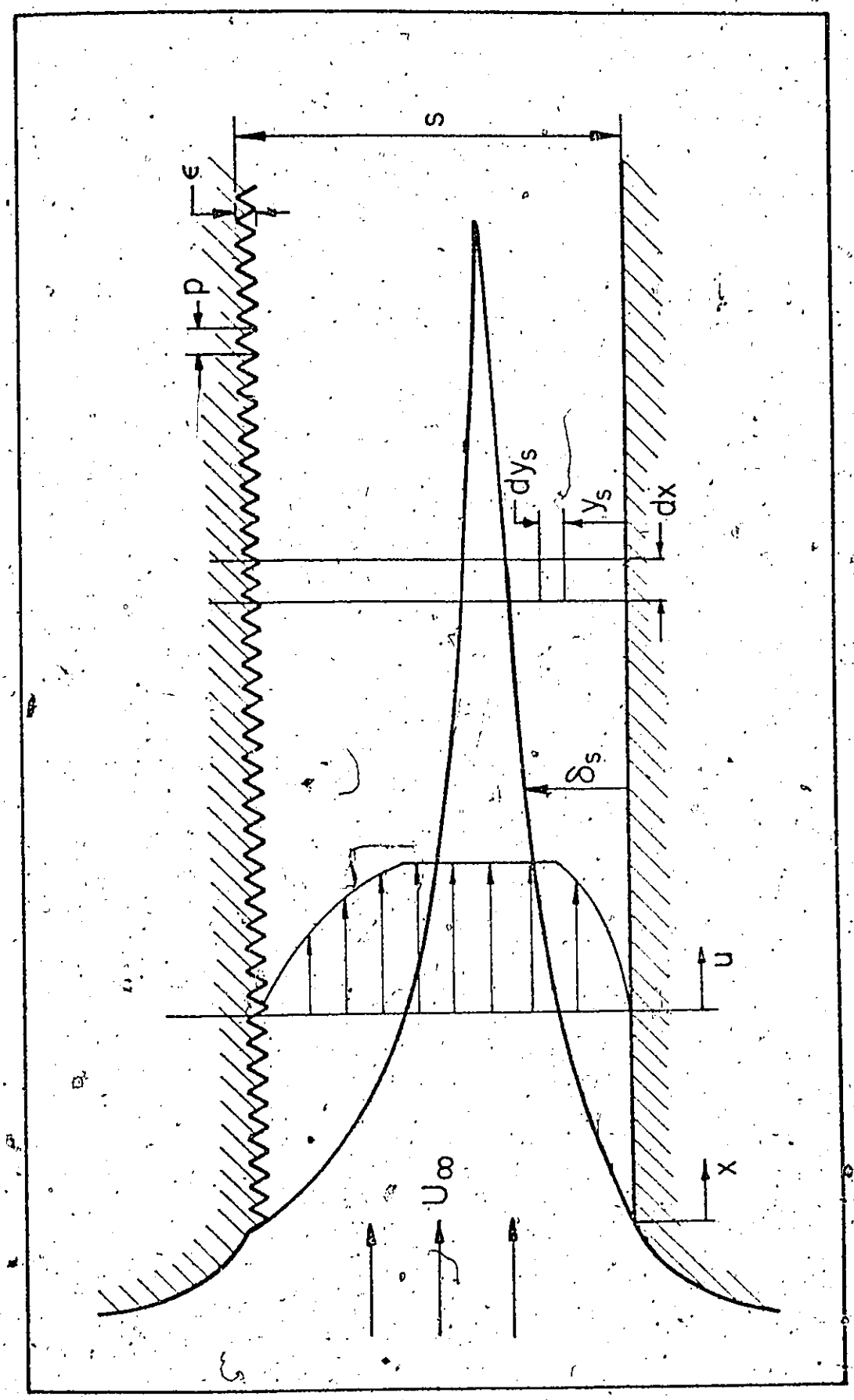

Figure 2.1 Idealized Model

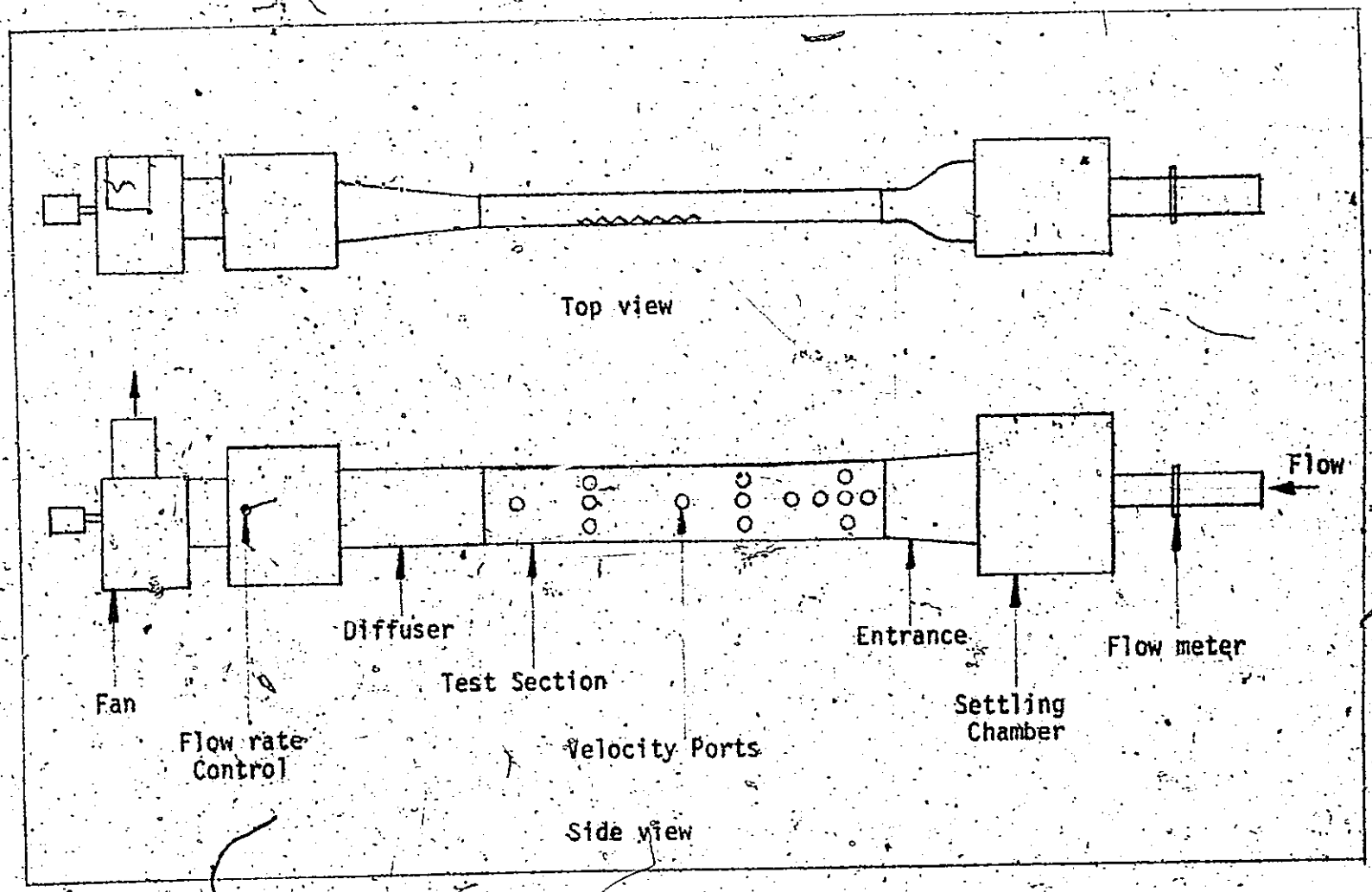

Figure 3.1 Schematical Description of Apparatus

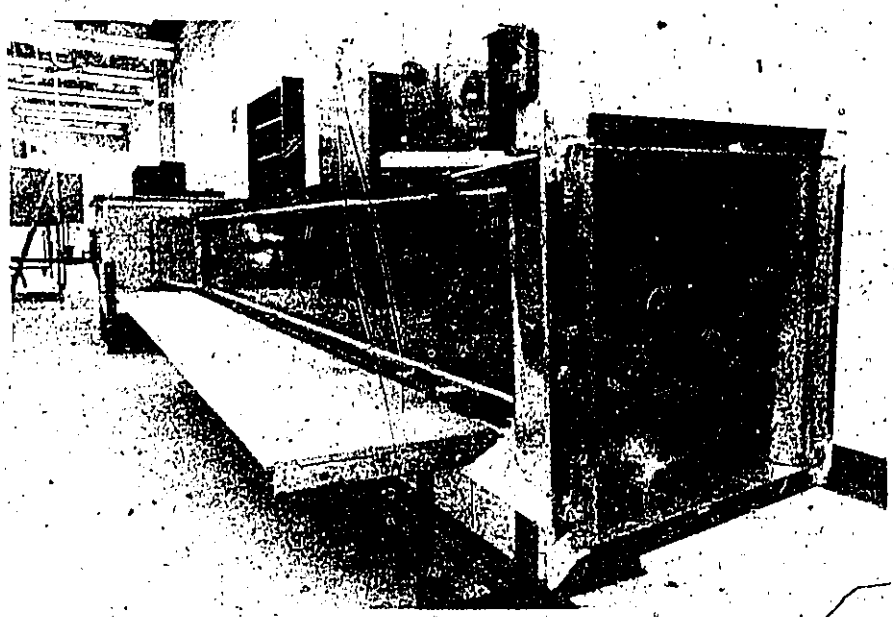

(a)

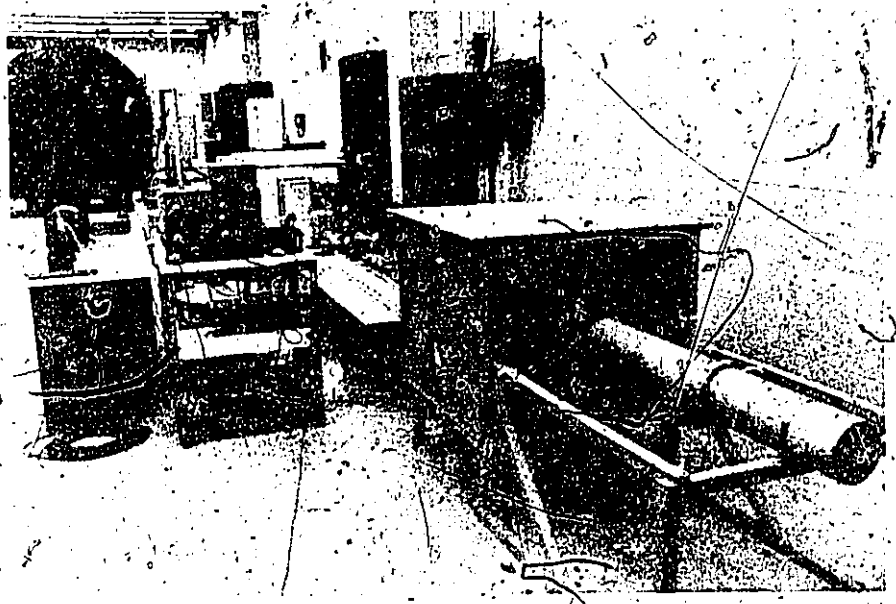

(b)

Figure 3.2 General View of Experimental Apparatus

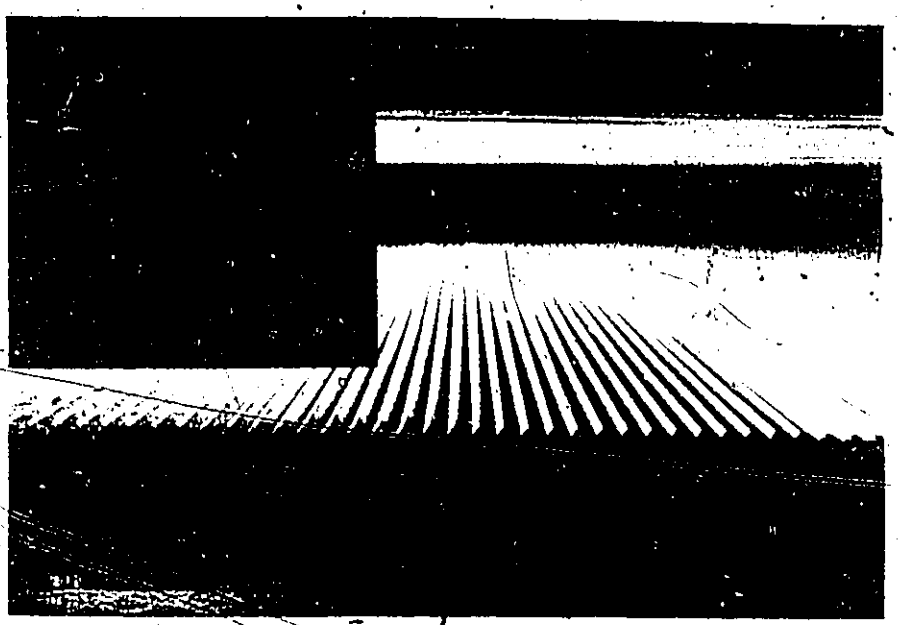

Figure 3.3 Rough Plate Profile

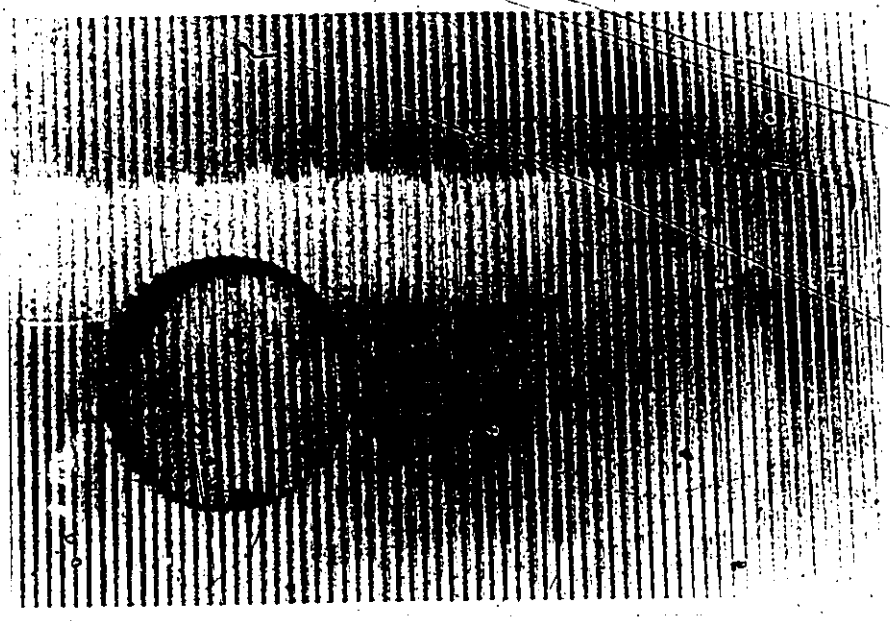

Figure 3.4 Velocity Measuring Ports

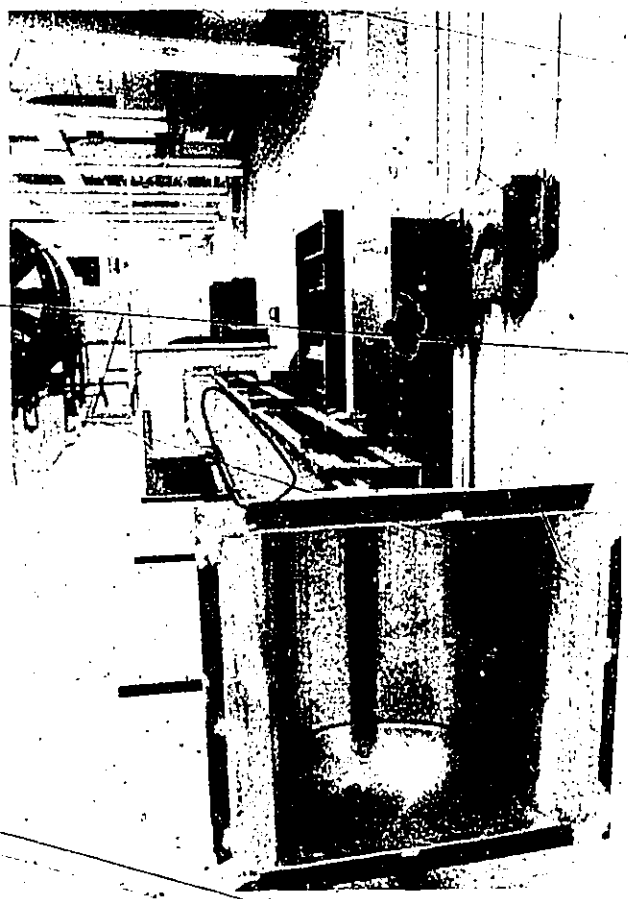

Figure 3.5 Static Pressure Taps

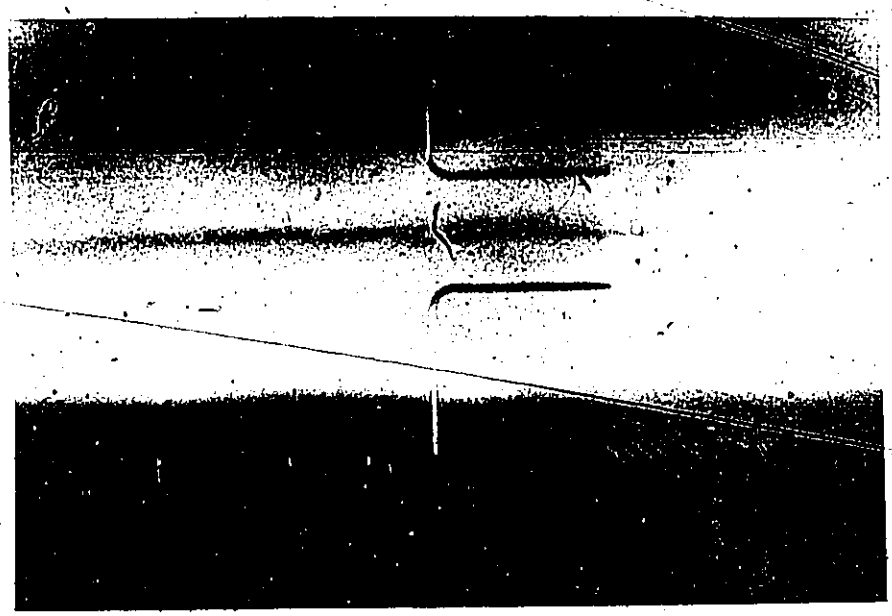

Figure 3.6 Single Pitot Tube Mounted in Position

Figure 3.7 Pressure Manifold and Clamps

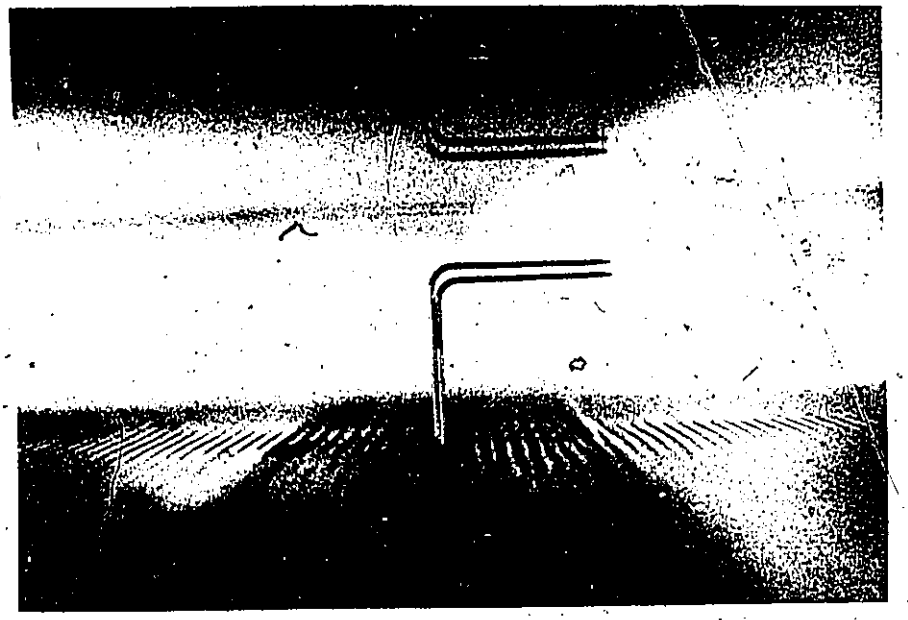

Figure 3.8 Double Pitot Tube Mounted in Position

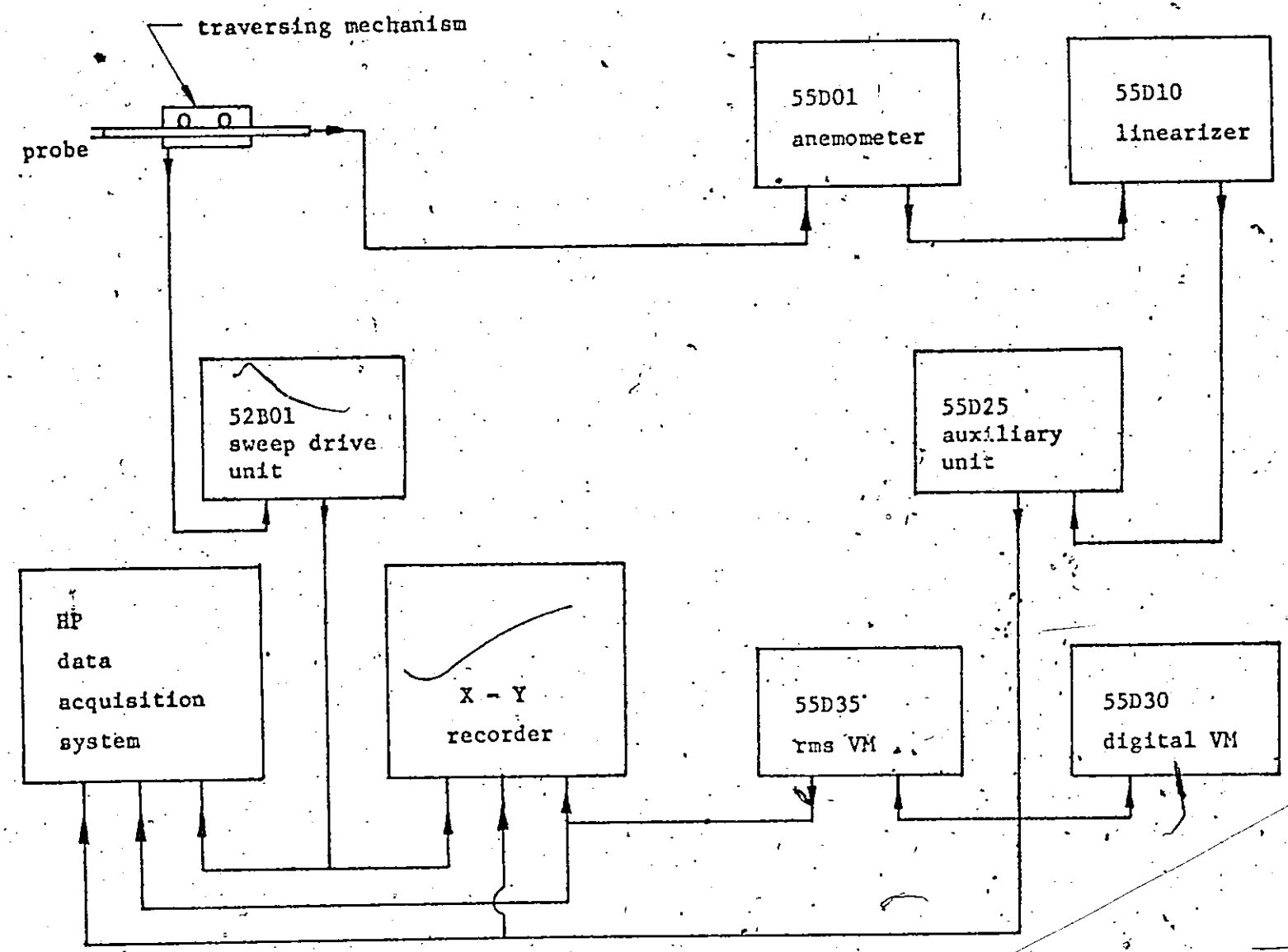

Figure 3.9a Flowchart of measurements

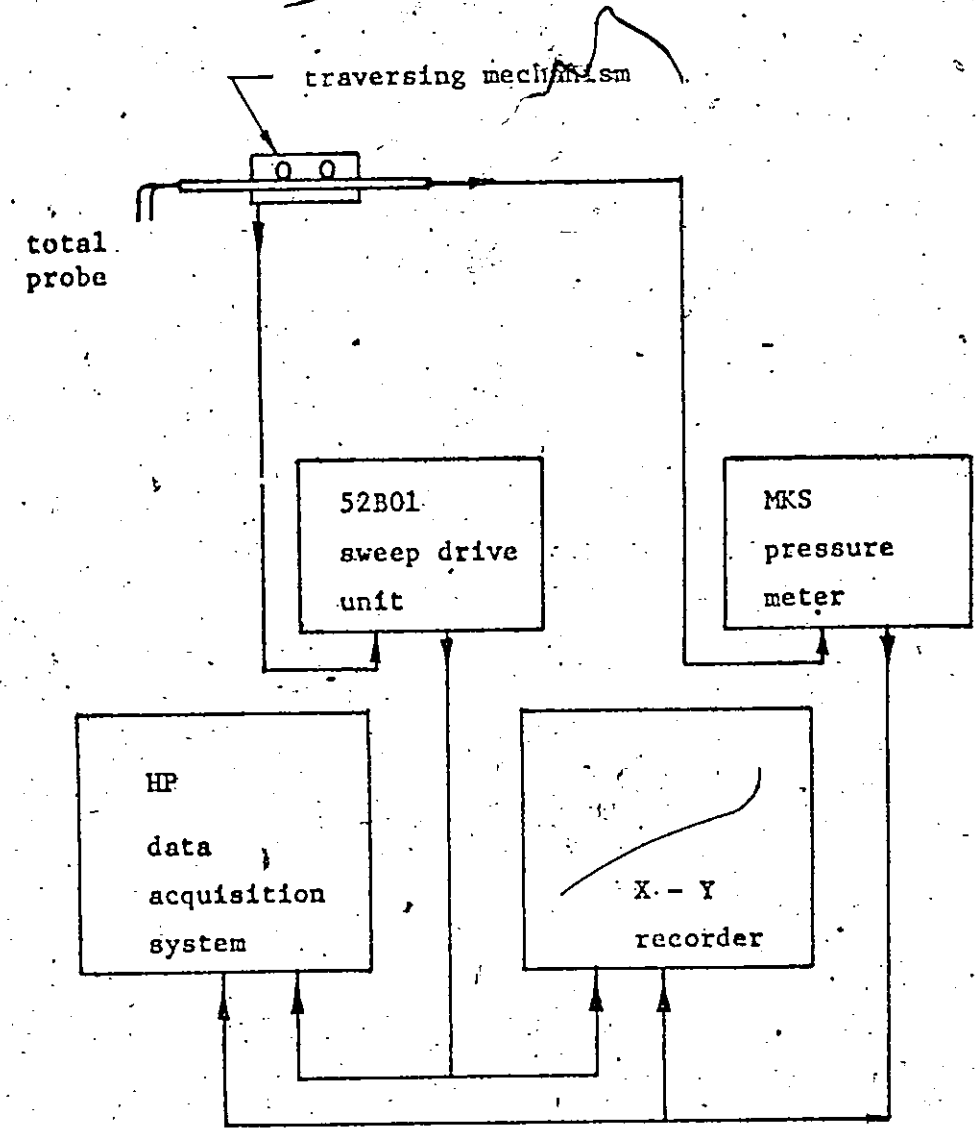

Figure 3.9b Flowchart of measurements

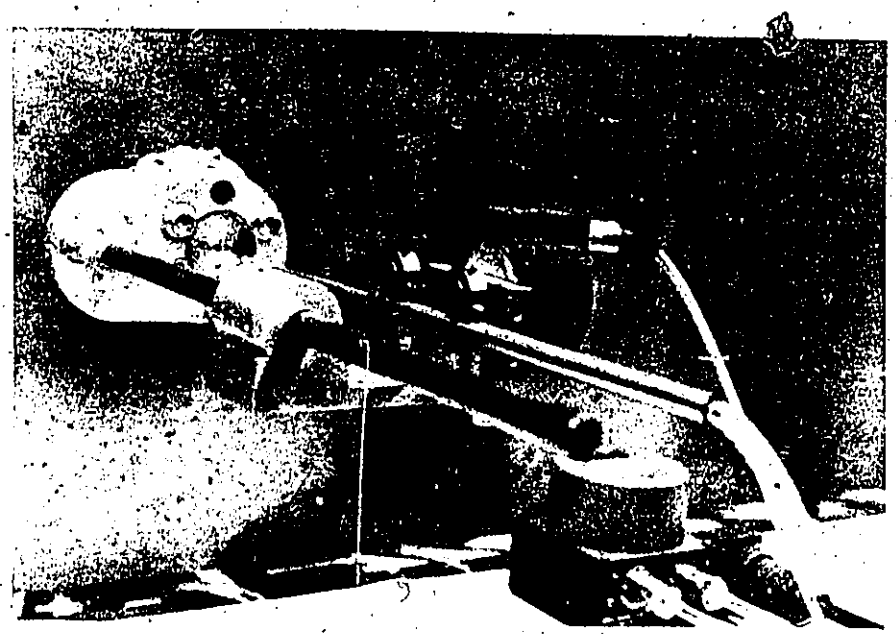

(a)

(b)

Figure 3.10 a, b Traversing Mechanism and Base

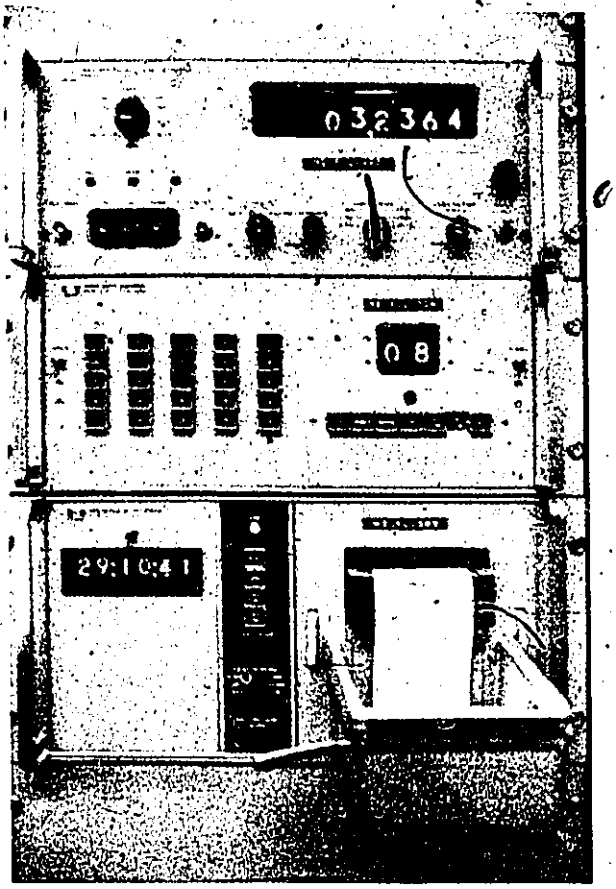

Figure 3.11 Hewlett-Packard Data Acquisition System

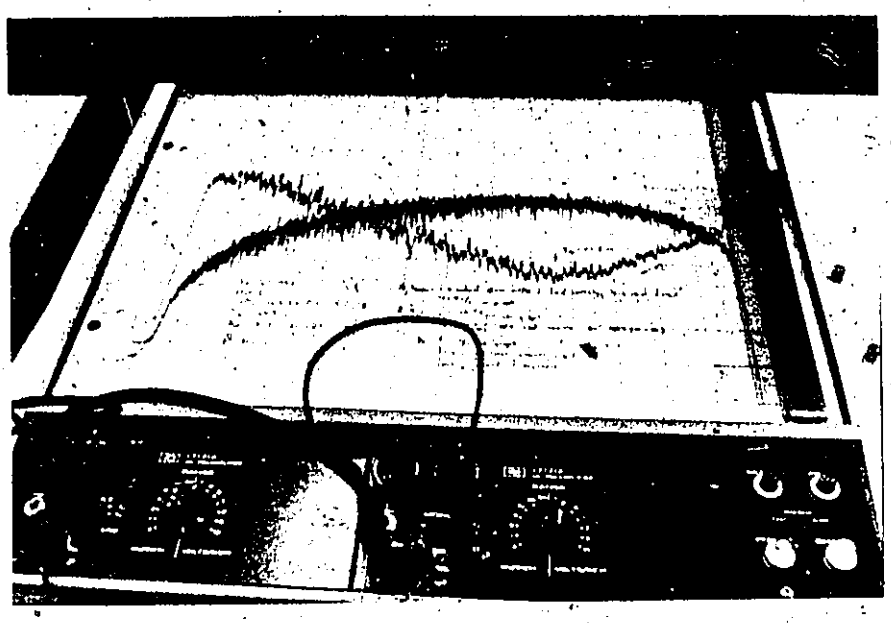

Figure 3.12 Hewlett-Packard X-Y Recorder

(a)

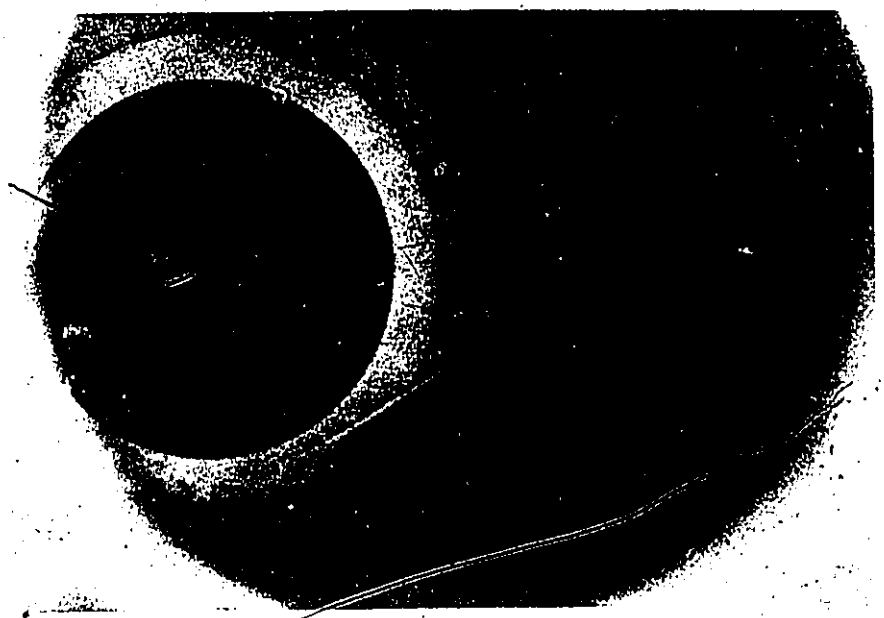

(b)

Figure 3.13 Orifice Meter

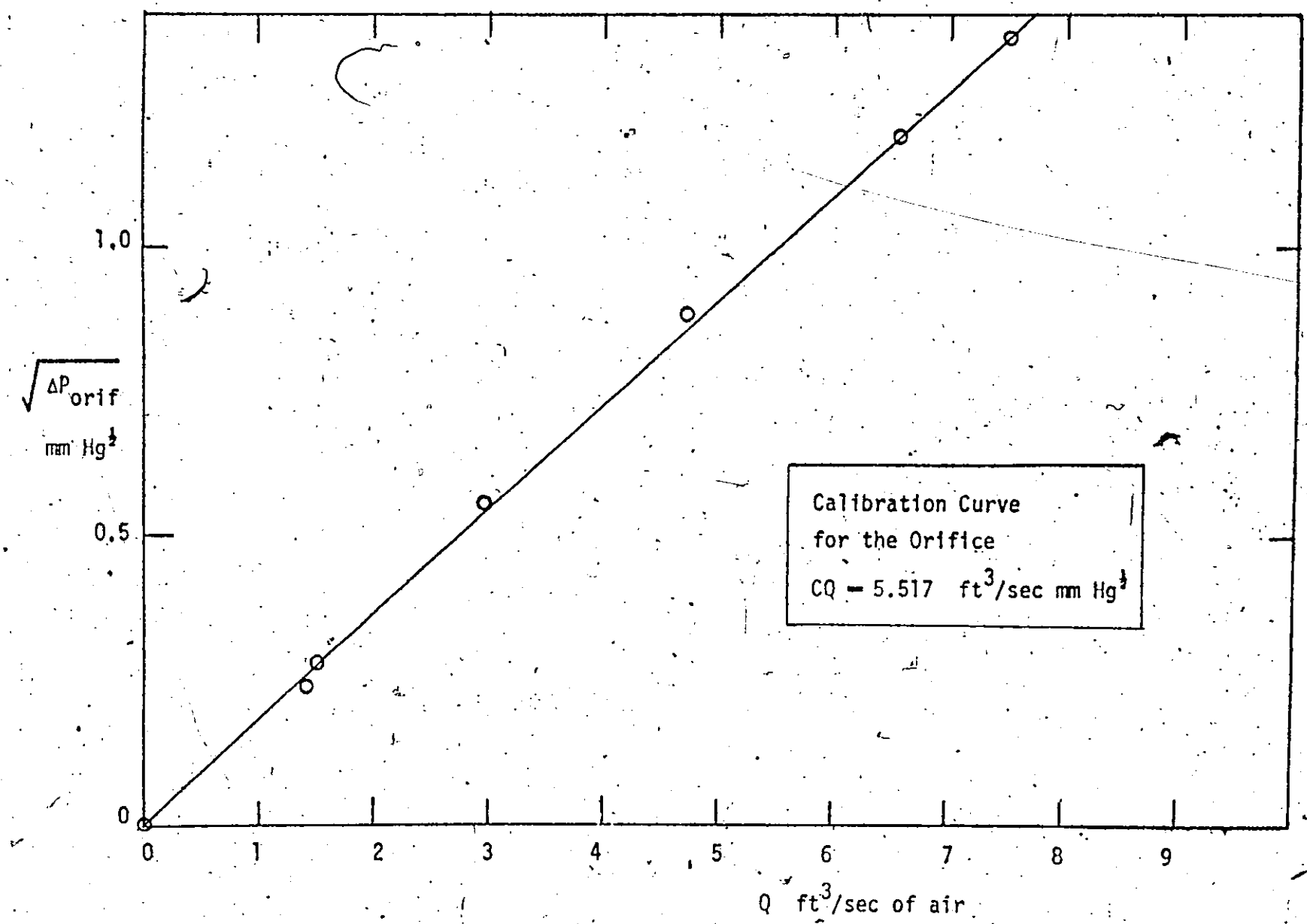

Figure 3.14 Calibration Curve for the Orifice Plate

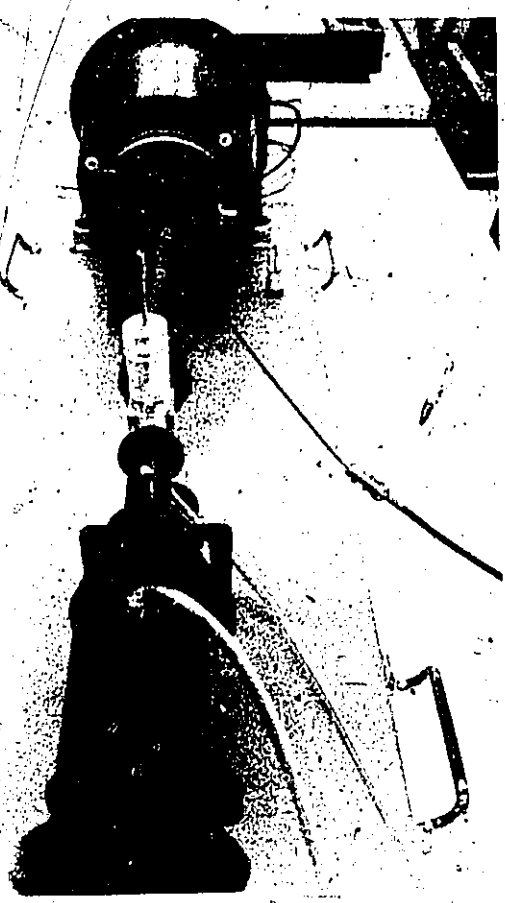

Figure 3.15 Hot-wire Calibration Apparatus

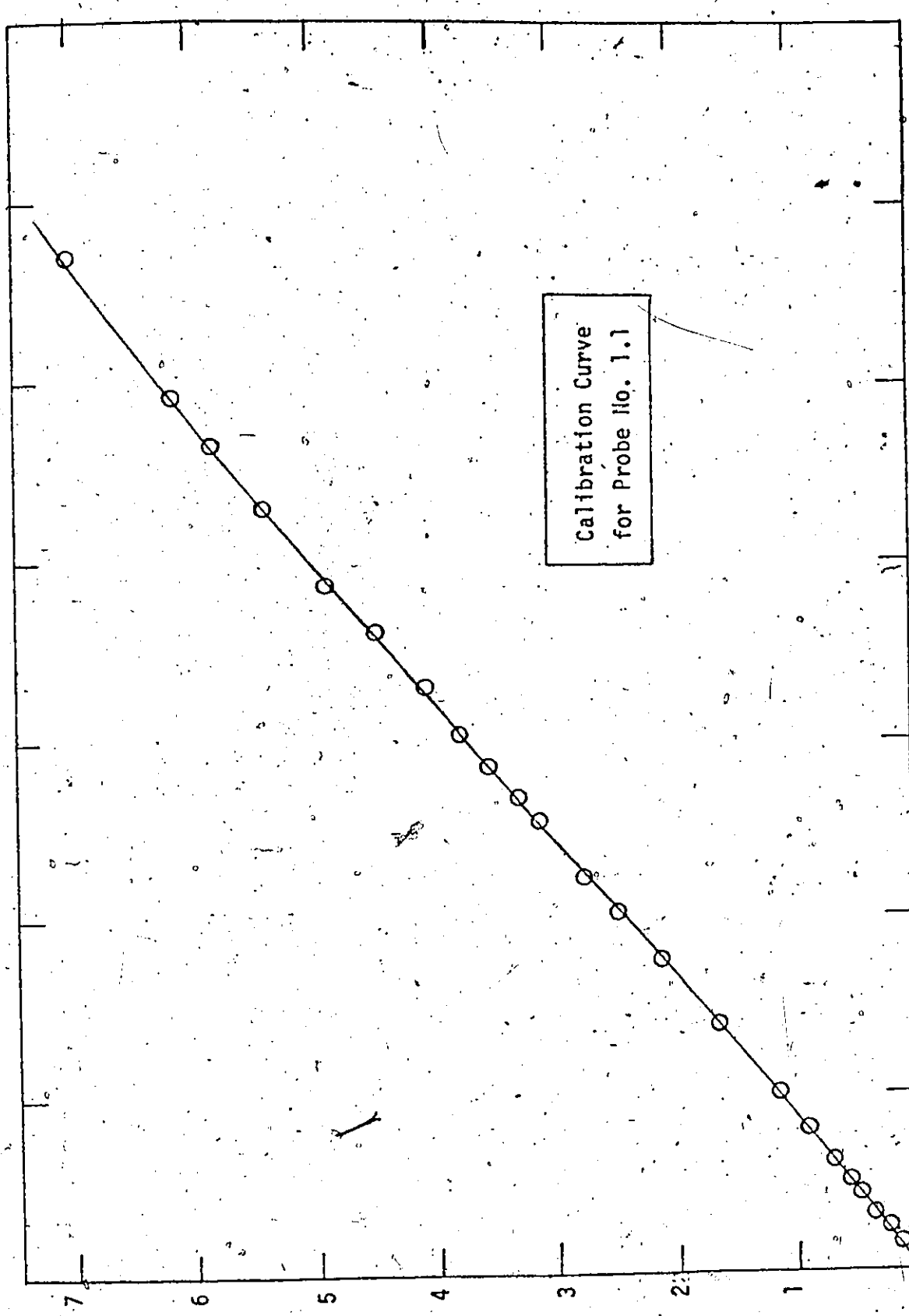

Figure 3.16 Typical Calibration Curve for a Hot-wire Probe

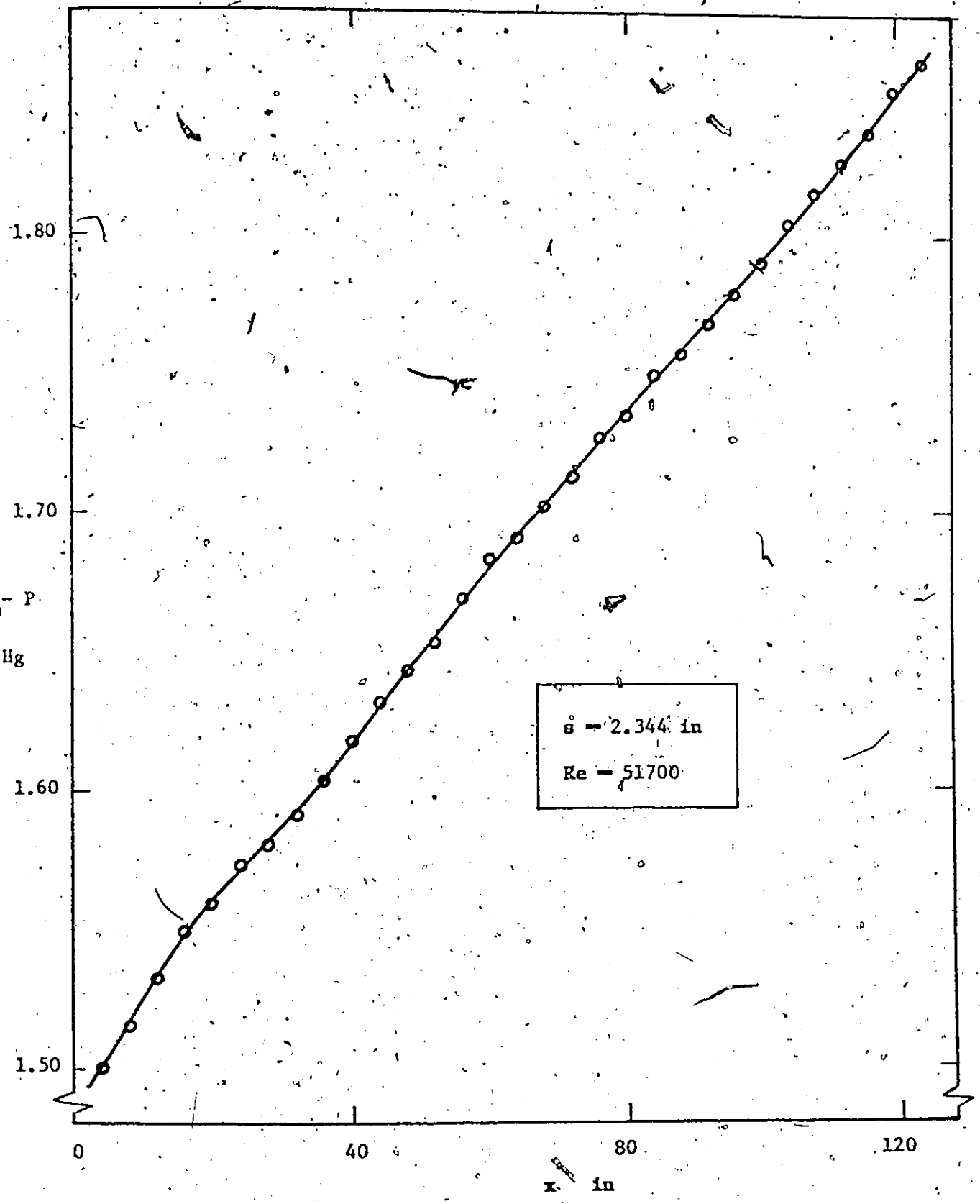

Figure 3.17 Pressure vs x

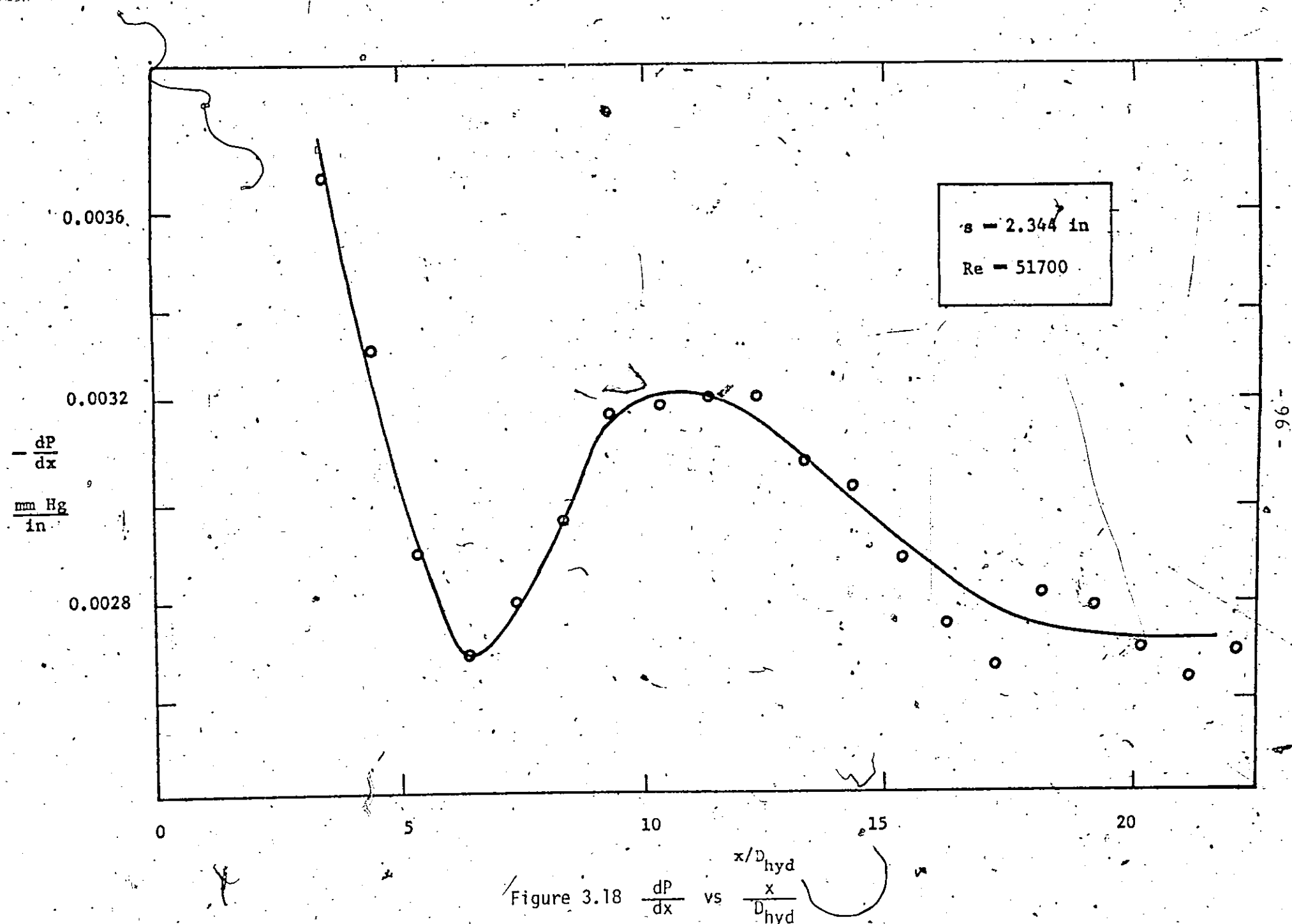

Figure 3.18 $\frac{dP}{dx}$ vs $\frac{x}{D_{hyd}}$

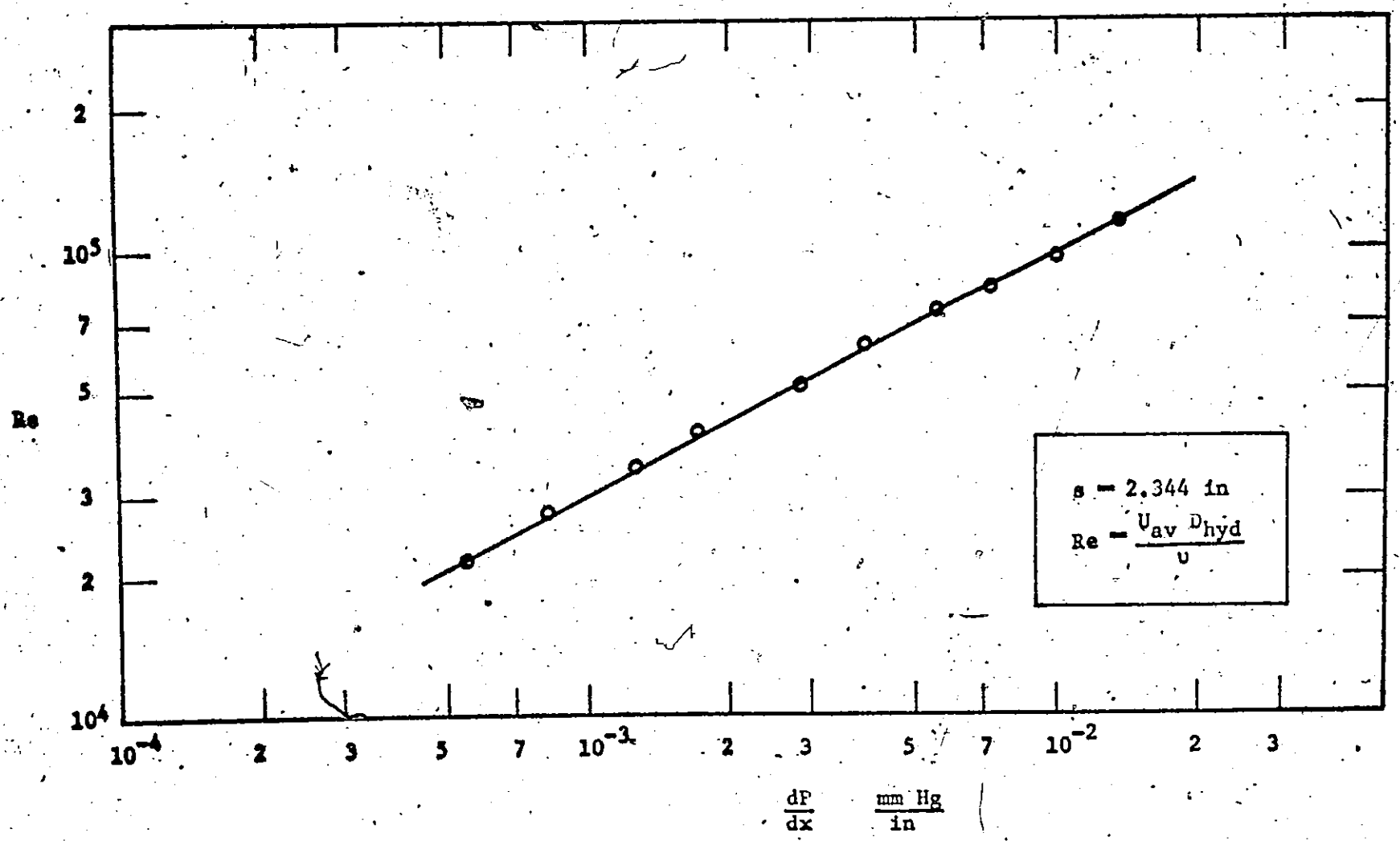

Figure 3.19 $\frac{dP}{dx}$ vs Reynolds Number

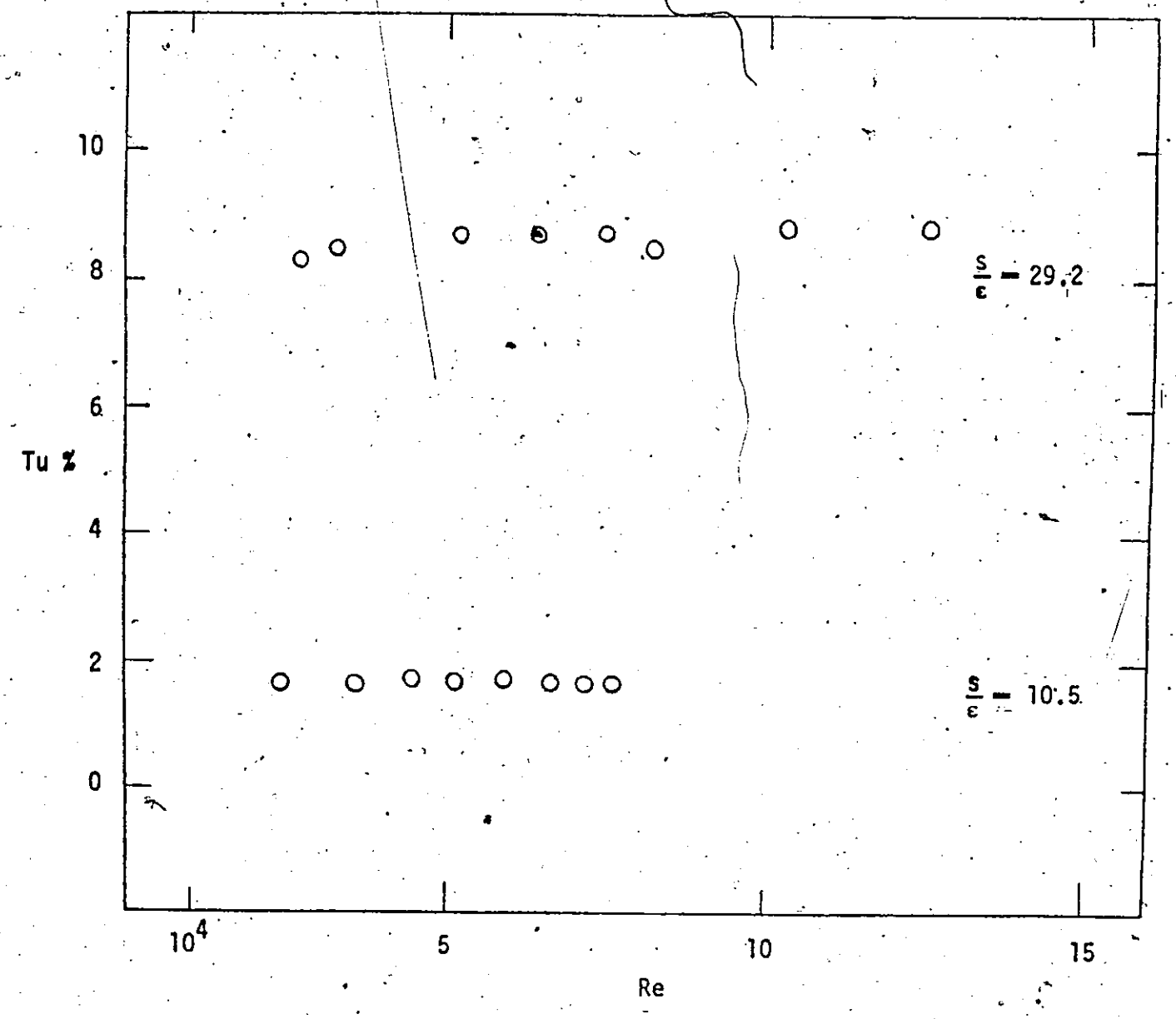

Figure 3.20 Turbulence Intensity vs Reynolds Number

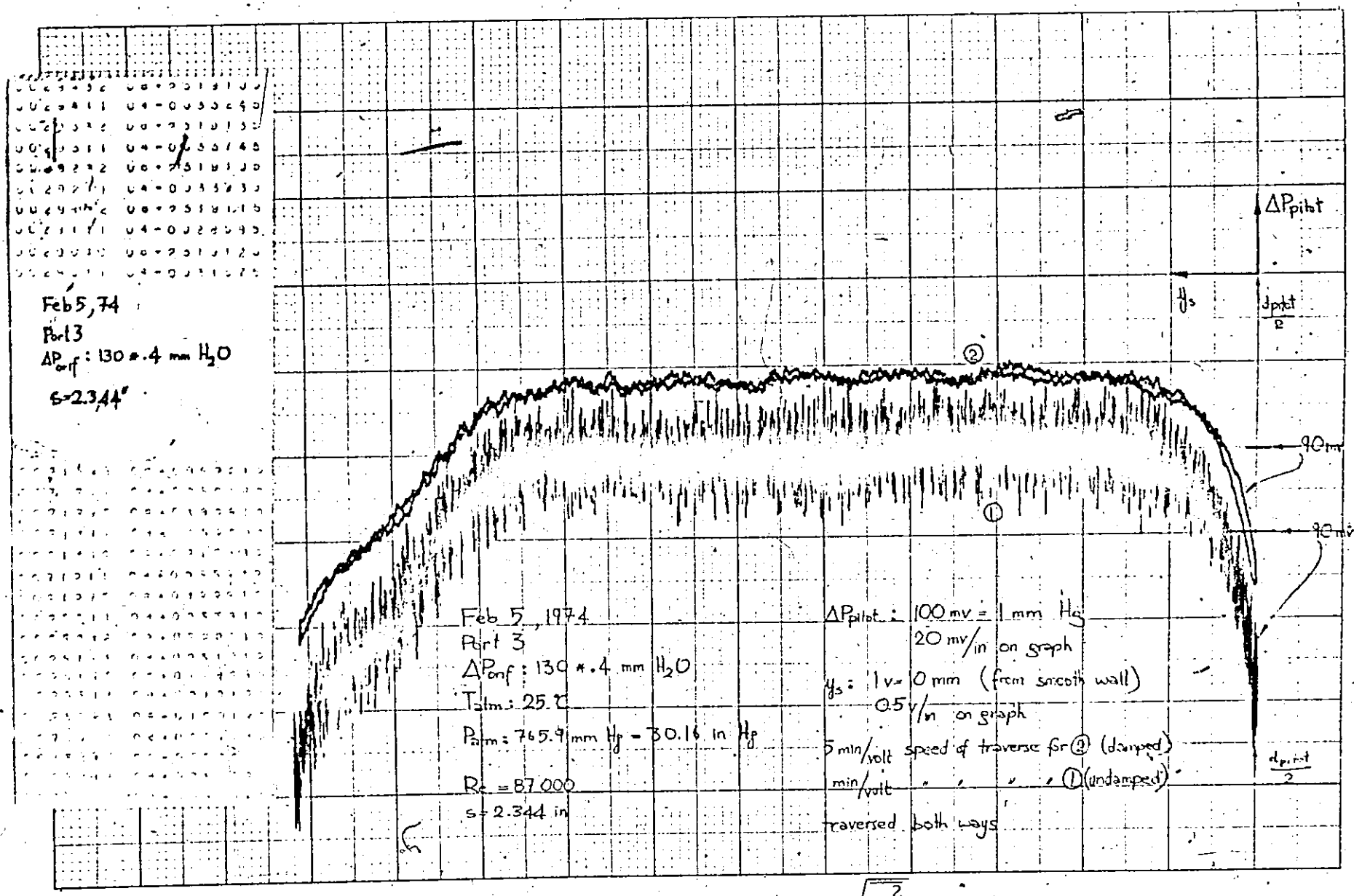

Figure 3.21 a Developing Velocity and $\frac{\sqrt{\overline{u'^2}}}{\bar{u}}$ Profiles

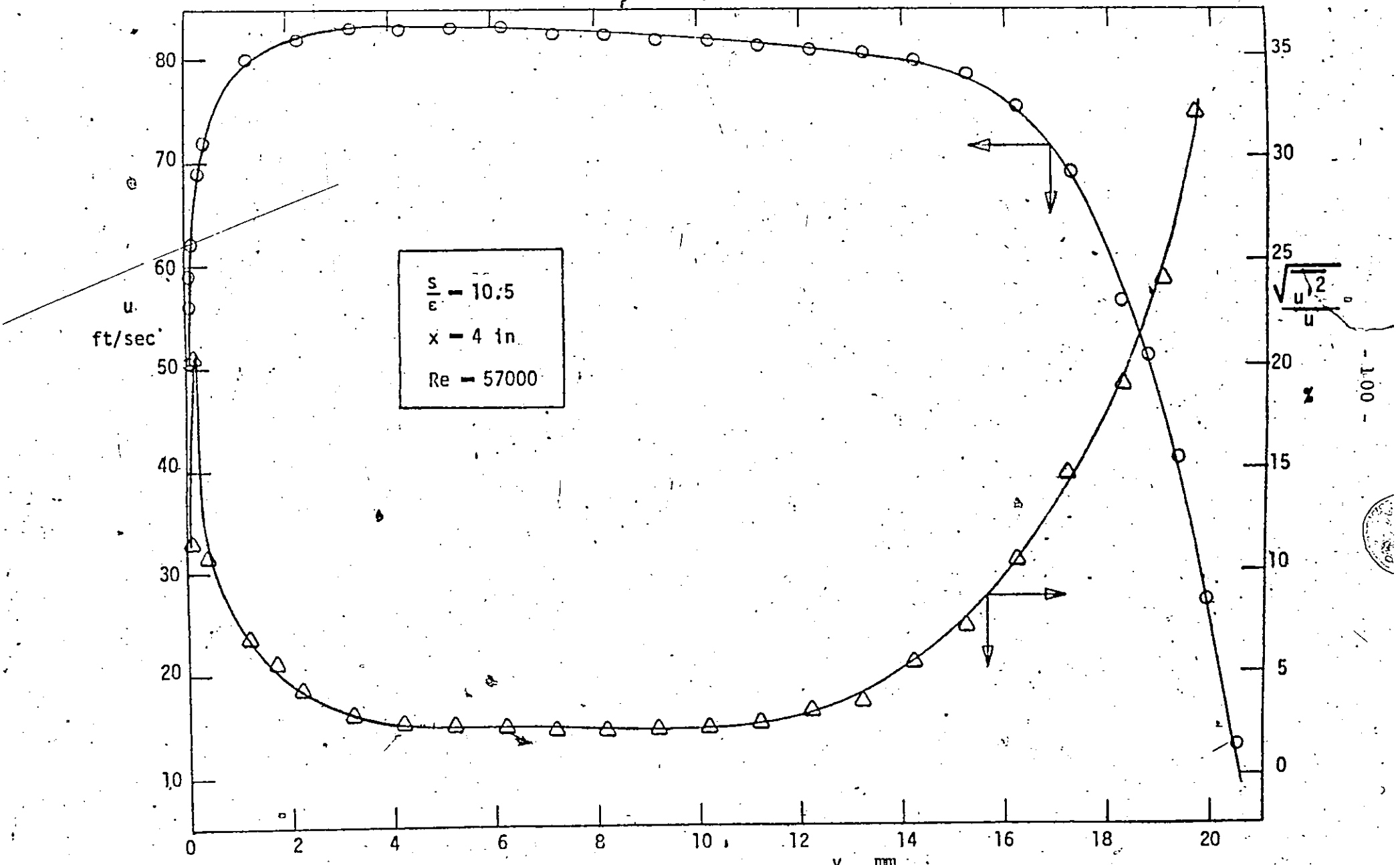

Figure 3.21 b Developing Velocity and $\frac{\sqrt{u'^2}}{u}$ Profiles

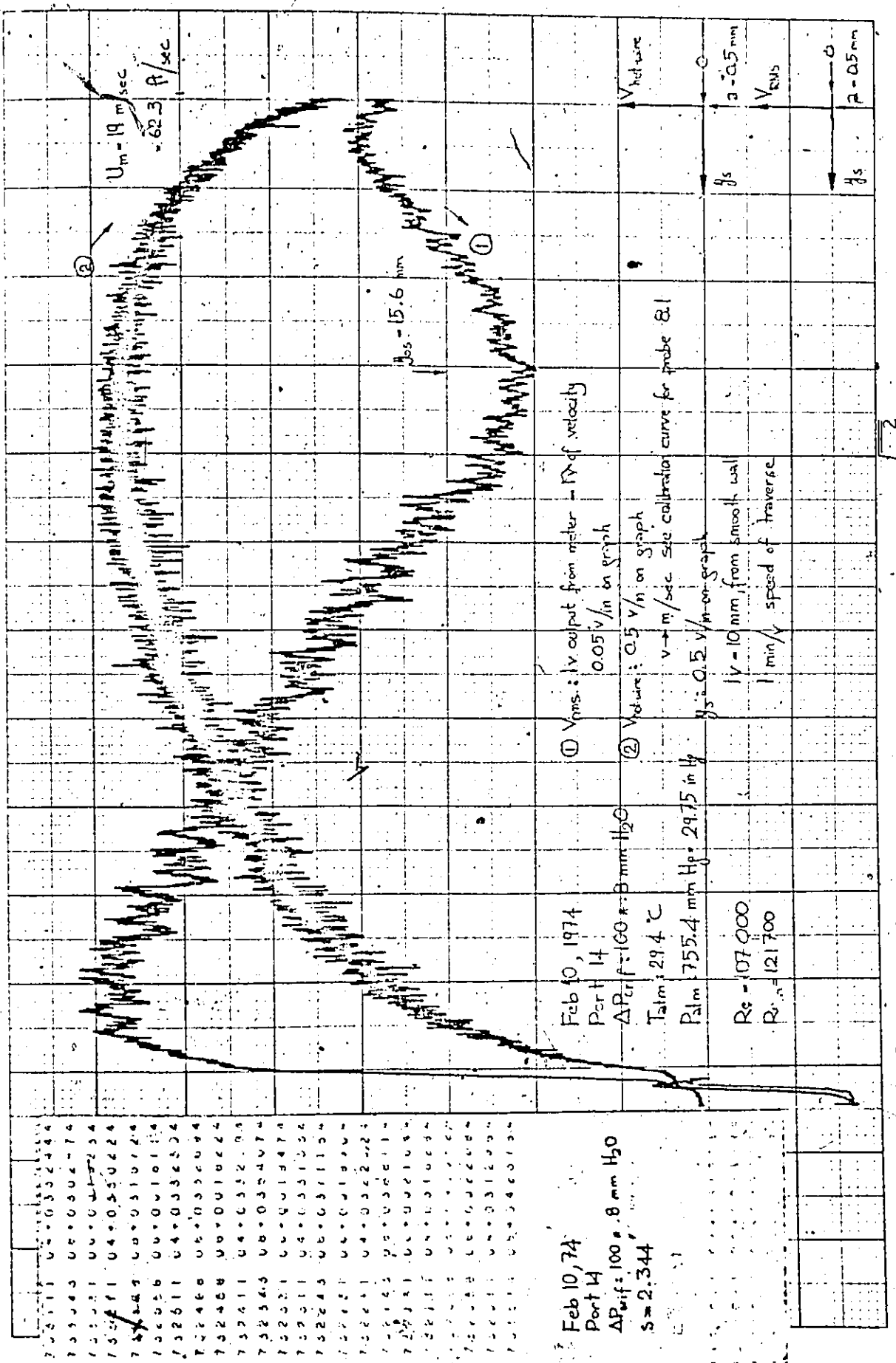

Figure 3.22 a Developed Velocity and $\frac{\sqrt{u'^2}}{\bar{u}}$ Profiles

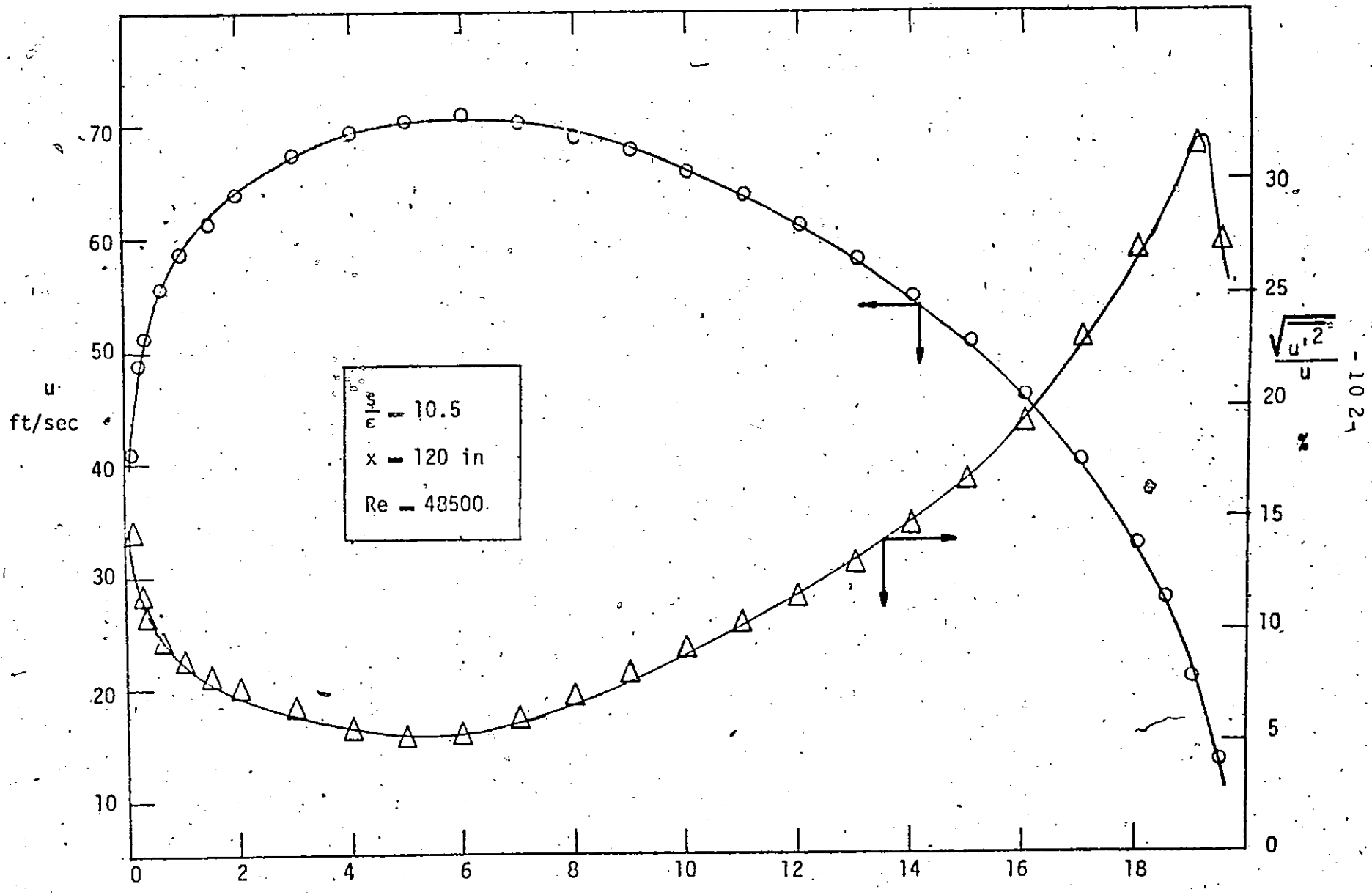

Figure 3.22 b Developed Velocity and $\frac{\sqrt{u'^2}}{u}$ Profiles

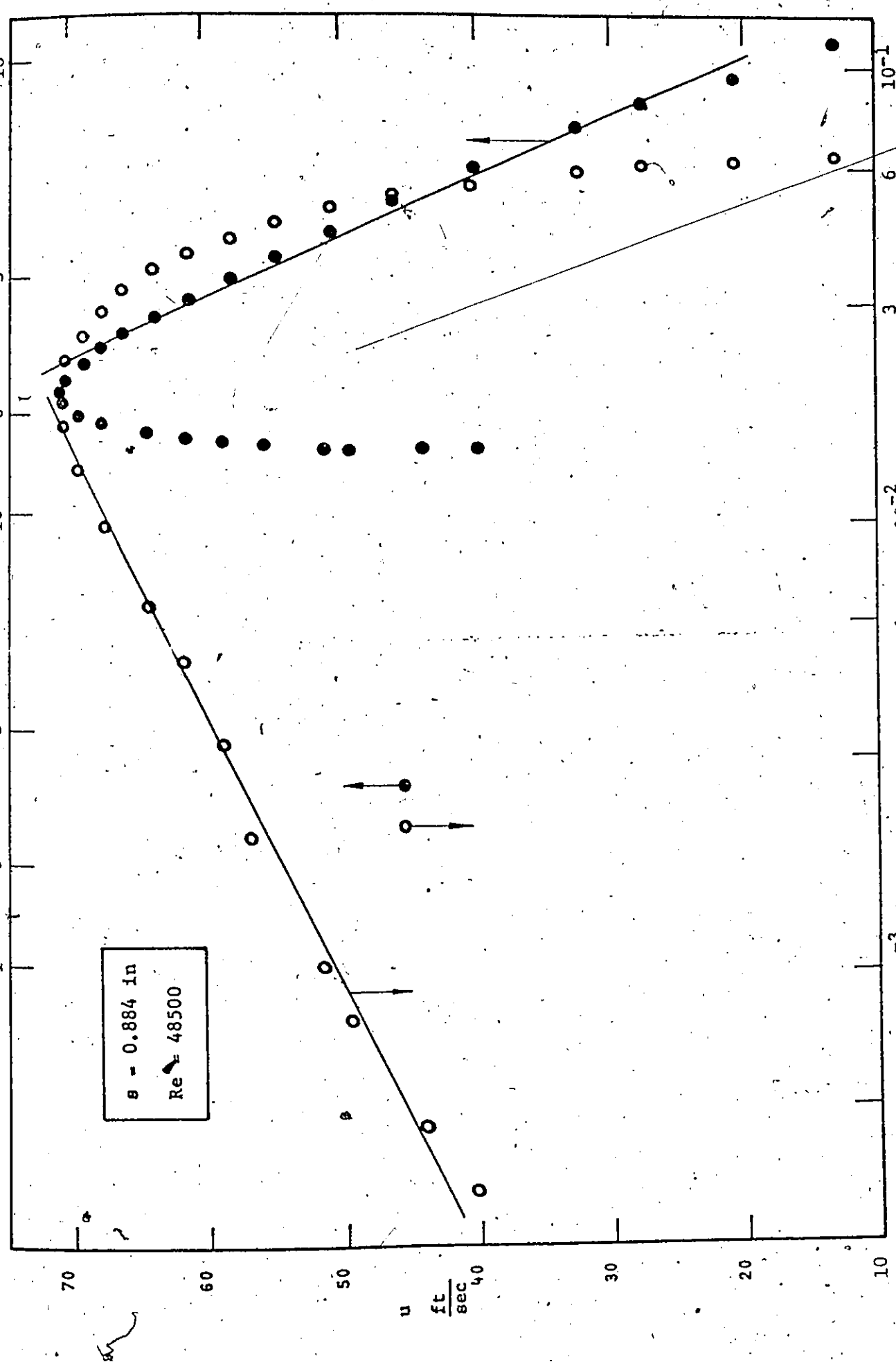

Figure 3.23 Logarithmic Velocity Profiles

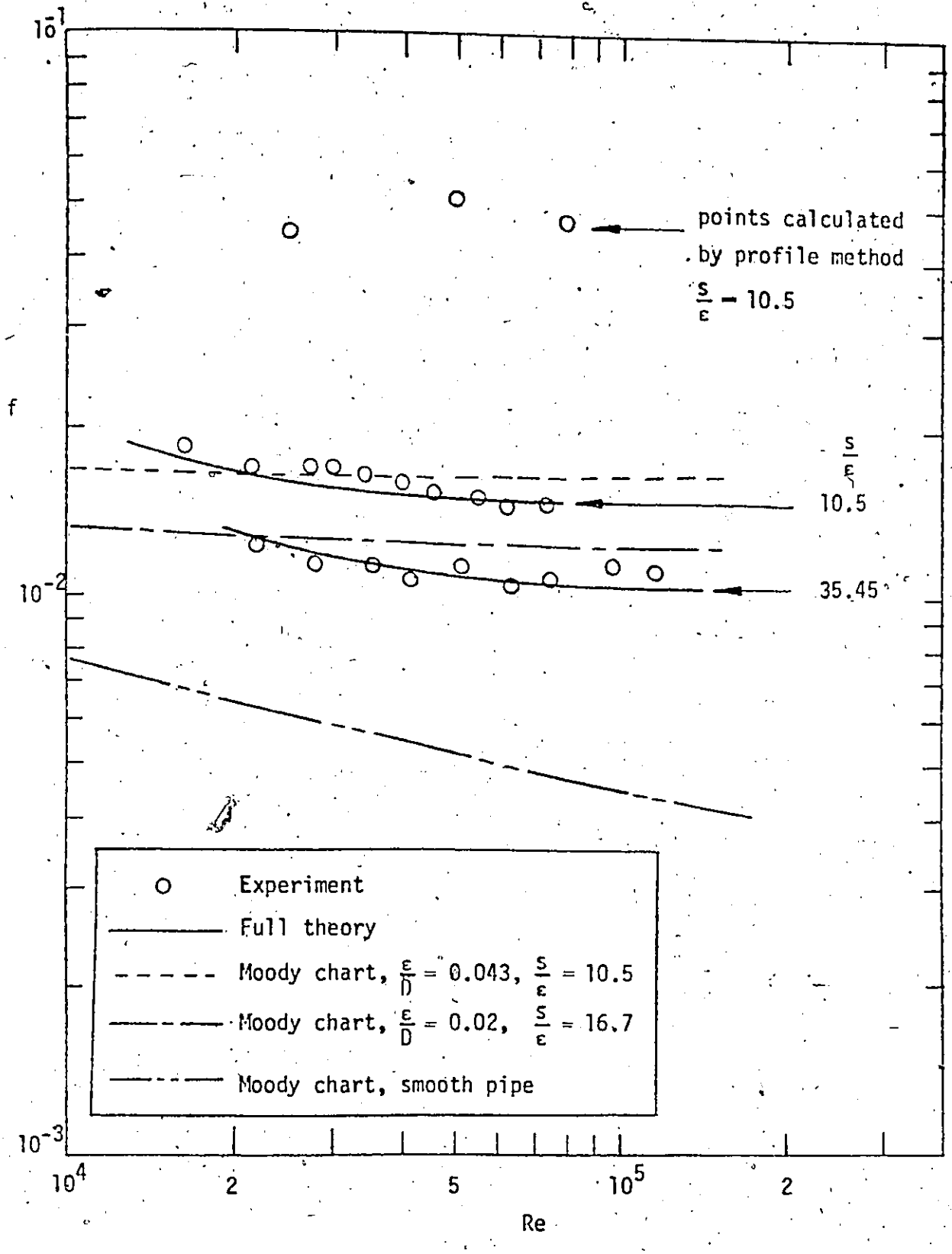

Figure 3.24 a Friction Factor vs Reynolds Number

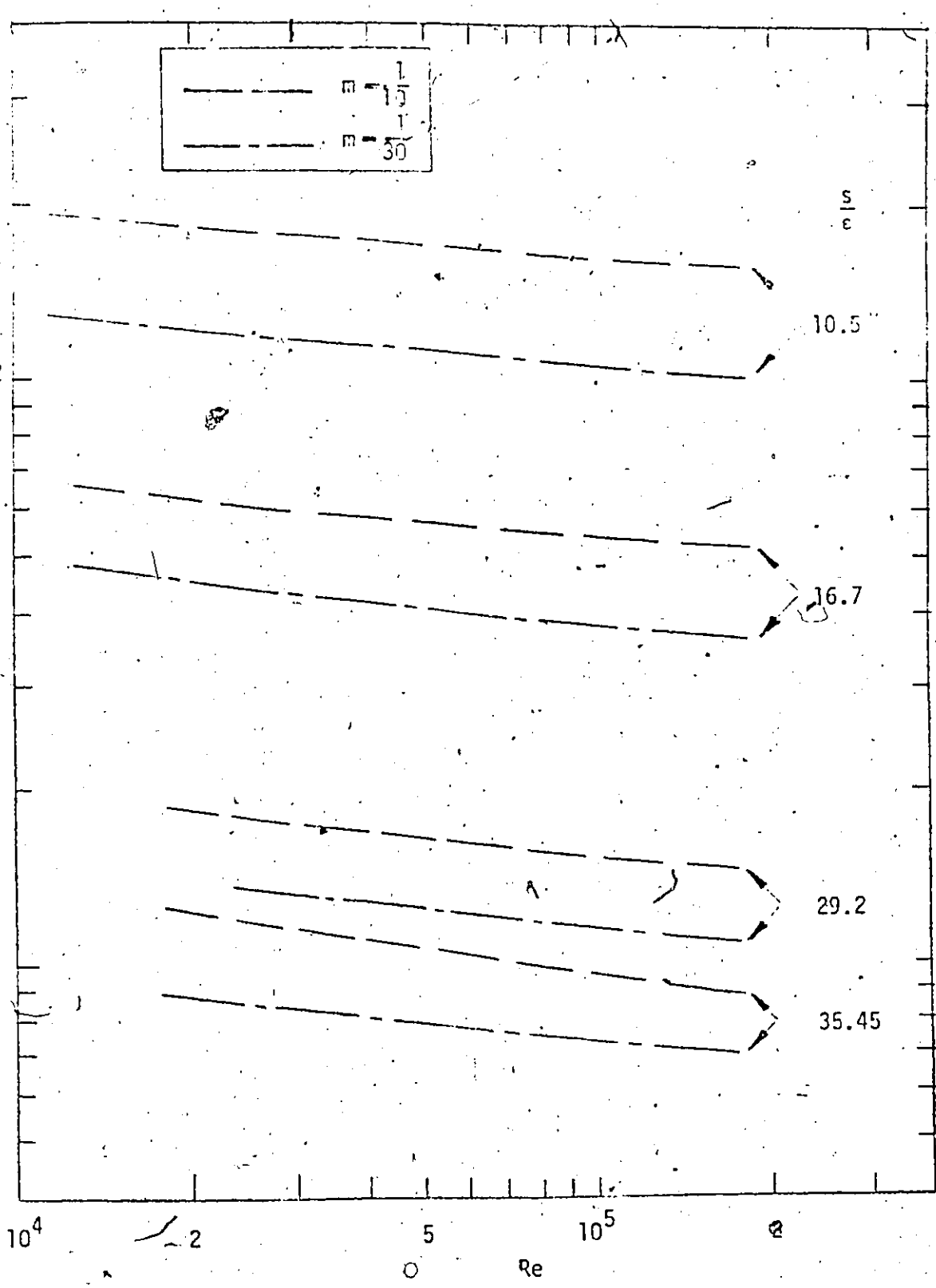

Figure 3.24 b Friction Factor vs Reynolds Number

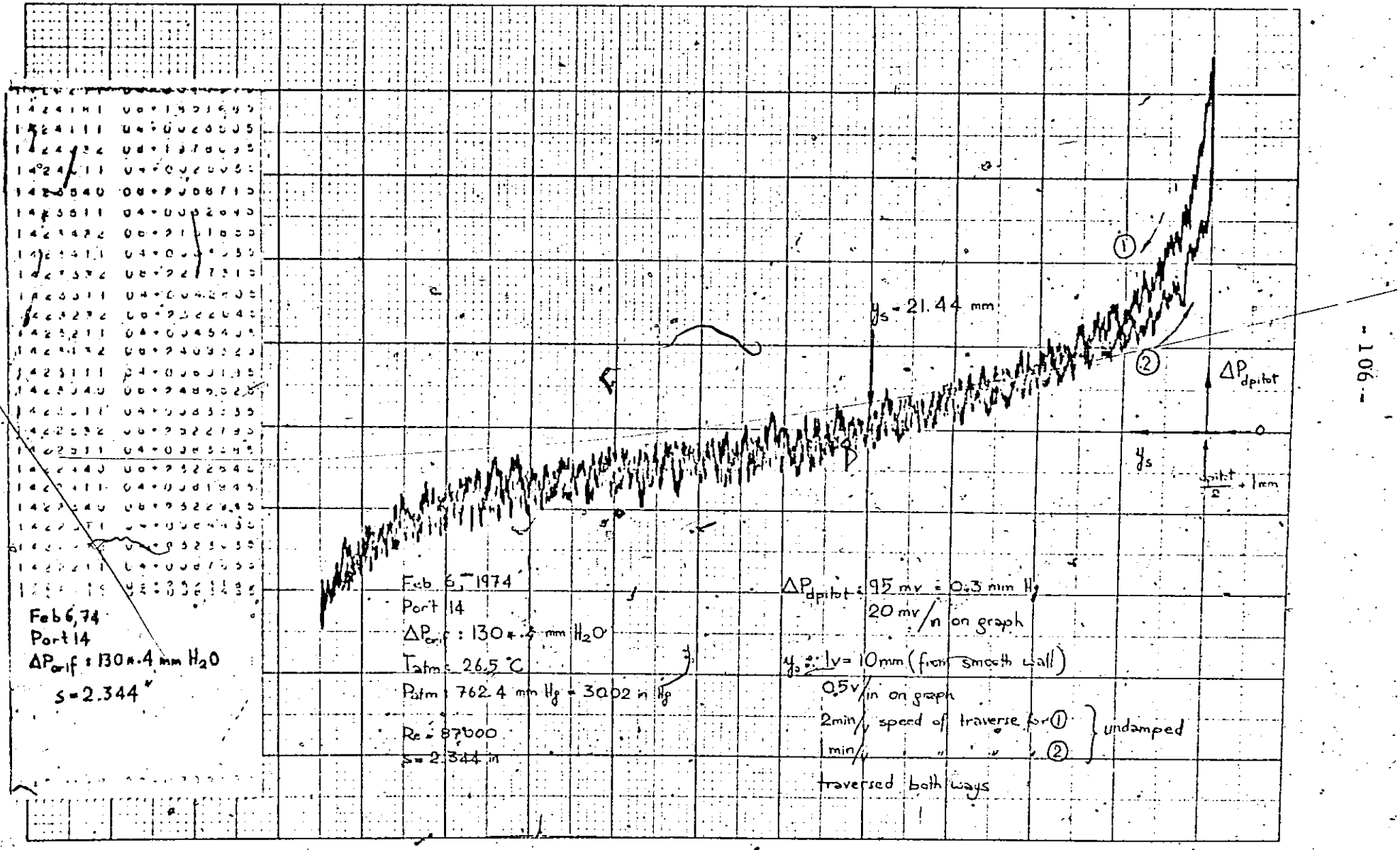

Figure 3.25 Double Pitot Tube Measurement

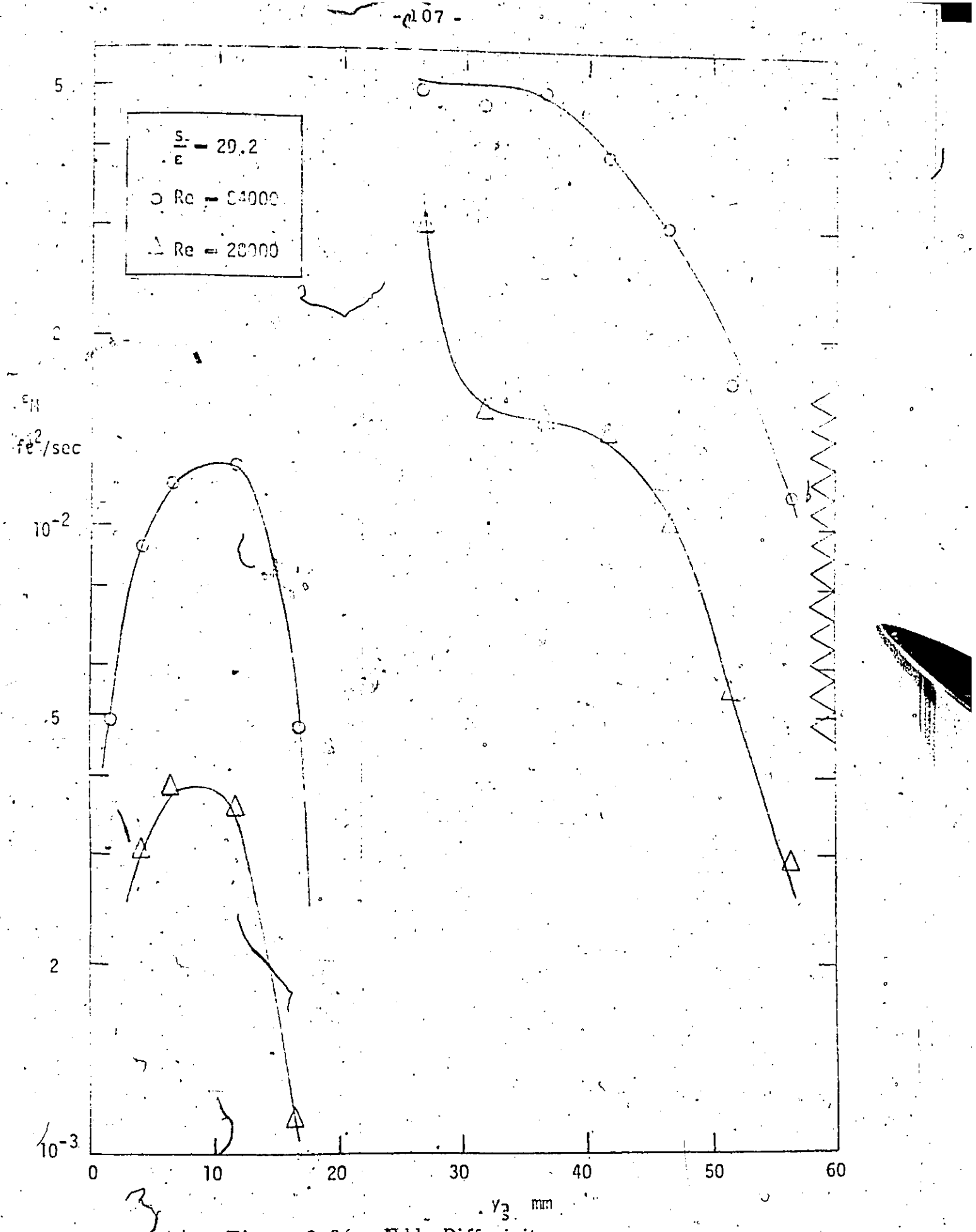

Figure 3.26 Eddy Diffusivity

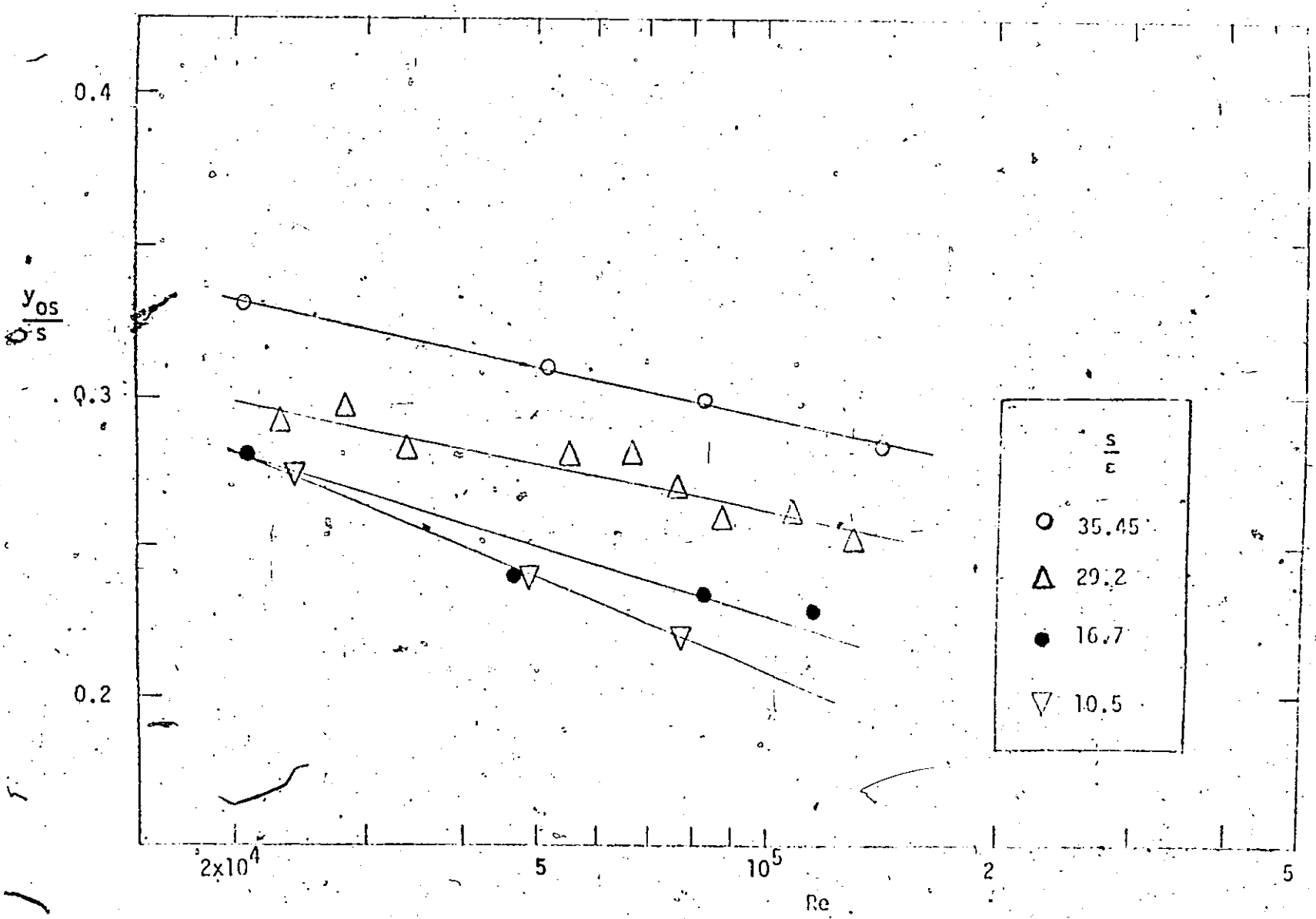

Figure 3.27 Zero Shear Point vs Reynolds Number

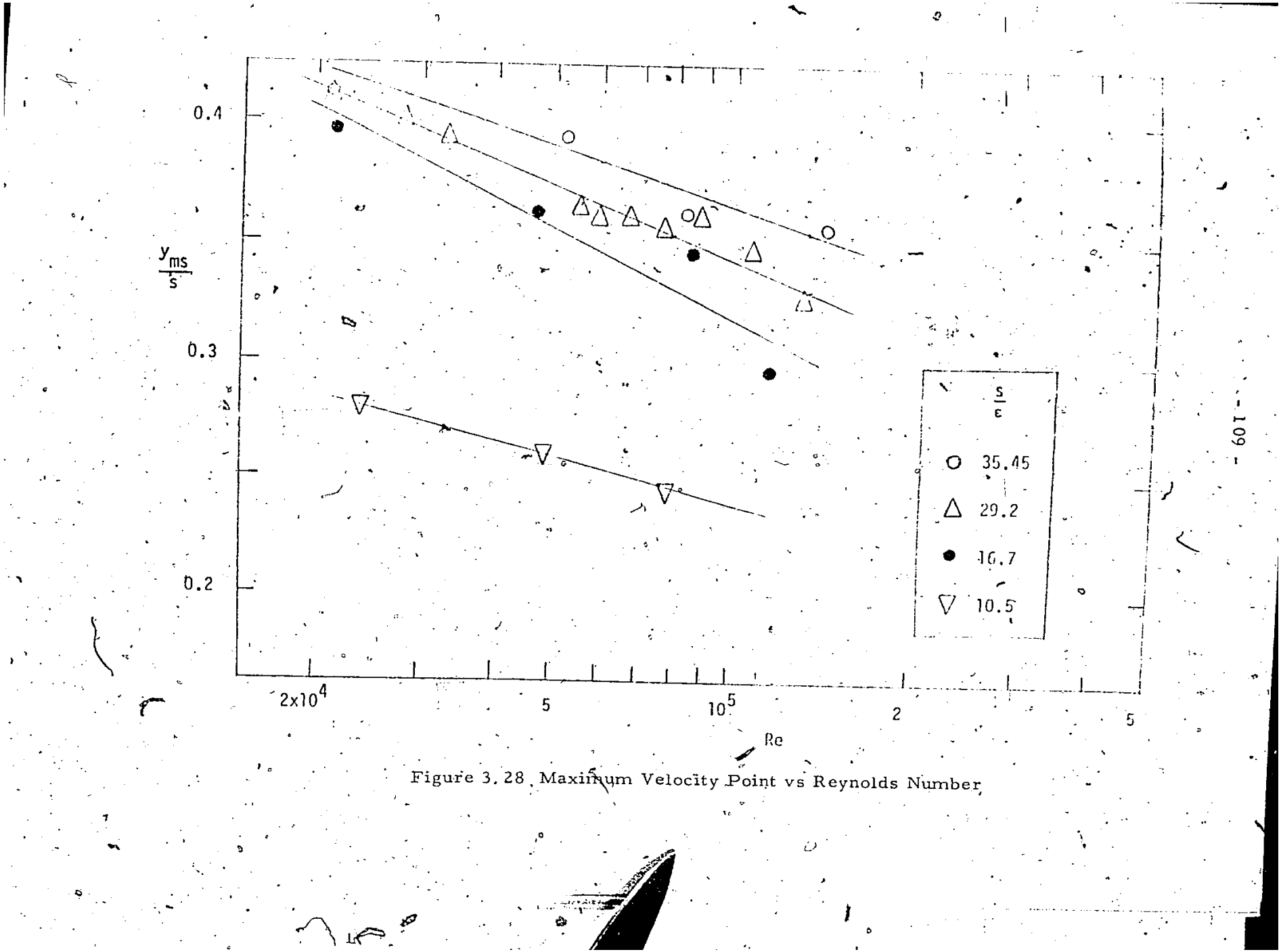

Figure 3.28 Maximum Velocity Point vs Reynolds Number

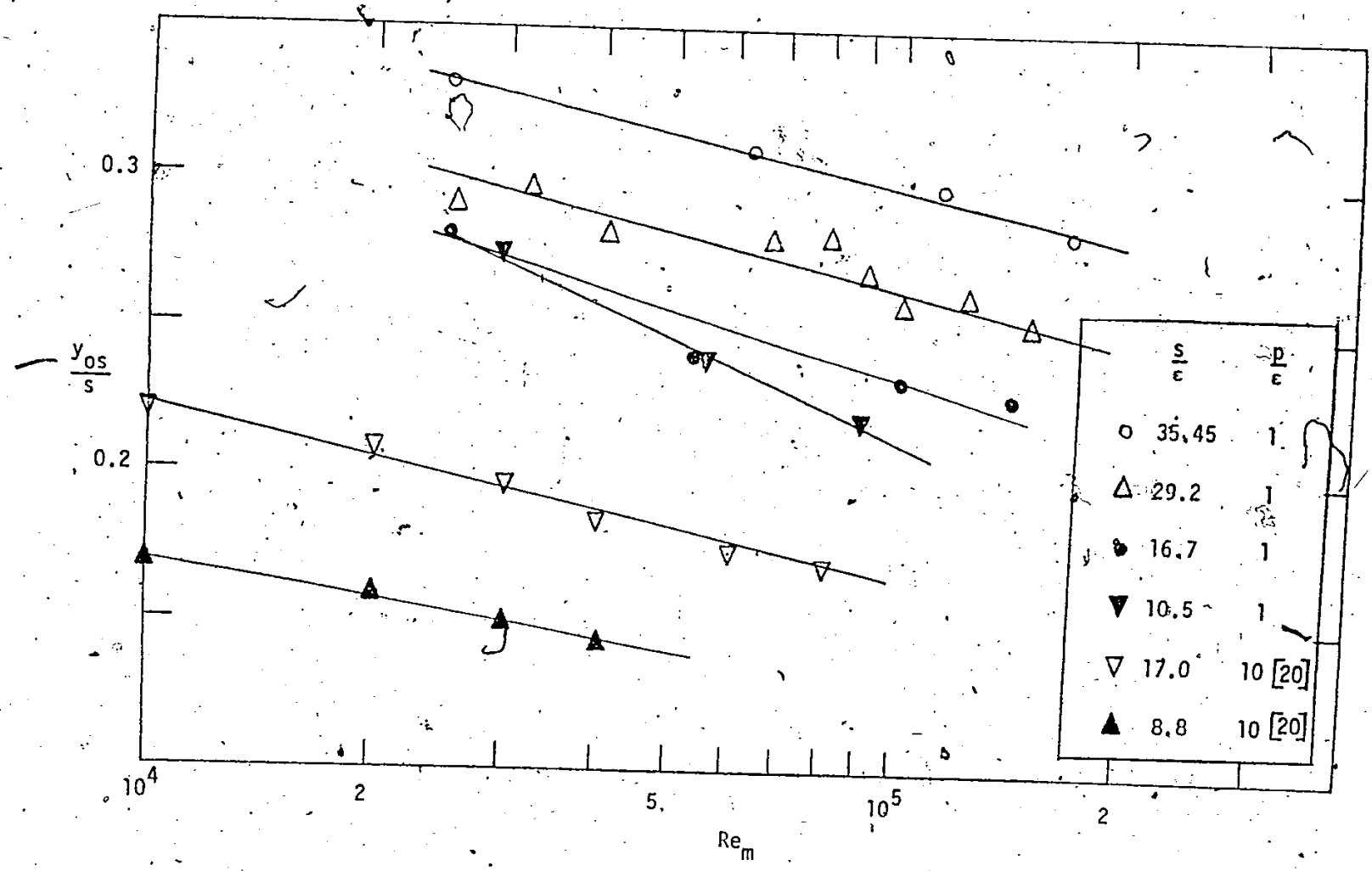

Figure 3.29 Zero Shear Point vs Reynolds Number Based on Maximum Velocity in the Channel

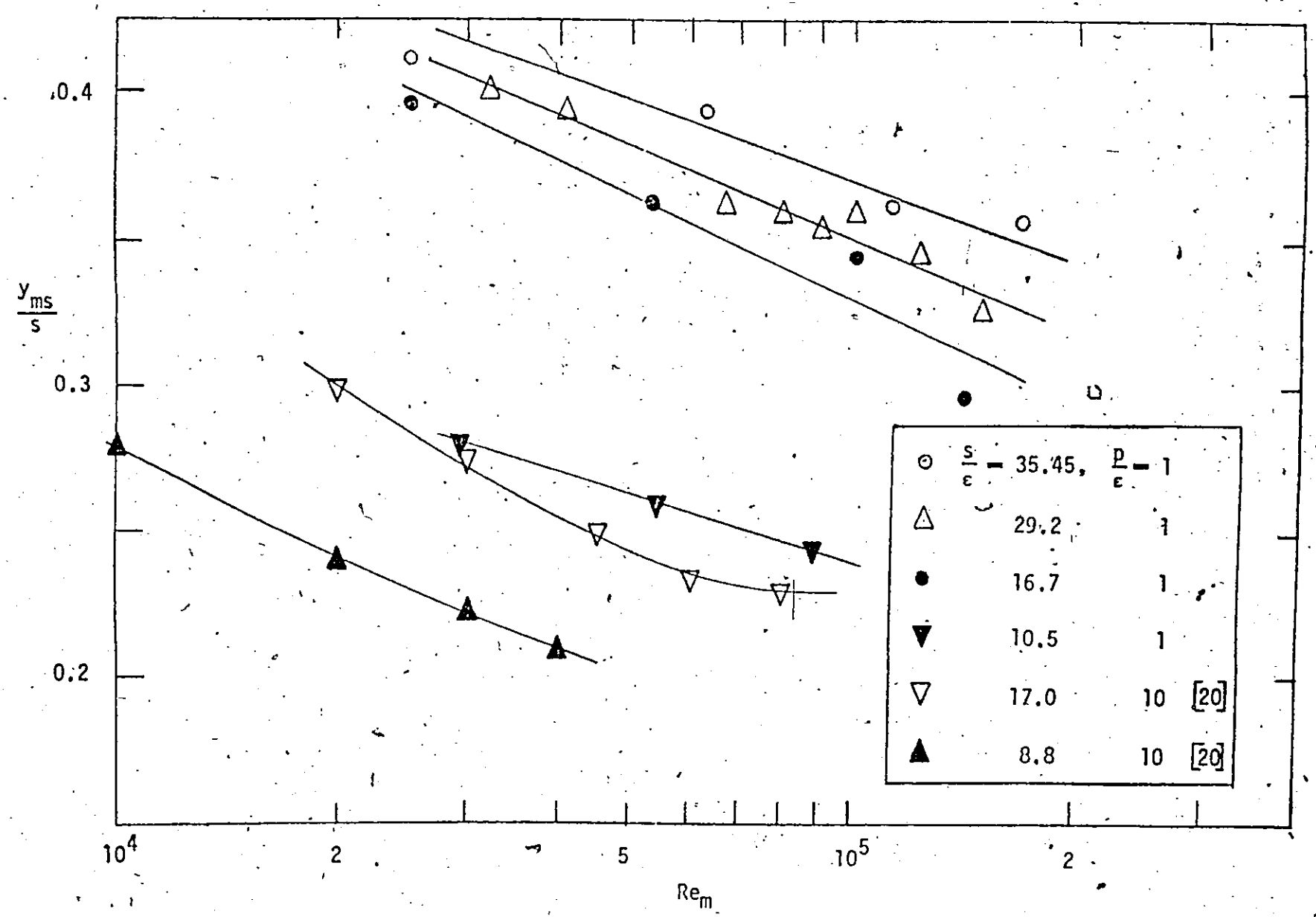

Figure 3.30 Maximum Velocity Point vs Reynolds Number Based on Maximum Velocity in the Channel

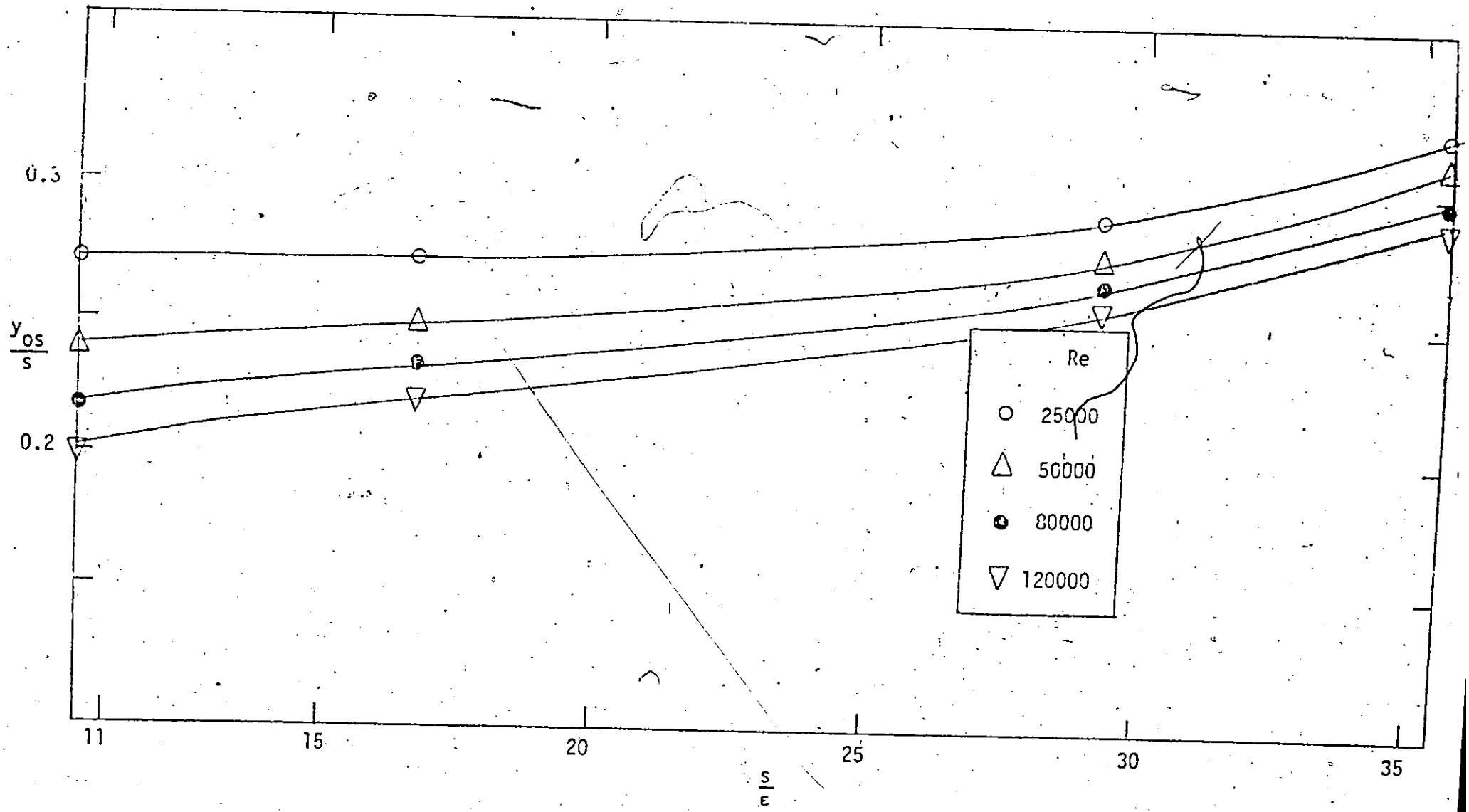

Figure 3.31 Zero Shear Point vs Channel Width to Roughness Height Ratio

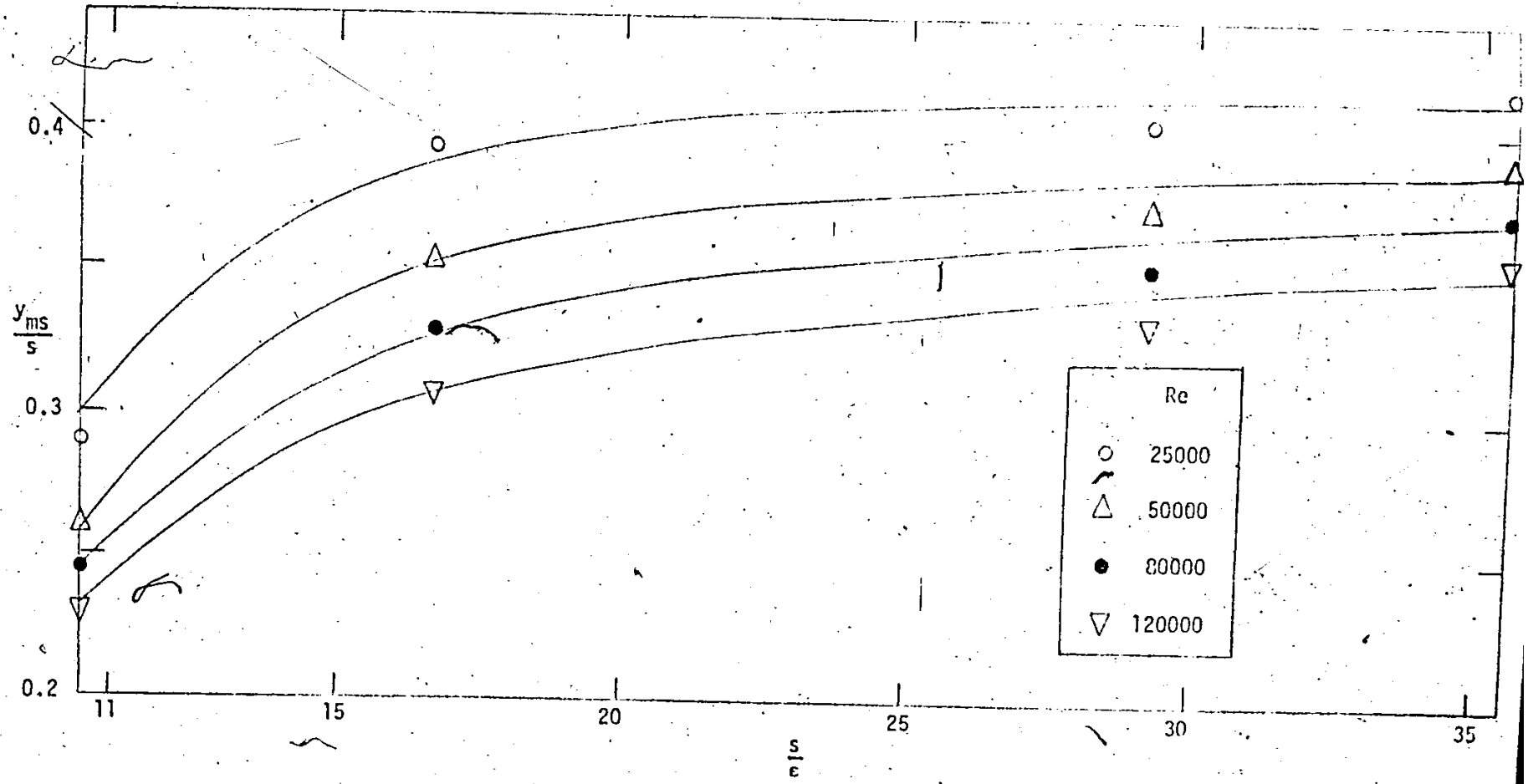

Figure 3.32 Maximum Velocity Point vs Channel Width to Roughness Height Ratio

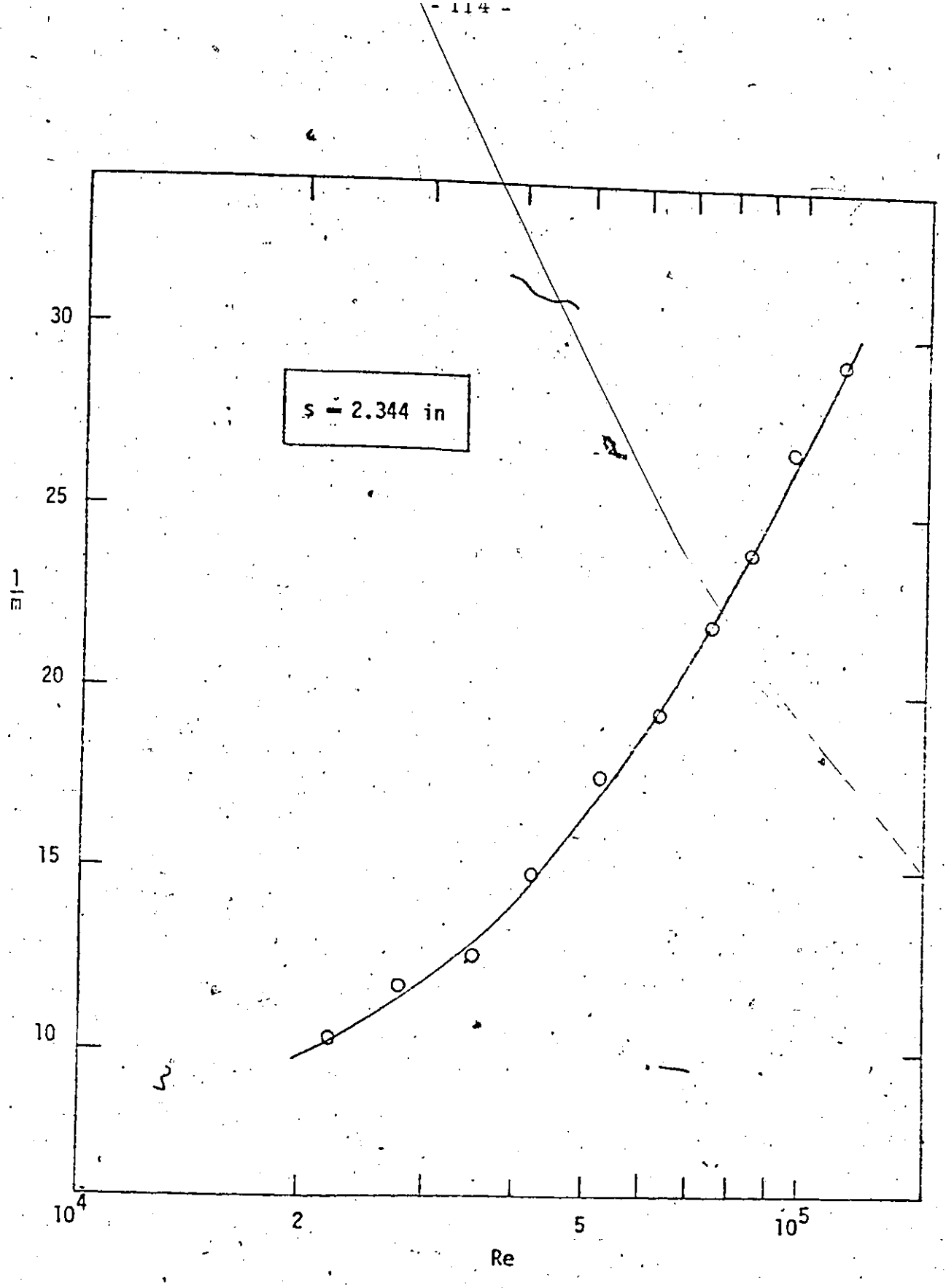

Figere 3.33 $\frac{1}{m^{\prime}}$ vs Reynolds Number